BlueMUSE

Phase A White Paper

March 14, 2025

Davor Krajnović[1], Johan Richard[2], Roland Bacon[2], Angela Adamo[3], Arjan Bik[3], Jérémy Blaizot[2], Nicolas Bouché[2], Jarle Brinchmann[4], Norberto Castro[1], Adéla ide Claeyssens[2], Luca Cortese[5,6], Emanuele Daddi[7], Stefan Dreizler[8], David Elbaz[7], Thibault Garel[2,9], Matthew Hayes[3], Mathilde Jauzac[10], Jean-Paul Kneib[11], Vianney Le Bouteiller[7], Floriane Leclercq[2], Angel Lopez-Sanchez[6], Anna F. McLeod[10], Cyrielle Opitom[12], Martin M. Roth[1], Jesse van de Sande[6], Russell Smith[10], Anthony Mark Swinbank[10], Tanya Urrutia[1], Anne Verhamme[9], Peter Weilbacher[1], Martin Wendt[13], Lutz Wisotzki[1], (*)

(*) Additional authors from the BlueMUSE Science Case document (Richard et al., 2019) contributed to this white paper by providing material for the BlueMUSE science cases.

Abstract

We present a set of science cases for BlueMUSE, a blue-optimised, medium spectral resolution, panoramic integral-field spectrograph proposed for the Very Large Telescope. With an optimised transmission down to 350 nm, a twice higher spectral resolution and a similarly large field-of-view compared to MUSE, BlueMUSE will open up a new range of galactic and extragalactic science cases facilitated by its specific capabilities. They will extend the discovery space beyond that possible with MUSE, presenting BlueMUSE as both a sister instrument to MUSE for linked observations, and as an independent tool for scientific discoveries.

In this document we outline the key science cases as drivers of the BlueMUSE design, as well as supporting science cases that define the associated Top Level Requirements. They are divided in three groups, based on the distance scales, covering the Milky Way and the Local Group, nearby galaxies and the distant universe. Presented cases, coming from the BlueMUSE science team as well as the community, provide only a fraction of examples for possible usage of BlueMUSE. They are primarily highlighted here as they drive and define the Top Level Requirements, but they also form the basis for future scientific aims of the BlueMUSE consortium.

BlueMUSE will be ready in early 2030s when the focus of most of the new large facilities (ELT, JWST) will be on the infrared. At that time, BlueMUSE will be a unique integral field spectrograph focusing on the Blue/UV part of the spectra observable from the ground. It will offer a strong synergy with other VLT instruments (e.g. MUSE, CUBES, Mavis), and a supportive role with ELT, ALMA, SKA, JWST, Euclid, Roman and Athena. BlueMUSE's unique survey capability, its large field-of-view and blue optimised sensitivity are attractive aspects for the ESO community, opening new scientific possibilities as well as serendipitous discoveries.

[1]Leibniz-Institut für Astrophysik Potsdam (AIP), An der Sternwarte 16, D-14482 Potsdam, Germany,

[2]Univ Lyon, Univ Lyon1, Ens de Lyon, CNRS, Centre de Recherche Astrophysique de Lyon UMR5574, F-69230, Saint-Genis-Laval, France,

[3]Stockholm University, Department of Astronomy and Oskar Klein Centre for Cosmoparticle Physics, AlbaNova University Centre, SE-10691, Stockholm, Sweden,

[4]Instituto de Astrofísica e Ciências do Espaço, Universidade do Porto, CAUP, Rua das Estrelas, PT4150-762 Porto, Portugal,

[5]Australian Astronomical Optics - Macquarie University (AAO-MQ), NSW 2109, Australia

[6]International Centre for Radio Astronomy Research, The University of Western Australia, Australia [7]Institut de Recherche des lois Fondamentales de l'Univers & AIM, CEA & CNRS, Université de Paris-Saclay, F-91191 Gif-sur-Yvette, France

[8]Institut für Astrophysik und Geophysik, Georg-August-Universität Göttingen, Friedrich-Hund-Platz 1, 37077 Göttingen, Germany,

[9]Observatoire de Genève, Université de Genève, 51 Ch. des Maillettes, 1290, Versoix, Switzerland,

[10]Centre for Extragalactic Astronomy, Department of Physics, Durham University, South Road, Durham DH1 3LE, United Kingdom,

[11]Laboratoire d'Astrophysique, Ecole Polytechnique Fédérale de Lausanne (EPFL), Observatoire de Sauverny, CH-1290 Versoix, Switzerland,

[12]Institute for Astronomy, University of Edinburgh, Royal Observatory, Edinburgh, UK, and

[13]University of Potsdam, Institute for Physics & Astronomy, Potsdam, Germany

Contents

1 Introduction

Over the past two decades, the integral-field spectroscopy became one of the preferred methods for mapping galactic and extragalactic objects and observing physical processes that shape them. The very high demand (Roth, 2024) for MUSE (Bacon et al., 2010) among all other instruments at the Very Large Telescope (VLT) is the most striking example of both how useful an integral-field spectrograph (IFS) can be and how much it is needed by the community to pursue the forefront research. Motivated by the desirability of IFS, and the proven quality of MUSE, our team is building a sister instrument, BlueMUSE. BlueMUSE is envisioned as an optical, seeing-limited, blue-optimised, medium spectral resolution, panoramic IFS, proposed for the VLT. Its properties are similar to MUSE in the sense of the large field-of-view (FoV) and high throughput, but its wavelength range is shifted to bluer wavelengths, while offering a higher spectral resolution and a better spectral sampling. On the other hand, BlueMUSE will be optimised for one mode and it will not be adaptive optics assisted instrument. Its single mode of operation and a fixed spectral and spatial format will simplify the overall fore-optics, as well as the operations. The main characteristics of BlueMUSE are presented in Table 1.

Characteristic	Value
Common wavelength range	350 - 580 nm
Spectral resolution	$R > 2600$, average 3500 over the wavelength range
Throughput including telescope and atmosphere	$> 15\%$ and average $> 26\%$ over the wavelength range
Field-of-View	> 1 arcmin^2
Operational efficiency	$> 70\%$ open shutter time
Image quality	$< 0.42''$ over common wavelength range
Stability	< 0.1 pixel and $< 10\%$ illumination within a night (without night calibration)
Spatial sampling	$0.2'' <$ spaxel $< 0.3''$
Spectral sampling	> 2 spectral pixels (goal 2.5)

Table 1: Summary of the perormance Top Level Requirements based on the science cases presented in this paper, which define the characteristic parameters of BlueMUSE.

In this document, we present the science cases that drive the top level requirements (TLRs)[1] which define the presented characteristics of BlueMUSE (Table 1). These should be viewed within the landscape of proposed instrumentation for the next decade, when BlueMUSE will start operating. The major facilities covering the optical and near-infrared wavelengths, such as the ELT, JWST, Rubin, Euclid and Roman, will all be optimised for the near infra-red. In this sense BlueMUSE will be a unique facility, offering synergetic links and exploring additional parameter space. While BlueMUSE is an evolution of the technology used on the very successful MUSE instrument, with a similar architecture and many similar systems (and therefore low risk), it is supported with new and distinct science cases making use of its blue spectral coverage, higher spectral resolution and a large field-of-view (FoV). Of the existing or upcoming instruments only MUSE and KCWI are on an 8-10m class telescope, and while they are comparable in some aspects (e.g. same FoV for MUSE, blue wavelengths for KCWI), the combination of BlueMUSE properties outlined in the table above make it a unique instrument for addressing important open questions in astrophysics, as well as an excellent choice to provide support for other facilities. In this respect, we list here several science cases showcasing such synergies and uniqueness of BlueMUSE. They are divided in the "Key Science Cases", which are uniquely adapted for BlueMUSE, and examples of additional science cases that strongly benefit from BlueMUSE characteristics. This list is, however, not exhaustive, and the range of possible science cases for which BlueMUSE will be an instrument of choice is large. Here we primarily focus on those science cases that define the *limits* of the instrument in terms of TLRs. They are divided in three

[1]TLRs are specified in ESO document 513867 "BlueMUSE Top Level requirements".

groups, each having a key science case that drives the properties of the instrument, as well as a set of supporting science cases that reinforce them.

2 Science cases - The Milky Way and the Local Group

State-of-the-art IFS have demonstrated the maturity of this technology (Roth et al., 2018) and its importance for stellar physics, for spatially resolved studies of ionised gas in nebulae and diffuse galaxy interstellar medium (ISM) and for comet studies. MUSE has proven to be a unique instrument for studying the formation and evolution of stellar objects at various stages of their life cycles (e.g. Kamann, Wisotzki, and Roth, 2013; Castro et al., 2021) while also enabling synergies with studies of the interstellar medium (e.g. McLeod et al., 2015).

The wide field of view (FoV) and spatial sampling of MUSE highlight its potential to resolve crowded stellar fields (Kamann, Wisotzki, and Roth, 2013; Roth et al., 2018) and systematically study dense stellar clusters that are otherwise inaccessible or prohibitively expensive to observe with other facilities. Large and homogeneous spectroscopic samples are essential for understanding stellar evolution (e.g. Castro et al., 2014) and extending this knowledge to more distant regions of the Universe, where resolved stellar populations and ISM studies are not feasible. By spatially resolving nebulae (HII regions, planetary nebulae, supernovae remnants), we are able to map radiative and mechanic feedback from massive stars directly on the surrounding gas, a key component of the baryonic cycle of galaxies (Schinnerer and Leroy, 2024). Furthermore, the wide FoV of MUSE has proven crucial for studying the physical and chemical properties of cometary comae (Opitom et al., 2020), showcasing the possibility for Solar System studies.

BlueMUSE will enhance and extend the capabilities of MUSE by covering the much-needed blue range of the optical spectrum, crucial for stellar and ionised gas physics and the study of non-sidereal objects. Notably, BlueMUSE science cases include the following:

- BlueMUSE will provide systematic maps of stellar properties and chemical compositions for very massive clusters in the Milky Way and nearby galaxies, such as NGC 2070 in the Large Magellanic Cloud. Its unique wavelength coverage in the blue range (400 – 500 nm) is essential for accessing key diagnostic lines, such as O II, Si II, Si III, Si IV and N II. Since hot stars are intrinsically blue, BlueMUSE's wavelength coverage aligns closely with the peak of their spectral energy distributions, offering significant advantages over MUSE. Additionally, the large spectral resolution of BlueMUSE will enable a more detailed exploration of the kinematics and the presence of binary within these environments.

- In our Galaxy and within the Local Group we will be able to map physical properties at the smallest physical scales (sub-parsec). These studies will be laboratories to understand the interplay between stellar feedback and the immediate surrounding medium. At intermediate distances (2 and 10 Mpc), the panoramic BlueMUSE field of view will enable to gather large samples of these populations, while also mapping the diffuse ionised gas component, physical conditions, abundances, and kinematics of the ionised gas in resolved nebulae. The wavelength range covered by BlueMUSE will provide emission lines sensitive to gas densities (e.g., O II$\lambda\lambda$3729,3726, Cl III$\lambda\lambda$5518,5535, Ar IV$\lambda\lambda$4740,4711), temperature (O III$\lambda\lambda$4363,4958,5007; Ne III$\lambda\lambda$3343,3968,3869) and enable direct abundance measurements. These will be fundamental to study the mixing time scales across different galactic environments. The blue range provides a possibility to cover the Ne Vλ3426 line[2], used as AGN diagnostic. The increased spectral resolution will enable us to better resolve the kinematics of the ionised gas and stellar component, important to understand the 3D structure of disk galaxies

- The spatial information provided by an IFS is essential for disentangling individual spectra in dense stellar environments, such as globular clusters (GCs). MUSE allowed for the retrieval of tens of thousands of spectra per cluster, enabling detailed studies of their chemical compositions and dynamics. Access to the blue-visible and near-UV wavelength regions with BlueMUSE will uncover critical spectral features that are highly sensitive to subtle abundance differences among distinct stellar populations within GCs. Moreover,

[2] BlueMUSE will have an extend wavelength range between 330 - 600 nm, for 1/3 of the FoV. The line will fall within the nominal wavelength region and the full FoV for objects further than $\sim$ 100 Mpc away

the increased spectral resolution will offer enhanced precision in measuring radial velocities, facilitating the detection of binary systems and probing stellar dynamics in the vicinity of intermediate-mass black holes.

- Due to their faintness, Ultra Faint Dwarf galaxies (UFDs) are only found as satellites of the dominant galaxies in the Local Group, but their nature offers unique laboratories to study the properties of dark matter. As the amount of baryons in these galaxies is rather small, one expects their star formation histories to be simple and lacking strong stellar feedback episodes. A consequence is that the dark matter (density) profiles are expected to be closely related to those of dark-matter-only simulations, making UFDs systems where the difference between intrinsic properties of dark matter can be studied, as well as potentially determine the nature of dark matter (e.g. is it “cold”, “warm” or “fuzzy”) and whether it is collision-less or self-interacting (e.g. Bullock and Boylan-Kolchin, 2017).

- Large FoV IFS have proven extremely useful to detect faint activity levels in comets, helping us understand how their activity evolves with varying distances from the Sun. A number of radicals are observable in the blue part of the optical range (e.g. CN and C3). BlueMUSE will allow us to gain in-depth insight into the production mechanisms of species in the coma of comets, as well as their activity. BlueMUSE will also offer unique opportunities for the observation of interstellar objects, which formed in other planetary systems and crossing pass through our own solar system.

2.1 Key science case: massive stars

Massive stars dominate the spectral energy distribution of star-forming galaxies across all redshifts, influencing their chemical and dynamical evolution. Through their high energy output, strong stellar winds, and explosive ends as core-collapse supernovae, massive stars significantly contribute to feedback processes that regulate galaxy evolution (Ceverino and Klypin, 2009). They serve as the ionising sources for H II regions, making them crucial for estimating star formation rates, understanding the diffuse ionised gas (DIG), and studying Lyα radiation. Additionally, massive stars provide insights into the chemical composition of contemporary stellar populations, offering an alternative to nebular abundance determinations using strong-line diagnostics (Bresolin et al., 2009). Hot stars are the key components of super star clusters, essential for understanding Population III stars and the re-ionisation of the early Universe. Furthermore, the recent detection of gravitational waves from stellar-mass black hole (BH) mergers has sparked significant interest in the origins of BH binaries, linking them to massive star binaries as their progenitors (e.g. Marchant et al., 2016).

The formation and evolution of massive stars remain poorly understood, particularly for the most massive stars (> 100 M$_\odot$; Vink et al., 2015) and during the later stages of their evolution, after they leave the main sequence and begin core helium burning (Langer, 2012). The theory of massive stars faces significant challenges related to stellar evolution, including the role of rotation, metallicity, stellar winds, convective overshooting, and binarity (Meynet and Maeder, 2000; Langer, 2012; Castro et al., 2014; Vink, 2018; Vink, 2018; Higgins and Vink, 2019; Wang et al., 2022). Systematic surveys are key for unraveling the evolution and nature of the most massive stars, providing homogeneous datasets in different environments and unbiased empirical constraints to theoretical models (e.g. Castro et al., 2014). For instance, understanding the behaviour of massive stars as a function of metallicity, particularly in metal-poor environments, is essential for exploring the early epochs of the Universe. Although theoretical models can simulate stars at such low metallicities, the parameter space becomes increasingly uncertain as metallicity decreases, complicating extrapolations to unresolved populations with metallicities below that of the Small Magellanic Cloud (Garcia et al., 2021; Lorenzo et al., 2022).

Massive stars are rare in the Universe compared to lower-mass objects, and obtaining large spectroscopic samples needed to study them requires demanding observational programs (Evans et al., 2011b). Photometry alone is insufficient to constrain stellar parameters for massive stars. Historically, identifying and characterising massive stars necessitated a laborious two-step process: selecting hot star candidates through photometry and then conducting follow-up spectroscopy (Massey, Neugent, and Smart, 2016). This approach is both expensive and incomplete. Moreover, spectroscopy of massive stars in star-forming regions is challenging due to nebular contamination and crowding. The capabilities of MUSE have already demonstrated a significant advantage in overcoming these limitations, offering unprecedented multiplexing capabilities (e.g Kamann et al., 2018a; Castro et al., 2018; Roth et al., 2018) However, the MUSE spectral range is not ideal for fully characterising the atmospheres and chemical compositions of massive stars, as it lacks coverage of critical diagnostic lines in the blue region of the spectrum. BlueMUSE will represent a significant advancement, providing the optical wavelength coverage required to observe these crucial blue diagnostic lines while achieving higher spectral resolution. This will enable more precise analyses of the atmospheres and compositions of massive stars, marking a major step forward in our understanding of these objects.

Why is BlueMUSE needed? The canonical stellar transitions used for stellar atmosphere analysis, chemical composition and spectral classification occur between 3500-5000 Å (Walborn and Fitzpatrick, 1990; Martins, 2018). The BlueMUSE wavelength range gives access to the following spectral features constraining stellar parameters, chemical composition and evolutionary stage of the stars (Fig. 1):

- Balmer lines as the principal surface gravity criteria in massive stars.
- Balmer jump at 3646 Å as effective temperature ($T_{\rm eff}$) criterion.
- Wind and classification diagnostics from He II λ4686 and nearby CNO lines.
- Si IV $\lambda\lambda$4089, 4116, Si III triplet λ4552, Si II $\lambda\lambda$4128, 4130, as well as He I (e.g., λ4387 or λ4471) and He II (λ4200 and λ4541) lines for $T_{\rm eff}$ and/or helium abundance.
- Crucial wavelength range for Wolf-Rayet (WR) emission (blue and red bumps), and O VI λ3811 (Crowther, 2007).

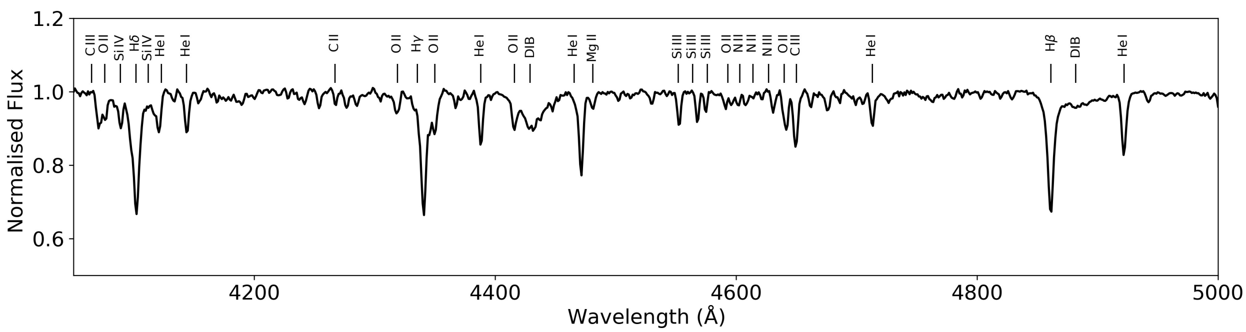

Figure 1: Early B-type spectrum with diagnostic lines in the blue relevant for hot, massive stars (from Gvaramadze et al. 2019).

In the hottest stars, range ($>$ 45000 K), where He I lines are weak or absent, optical lines of N III, N IV and N V are used as temperature criteria in this blue optical range (Rivero González et al., 2012). The 4000-5000 Å range encloses many transitions to measure $T_{\rm eff}$ and log(g): C II, C III, N II, N III, N IV, N V, O II, O III, Si II, Si III, Si IV and Mg II. These transitions also provide the chemical composition of the stars and surrounding interstellar medium (ISM) (Martins et al., 2015). At lower temperatures ($T_{\rm eff}$ >10000 K), Fe II lines are available and can be added to the chemical composition and stellar parameter analysis. The expected spectral resolution of BlueMUSE will be suitable to estimate $T_{\rm eff}$, log(g) as well as abundances, as demonstrated by earlier studies using FORS and LRIS-B (e.g., Kudritzki et al. 2012; Kudritzki et al. 2016).

BlueMUSE will enable unique science for two major reasons: (1) *Multiplex+Sensitivity*: The current state-of-the-art has been set by the VLT-FLAMES Massive Star Survey (Evans et al., 2005a; Evans et al., 2005b) that yielded a total of 803 spectra from an effort of more than 100 hrs VLT time. BlueMUSE will be up to two orders of magnitude faster, depending on the size of a cluster, which has already been demonstrated with MUSE in globular clusters, providing up to 1000 stellar spectra per pointing (Husser et al., 2016). (2) *Crowding*: Analogous to point spread function (PSF) fitting CCD photometry (Stetson, 1987), the IFU concept is vital to deblend heavily crowded fields and yield cross-talk free spectra of stars with overlapping images (see Kamann, Wisotzki, and Roth, 2013). Again, the state-of-the-art can be appreciated from existing results obtained with the VLT-FLAMES Tarantula Survey (Evans et al., 2011a; Evans et al., 2011b) that has provided multi-epoch fibre spectra of different spectral resolution for more than 800 stars, however severely hampered by nebular contamination, and completely unable to address crowded regions. In contrast, from four MUSE pointings on the R136 region with a total exposure time of 2680 s, Castro et al. (2018) were able to extract 2255 spectra, out of which 588 show a S/N>50. In the foreseeable future, no other instrument[3] will have such capability.

Derived TLRs for the Key Science case: massive stars. Characterising the physical parameters of massive stars requires at least a moderately high-resolution optical spectroscopy in the blue, while the large field-of-view will allow efficient observations of star forming region. A summary of TLRs for this science case is presented in Table 2.

TLR	Value	Comment
Wavelength range	350 - 580 nm	
Spectral resolution	R $\geq$ 3500	
Field-of-View	$\geq$ 1 arcmin^2	goal 2 arcmin^2
Sensitivity		same as MUSE (or better)
Spatial sampling	$0.2'' <$ spaxel $< 0.3''$	sample seeing with $\sim$ 2 spaxels
Spectral sampling	$>$ 2 pixels	
Image quality	natural seeing	
Stability	0.1 pixels	

Table 2: TLR for the Key science case: massive stars.

2.2 Physical properties and statistical studies of resolved nebluae

Stellar feedback, originating at the scales of stars, plays a fundamental role in regulating stellar mass growth and metallicity content in galaxies. The sensitivity, multiplexing capabilities, and wide FoV of BlueMUSE will enable us to study different feedback processes while sampling diverse galactic environments. Galaxies at 2 –10 Mpc distance are optimal targets. Efficient mosaics will enable us to sample scales below 10 pc, while covering large areas of the disks (McLeod et al., 2021; Della Bruna et al., 2021; Emsellem et al., 2022; Della Bruna et al., 2022a). In this front, BlueMUSE data will open a unique window at the 350-550 nm, which will enable us to perform statistical studies of populations from a few tens to several thousands of feedback sources (i.e census of massive stars and star clusters bright at these wavelengths), as well as their effect on HII regions (ionisation state, densities, direct abundance measurements using auroral lines). The broad coverage will also enable to gather and study the physical conditions of populations of supernova remnants (SNR; e.g. McLeod et al., 2021) and planetary nebulae (PNe; Scheuermann et al., 2022) and the DIG. An example is shown in Fig. 2, a 20 tile mosaic of a nearby spiral galaxy M83 (5 Mpc). The M83 MUSE mosaic enable us to extrapolate the type of data quality and incredible source of information that will be stored in the BlueMUSE 3D cubes. With BlueMUSE's factor of 2 better spectral resolution it will be possible to better quantify the kinematics in the regions with low velocity dispersion, and to disentangle broadening in the ionised gas due to thermal emission or shocks.

On the other hand, BlueMUSE will also play a fundamental role in mapping single nebulae in the Milky Way and Local Group (e.g. McLeod et al., 2019). These studies, while conducted on smaller sample of objects, will enable us to have a complementary view of star formation, feedback and their effect on the immediate surroundings mapping ionised gas kinematics, metal abundances, and ionisation states at sup-parsec scales within single HII regions, SNRs, PNe.

Star forming regions are embedded in optically thick dusty clouds, potentially affecting the observations at blue wavelengths. Studies, however, show that the deeply embedded phases are of very short duration ($< 2 - 3$ Myr, e.g Corbelli et al. 2017; Messa et al. 2021). Furthermore, very early on, strong stellar feedback, arising from radiation and stellar winds, before supernova explosions can occur (e.g. Kruijssen et al., 2019), is able to open low density channels along the collapsing clouds through which we can see very young stellar populations (e.g. 30Dor, NGC602). While the observational limits posed by the optical depth of the targets have to be taken into

[3]We note that MOONS, although high multiplex, covers a much redder wavelength range.

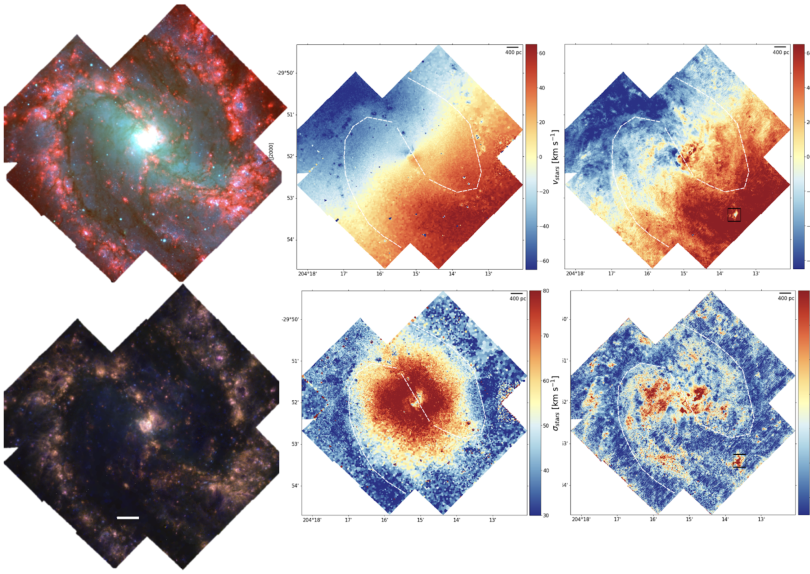

Figure 2: Three colour images obtained from a 20 tile MUSE mosaic of M83 (the white bar indicate 20″ or 400 pc). The top left image shows the pseudo-V and R bands and Hα map, the bottom left shows the Hα, [SII], [OIII] composite. The four right plots show the kinematics of the stellar (central) and ionised gas (right) components at scales of $\sim$ 20 pc. The velocity maps (top) show the regular stellar and gas disk rotation as well as small scale variations in the ionised gas. The velocity dispersion of the stellar light reveals the bulge component of the galaxy, while the gas shows larger broadening in regions coinciding with shocked gas (data from Della Bruna et al., 2022b; Della Bruna et al., 2022a).

account, the large FoV of BlueMUSE and demographic studies of a statistically significant sample of resolved nebulae, will ensure that this will not be a limitation or introduce biases.

Spectroscopy of line and continuum emission resulting from energy loss of ionised and neutral gas is fundamental to understanding the physical conditions and abundances in circumstellar, interstellar and intergalactic media and hence an essential probe of stellar and galaxy evolution. This gain relies on the presence of many diagnostic nebular lines in the blue wavelength range, which are of astrophysical importance and have been well studied spectroscopically (Fig. 3).

A long standing controversy concerns the light element abundances of nebulae (PNe and H II regions in particular, but not restricted to these) determined from the traditional, and strong, collisionally excited lines (CELs) compared to the fainter recombination lines of the same elements (mostly C, N and O). Many studies (e.g., Liu 2006; Tsamis et al. 2003; García-Rojas et al. 2006; Esteban et al. 2014) have shown differences between abundances from CEL and optical recombination line (ORL) determinations, called the abundance discrepancy factor (ADF), from values of a few for H II regions up to >50 for some PNe (Peimbert et al., 2014). If CEL abundances are wrong by large factors then the use of these lines for studies of the ISM in general, and of distant galaxies in particular, becomes problematic (Esteban et al., 2009; López-Sánchez et al., 2012); if, on the other hand, ORL abundances are not representative, then the physics of circumstellar media, and by association the ISM, is poorly understood, or the atomic physics required for recombination line abundance determination needs revising.

Why is BlueMUSE needed? The current MUSE range, while including some N II and C II ORLs, does not include the strongest ORLs of O II and O III (4300–4700 Å) which are crucial for exploring the ADF problem, since ORL and CEL O^{+} and O^{++} abundances (the latter from the very strong [O II] λ3727, and [O III] $\lambda\lambda$4959, 5007, lines) can be spatially compared. Other important ORLs of C II and C III together with Ne II ORL's (c.f. the spectral compilations of Sharpee, Baldwin, and Williams 2004 and Fang and Liu 2011) also require a bluer spectral range (see Fig. 3). Coverage in the 350 to 580 nm will allow us to sample electron densities (n_e : [OII] 3729,3726, [Cl III] 5518,5535 , [Ar IV]4740,4711) and ionised gas temperature (T_e : [OIII]4363,4958,5007) and determine abundances for HII regions, SNRs, PNe with direct methods. Higher spectral resolution is a strong advantage since the emission line spectrum is crowded, with many H and He recombination lines in addition to the CELs, thus line blending can be a problem particularly for the extraction of faint ORLs (see Fig. 3).

The use of a panoramic IFS is essential to sample the entire face of ionized nebulae that can be subject to different mechanisms of excitation (photoionization, shocks) and hydrodynamical effects, as well as spatially varying distributions of chemically enriched material. The large FoV of BlueMUSE is of strong significance here, and it provides an advantage over any other blue optimised IFS with a similar (or even larger) spectral resolution, such as KCWI. The larger size of BlueMUSE enables it to be $\sim$ 6 times faster than KCWI: to map a 2×2 mosaic

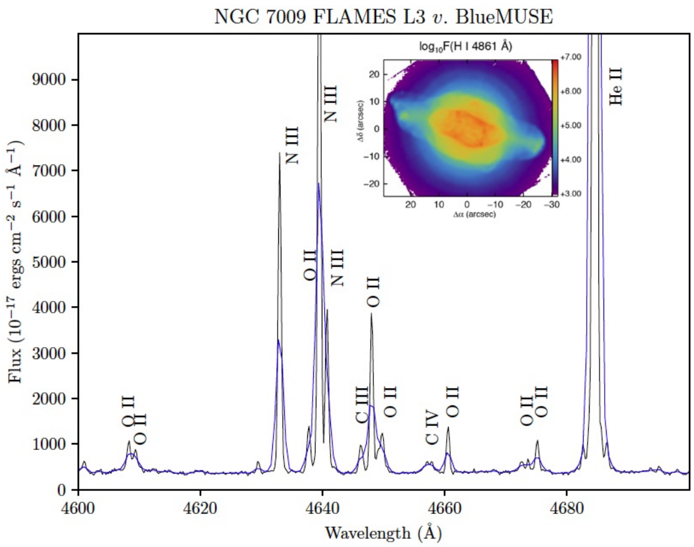

Figure 3: BlueMUSE simulated spectrum (in blue) of the rich 4600–4700Å region of a $2'' \times 2''$ region in NGC 7009. The spectrum was formed by smoothing and rebinning the FLAMES Medusa L3 spectrum (shown in black, see Tsamis et al. 2008) to the BlueMUSE resolution and pixel size. This region is rich in recombination lines of N III and C II and in particular the multiplet M1 of O II, which can be used to measure the O^{++} recombination line abundance. It is clear from this example that BlueMUSE will be very powerful for measuring these recombination lines over large areas of resolved Galactic and Local Group ionized nebulae. (Inset) Example of an emission line map across the planetary nebula NGC 7009, illustrating the spectroimaging capabilities of a large IFU for such objects (Walsh et al., 2018).

of a system with size similar to 30Dor (Castro et al., 2021) KCWI would require 24 hours compared with 4 hours used with MUSE (which has the same FoV as BlueMUSE). While KCWI can offer higher spectral resolution and higher precision for kinematics studies, BlueMUSE is much more suited for statistical surveys of extended objects such as resolved nebulae.

Derived TLRs for the science case: physical and statistical studies of resolved nebulae. Critical aspects of BlueMUSE for this science case are its ability to cover lines blue-ward of the [O III] $\lambda\lambda 4959, 5007$ doublet, at a medium high spectral resolution (~ 3500) in order to resolve the [OII] doublet, as well as disentangle kinematics in star forming regions. A spatial sampling of $0.2''$ to $0.3''$ would be sufficient to sample the PSF at seeing limited conditions. A summary of TLRs for this science case is presented in Table 3.

TLR	Value	Comment
Wavelength range	350 - 580 nm	
Spectral resolution	≥ 3500	≥ 2800 at 370 nm
Field-of-View	≥ 1 arcmin^2	goal: 2 armin^2
Sensitivity	$\sim 5 \times 10^{-18}$ergs/s/cm^2/Å	for e.g. [OIII] 4363 or [OII] 3727
Spatial sampling	$0.2'' <$ spaxel $< 0.3''$	sample seeing with ~ 2 spaxels
Spectral sampling	> 2 pixels	
Image quality	natural seeing	
Stability	0.1 pixel	

Table 3: TLR for the science case: physical and statistical studies of resolve nebulae

2.3 Globular clusters

MUSE allowed, for the first time, a detailed spectroscopic investigation for tens of thousands of individual stars in Galactic globular clusters (GCs) and even in massive star clusters in the Magellanic Clouds (see Section 2.1). For most clusters, this corresponded to an increase of the spectroscopic samples by two orders of magnitude. Thanks to the combination of the IFS and high spatial resolution space based imaging (e.g. Hubble Space Telescope), it also became possible to advance to the heavily crowded cluster centres. This enabled detailed studies of the kinematics of the clusters (e.g. Kamann et al., 2018a; Pechetti et al., 2024), binary searches (Giesers et al., 2018), and the measurement of stellar parameters (Husser et al., 2016). A combination of radial velocities obtained with IFS observations and proper motions from high-resolution imaging campaigns is the most promising way of detecting intermediate-mass black holes (IMBH) in the interiors of GCs (e.g Häberle et al., 2024).

It is now well established that GCs host at least two chemically different stellar populations with differences in light elements like sodium or oxygen, and possibly helium (Bastian and Lardo, 2018). In some GCs the multiple stellar populations show even more complex chemical pattern, including iron spread. The origin of these complex chemical patterns are still unknown. It is currently debated in the community whether they are linked to the way GC formed or more to their evolution in the host galaxy. So far high-resolution spectroscopy has been used to infer the abundance differences, hence the studies were restricted to rather small stellar samples in the outskirts of the clusters. With MUSE, abundance differences between the populations can be measured by co-adding the spectra of stars for which the population has been determined previously from precise photometry. The extremely high signal-to-noise ratios (S/N) of the combined spectra compensate for the relatively low spectral resolution. MUSE is, however, not covering the full parameter space; some stars are not well represented, such as horizontal branch and potentially blue hook stars, extremely low mass white dwarfs, or interacting binaries. As these objects probe the binary evolution in dense stellar populations, their study is important for understanding the overall dynamical evolution of the cluster.

Why is BlueMUSE needed? BlueMUSE will be a significant improvement and therefore the next major step towards a more complete understanding of the formation and evolution of GCs. Low mass stars have significantly more spectral lines in the visual-near-UV spectral range covered by BlueMUSE compared to the red-near-IR range covered by MUSE, including strategic lines for spectral analysis like the Ca II H & K, CN molecular lines, and many more. Furthermore, this wavelength range has minimal telluric emission in the sky spectrum and also covers the full Balmer series (except Hα), which is of high importance for early-type stars. Another important point is BlueMUSE's increased resolution (R$\sim$3500 on average) which will reduce the blending of spectral lines (e.g. Hollyhead et al., 2017), and allow a higher precision in determination of the radial velocities (RV), in particular considering the higher information content of the blue spectral range (Wendt et al., 2024). Tests show that while BlueMUSE is predicted to match the performance of MUSE in AO model in terms of extracting the equal number of stars from crowded regions, it should surpass MUSE in terms of the precision to which the physical properties of extracted sources can be determined (see BlueSi simulations in Section 6.2). The higher RV precision in combination with the improved sensitivity for spectral differences would allow for a chemo-dynamical separation and investigation of multiple populations in globular clusters. This will enhance current dynamical studies, enable more precise characterisation of binaries, the segregation state and allow determinations of IMBH masses. Furthermore, detailed studies of stellar rotation would become feasible. Stellar rotation has recently been confirmed to play a crucial role in shaping the colour magnitude diagrams of young and intermediate age clusters (e.g. Kamann et al., 2018b; Kamann et al., 2020). In general, BlueMUSE will allow to extend investigations of multiple populations from red giants to turn-off and main sequence stars, down to the high-mass end of the Brown Dwarf companions, while the planetary mass regime will not be achievable.

Derived TLRs for the science case: globular clusters. The main characteristic of BlueMUSE is to provide spectroscopy in the wavelength range of 350-600 nm. Higher spectral resolution than MUSE leads to more precise radial velocity measurements and better constrain the kinematics of star clusters. Higher spatial resolution is preferred to study crowded fields such as the centres of star clusters. A larger FoV is also desirable as it would allow us a more efficient mosaicking with 0.2 to 0.3 arcsec spaxels sampling. The lines of interest covered by BlueMUSE are: Mg triplet at 517 nm important for kinematics. CN molecular band at 384 nm important to discern multiple populations in GCs. CaII H&K lines, as well as the strong diffuse interstellar molecular bands at 443 nm. A summary of TLRs for this science case is presented in Table 4.

2.4 Ultra-Faint Dwarf Galaxies

The most natural place to constrain the nature of dark matter is to study the most dark-matter dominated systems we know: the Ultra-Faint Dwarf galaxies (UFDs) in the Local Group. In these very faint, $M_V > -7.7$ and $L \approx 10^5 L_\odot$, and very metal-poor ([Fe/H]$\lesssim -2$) systems (Simon, 2019), baryons might only make up $1/500^{\text{th}}$ of the total mass (e.g., McConnachie 2012; van Dokkum et al. 2015). UFDs are also stellar systems in which the impact of supernovae and massive stars feedback are expected to be largest, thus making them crucial

TLR	Value	Comment
Wavelength range	350 - 580 nm	goal > 336 nm
Spectral resolution	R $\geq$ 3500	on average
Field-of-View	> 1 arcmin^2	goal 2 arcmin^2
Sensitivity		similar to MUSE
Spatial sampling	$0.2'' <$ spaxel $< 0.3''$	sample seeing with ~ 2 spaxels
Spectral sampling	> 2 pixels	
Image quality	natural seeing	
Stability	0.1 pixels	

Table 4: TLR for the science case: globular clusters

laboratories for the study of baryonic physics in galaxy formation. Furthermore, as baryonic feedback effects (i.e. from star formation) are not expected to be strong, these objects are also unique laboratories for investigating the properties of dark matter particles, potentially allowing a distinction between such models as cold, warm and (several types of) self-interacting dark matter (e.g. Zoutendijk et al., 2021).

UFD candidates are now identified with great efficiency in wide-field imaging surveys such as SDSS, DES or Pan-STARRS (Belokurov, 2013; Drlica-Wagner et al., 2015). The Vera C. Rubin Observatory is expected to greatly increase the number of photometrically identified UFD candidates. However to confirm their nature and to study their dark matter content and the abundance patterns of their constituent stars, spectroscopic follow-up is mandatory. Traditionally this has been done with multi-object spectrographs (MOS, Li et al. 2017), but such follow-up requires a) pre-selection of member stars, and b) significant distances between the targeted stars to avoid slit/fibre collisions. Moreover, dynamical studies require sampling of stars both at the nucleus and at large radii. A wide-field integral field spectrograph offers the perfect alternative to a MOS since one can get away from pre-selection and the density of spectra is orders of magnitudes higher than for a MOS. Moreover, the PSF-fitting crowed field technique described above (§ 2.1 and 2.3) allows to de-blend overlapping stellar images which would not be possible with any other spectroscopic technique (Zoutendijk et al., 2020; Vaz et al., 2023).

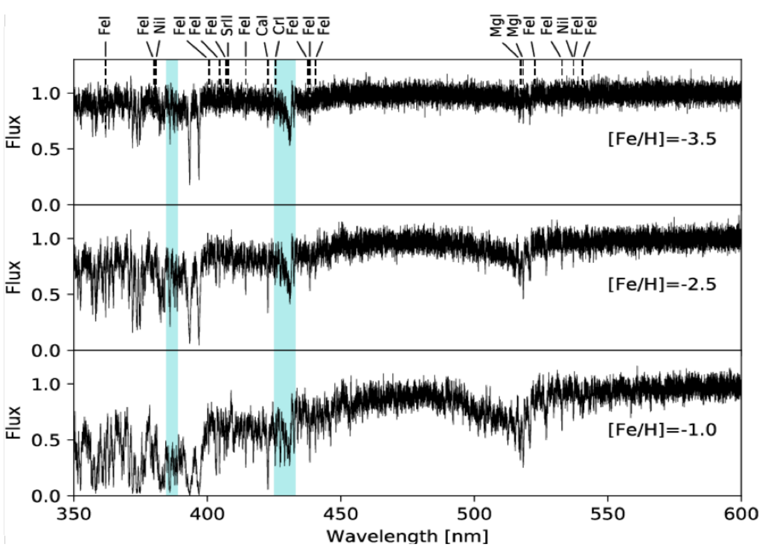

Figure 4: Example spectra of RGB stars at three different metallicities and for S/N=20 at BlueMUSE's spectral resolution. The chemical elements and molecular bands (in blue), which are accessible at this resolution and S/N, are indicated above the top spectrum. Image credit: Pascale Jablonka, private communication.

Why is BlueMUSE needed? The typical velocity dispersion of UFDs is of the order of a few $\mathrm{km\,s^{-1}}$. While MUSE itself can be used to determine velocities of individual stars, the velocity uncertainties with BlueMUSE will be at least a factor of two smaller, given its higher spectral resolution. This is critical as the membership of the stars within a dwarf is determined in a statistical way based on the radial velocities, and, crucially, their uncertainties.

In the most metal poor systems the rich set of absorption lines in the blue wavelength range will allow measurement of radial velocities in stars that are not accessible within the MUSE wavelength range. Currently, only about 1/3 of the stars extracted from MUSE FoV can be used for radial velocity measurements (e.g. Zoutendijk et al., 2020) due to their low metallicities and the lack of absorption lines in the red part of the optical spectrum. Since many spectral features lie at wavelengths < 5000 Å, a good sampling of this range is essential for stellar abundance determinations, as already mentioned in §2.1. At low metallicities, [Fe/H] < -2, the red part of the stellar spectrum has relatively little information, while, as shown on Fig. 4, the blue part is still rich in spectral features including important molecular bands such as CN and CH.

In order to unveil the modes of star formation in UFDs and the extent of their chemical evolution, it is mandatory to accurately determine the atmospheric parameters (effective temperature, gravity, [Fe/H]) of a large sample of stars, as well as their chemical patterns (e.g., abundances in α, iron-peak, neutron capture elements etc...), their mean values and their dispersion. In that respect, BlueMUSE will open-up an entire new region of parameter space, allowing much better constraints, although analysis methods must also be improved as the spectral resolution is lower than is usually used for these studies. In addition, BlueMUSE will provide large samples of secure member stars which allows for efficient follow-up with higher resolution spectrographs, for example to measure the abundances of neutron capture elements, which are both constraining the galaxy chemical evolution path and the nucleosynthesis origin of the r-process (e.g., Ji et al. 2016). Revisiting known (i.e. already observed with MUSE) and studying new UFDs, to be discovered by the upcoming imaging surveys (e.g. Euclid, LSST, Rubin), with BlueMUSE is a prospective way to solve some of the basic problems related to the formation and evolution of galaxies.

TLR	Value	Comment
Wavelength range	380 - 580 nm	goal 350 nm
Spectral resolution	>3500	on average
Field-of-View	> 1 arcmin^2	goal 2 arcmin^2
Sensitivity	r=24.5 mag within 5h	
Spatial sampling	$0.2'' <$ spaxel $< 0.3''$	sample seeing with ~ 2 spaxels
Spectral sampling	> 2 pixels	
Image quality	natural seeing	
Stability	0.1 pixels	

Table 5: TLR for the science case: ultra-faint dwarf galaxies

Derived TLRs for the science case: ultra faint dwarf galaxies. To efficiently map UFDs one needs a panoramic IFS, of a medium spectral resolution with wavelength coverage blue-ward of 5000 Å. For the estimation of stellar abundances and in particular the detection of unique enrichment episodes, it is essential to have wavelength coverage to 3500 Å (Bland-Hawthorn and Freeman, 2004). BlueMUSE will also allow to reach r=24.5 in a respectable ~ 5 hours. While UFDs are relatively large on the sky, mild mosaicking (i.e. two FoVs) will suffice and allow an efficient survey of any sample of newly discovered UFDs. A summary of TLRs for this science case is presented in Table 5.

2.5 Comets and the Solar System bodies

Comets are pristine relics of the protoplanetary disk where the planets formed and evolved, and preserve in their nuclei important clues about the early solar nebula. One of the main questions to answer about comets is the physical origin of the radicals (CN, C_2, C_3) in particular their locus of production within comets. Ground-based observations of comets can only detect the coma, not the nucleus. However, the nucleus strongly influences the morphology of the coma via processes such as nucleus rotation, obliquity, and active regions on its surface. Mapping the coma morphology using an integral-field spectrograph allows us to study the underlying processes that shape the coma and set constraints on the properties of the nucleus, the fundamental truth we are seeking.

To uncover the origin of radicals (CN, C_2, C_3) observed at optical wavelengths in the coma of comets, one needs to study species parentage. It is a complex problem, as some radicals can have several possible parents or be released by different mechanisms, which are not easy to identify. However, a better understanding of those mechanisms is crucial to link optical observations of comets to nucleus ice abundances. Mapping the coma morphology, using an IFS, and comparing the spatial distribution of the gas and the dust, allows us to study the underlying processes that shape the coma and produce radicals such as CN, C_2 or C_3 and also to set constraints on the properties of the nucleus.

In addition to comets from our own solar system, an IFS such as BlueMUSE will offer unique opportunities for the observation of interstellar objects (ISOs), which formed in other planetary systems and are crossing through our own solar system. Observations of these interstellar comets with a sensitive IFS will allow characterisation of their composition and a potential discovery of new emission-lines from elements not detected in solar system comets. Compared to what is known about the composition of solar system comets, studying ISOs will bring invaluable information on the formation conditions of planetesimals in other planetary systems. In general, panoramic IFS allow us map the morphology of gaseous species in the coma of the outgassing object to study the underlying processes that shape it, and set constraints on the intrinsic properties and composition of the nucleus, as well as the processes governing the release mechanisms of radicals in the coma.

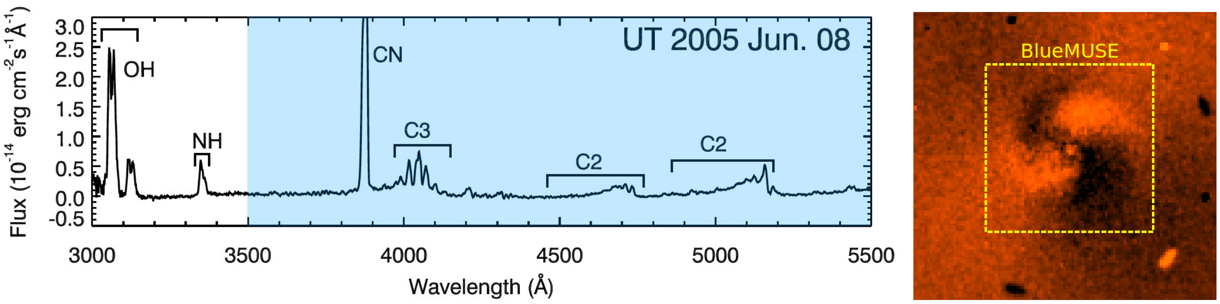

Figure 5: (Left) typical coma spectrum of comet 9P/Tempel 1, as observed at a distance of 1 AU (Meech et al., 2011). The BlueMUSE coverage (blue-shaded region) covers multiple radicals like CN, C_2 and C_3 including several groups of transitions. (Right) Example of morphology expected in the central region of the coma within the BlueMUSE FoV (as seen in comet Lemmon, Opitom et al. 2015). Spiral structures like this one can be observed depending on the activity, the orientation and the geometry of the observation.

Why is BlueMUSE needed? The wavelength range of BlueMUSE allows for a simultaneous coverage at $350 < \lambda < 500$ nm of multiple radicals (Fig. 5, left). In particular, in the CN (388nm), C_2 (517 nm), C_3 (405 nm) group, as well as N2+ (391 nm) and CO+ (400 and 425 nm), while NH (around 335 nm) would be a useful goal, many transitions that can be studied individually in a single IFS observation over a large spatial scale, which is impossible to do efficiently with narrow-band filters or long-slit spectroscopy (e.g., Dorman, Pierce, and Cochran 2013). In addition, observations with an IFS (e.g., Vaughan, Pierce, and Cochran 2017) allow to simultaneously study several gas species and the dust without any concern about the effects of rotation (typically a few hours). Observing these radicals with BlueMUSE allows us to gain in-depth insight into the production mechanisms of species in the coma of comets, as well as their activity. Large spatial structures are expected over the BlueMUSE field-of-view based on current narrow-band observations, such as spiral-like structures (Fig. 5, right). One of the hypotheses that can be directly tested with BlueMUSE is whether dust grains could be a source of production for the CN. In this context BlueMUSE can uniquely help in mapping gaseous emission bands of abundant species in comets (or any solar system body that is gassing out) as well as colours scattered by the dust, allowing detailed studies of the spatially resolved physical properties of these objects.

Derived TLRs for the science case:comets and the Solar Systems bodies. The coma's extended nature makes large field of view IFS crucial for studying the physical and chemical properties of cometary comae. Cometary lines are very narrow, but high spectral resolution of ∼3500 like that of BlueMUSE is sufficient to study the spatial distribution of gaseous species. The main spectral features are found in the blue part of the spectrum down to the UV region, but the spectral region accessible from the ground and covered by BlueMUSE covers the species of importance. A summary of TLRs for this science case is presented in Table 6.

TLR	Value	Comment
Wavelength range	350 - 520 nm	goal 335 nm
Spectral resolution	≥ 1000	
Field-of-View	≥ 1 arcmin^2	
Sensitivity		
Spatial sampling	$0.2'' <$ spaxel $< 0.3''$	
Spectral sampling	> 2 pixels	
Image quality	natural seeing	
Stability	0.1 pixel	

Table 6: TLR for the science case: comets and Solar System bodies

3 Science cases - Nearby galaxies

While MUSE has made an incredible leap forward for star formation and feedback over the entire spectrum of star-forming galaxies accessible in the local Universe (Erroz-Ferrer et al. 2019; Kreckel et al. 2019; Sánchez-Menguiano et al. 2020; Emsellem et al. 2022), BlueMUSE will provide critical information for determining the properties of the ISM, H II regions, stellar populations and kinematics, young and old stellar clusters in all kind of star-forming galaxies, as well as intergroup stellar and gaseous distributions. Some of the unique science cases for BlueMUSE are listed below.

- Observations of nearby low-metallicity (extreme) starburst galaxies. These systems offer an opportunity to study galaxy formation under conditions similar to those of the first galaxies. Such galaxies contain rare massive stars, are likely to host superluminous supernovae (hypernovae), have "porous" ISM which enhances the escape of Lyα and Ly continuum radiation, and they enable studies of star formation and its feedback effects, including outflows and the enrichment of the IGM. In these respects, these galaxies are close analogues of the faint galaxies in high-z surveys, that dominate the star formation budget. Observations of massive stars, including the Wolf-Rayet populations, fundamental for the production of ionising radiation, will be fundamental to address the stochastic sampling of the IMF, a topic that has major repercussions to all fields dealing with SFR tracers based on H emission lines.

- Study of H II regions and diffuse interstellar gas properties (temperature, densities, metallicities, optical thickness) by using critical lines like [O II] $\lambda\lambda$3726,3729 and [O III] $\lambda\lambda$4363,4959,5007 will enable BlueMUSE to provide a new view on the interstellar medium (ISM) in general. Previous studies have revealed a pervasive turbulent nature of the ISM, but the physical mechanisms for its creation are not understood. This is fundamentally linked to gas flows in galaxies. For example, metallicity variations at galactic scales are fundamental to understand time scales for gas inflow and gas mixing. With BlueMUSE observations, the determination of the supersonic gas motions and their spatial distributions within galaxies will fall for the first time within capabilities of an IFS.

- Given the faintness of the low surface brightness galaxies (LSB) it is not surprising that, while they might comprise up to 50% of local galaxies, their general properties, nature and origin are still poorly known. We still need to understand what is the shape of their luminosity function and how it combines with the general luminosity function of z=0 galaxies. LSB galaxies are sources of star formation in a low density regime, which might be reflected in the initial mass function. The stars or emission-line gas in the LSB galaxies are likely to move almost exclusively under the gravitational influence of the dark matter, and therefore these galaxies are excellent probes of dark matter models, as well as modified gravity theories. This science case focuses on the census of the star formation and dynamical properties of LSB, as probes of galaxy evolution.

- The environment plays a major role in shaping galaxies and determining their subsequent evolution. The range of possible physical processes that operate is large, but we are missing a clear picture about which process is dominating a certain type of transformation. Moreover, while it is clear that the processes can be, broadly speaking, either linked to the gravitational perturbations or to hydrodynamical interactions (for example of the cold ISM and warm IGM), their relevance with respect to the environmental density, galaxy (stellar) mass and the interaction epoch (local or intermediate redshift universe) remains a major challenge to our understanding.

- PNe are versatile probes of the distance, kinematics and stellar populations in nearby galaxies. MUSE observations demonstrated that PNe luminosity function can be used to distance of 40 Mpc, overlapping with the second rung of the distance ladder, and offering an possibility of an independent probe of the Hubble constant. Furthermore, the relative number of PNe per stellar mass of the underlying population can be an interesting probe for post-RGB evolution, especially at the high metallicities found in the cores of ellipticals. The challenge is to find PNe against the high continuum in sufficient numbers. While PNe are detectable in large numbers at larger radius in MUSE observations, galaxy cores remain challenging, which can be directly addressed using high spectral resolution of BlueMUSE.

- Detailed dynamical studies of stars in present-day galaxies provide a fossil record of their individual assembly history. In particular the high-order kinematic moments, i.e. the skewness and kurtosis of the line-of-sight velocity distribution, reveal complex stellar orbital structures that go undetected when measuring the velocity and velocity dispersion alone. High-order kinematic measurement will be crucial for revealing the dynamical properties of low-mass spirals and spheroidals ($\log M_*/M_\odot < 9.5$) that break away from fundamental galaxy scaling relations. High-precision measurements of the stellar orbits in galactic disks are required to understand how minor mergers impact the formation and evolution of galaxy structure, which can be used also to place our Milky Way in a cosmological context.

As discussed in Section 2.2, dust can have a significant influence on the observations at blue wavelengths. This is shared with most science cases in this section, where the foreground extinction or extinction within the targets can influence the observational results. An exception is the Key Science Case (Section 3.1) targeting low-metallicity galaxies, which are not expected to suffer from heavy extinction. In other science cases, the effects of dust can be mitigted by a careful sample selection (e.g. dust free galaxies), targeting regions that are less dusty (e.g. outskirts of disks) or by relaying on the large FoV that can cover a substantial region and obtain a statistical sample of dust free nebulae. Crucially, these approaches do not introduce an observational bias with respect to the physical properties that the science cases are targeting (e.g. stellar kinematics, distance, stellar populations properties, etc). Even if dusty systems are being targeted with BlueMUSE, it can be used in synergy with instruments at other wavelengths, also beyond the optical range, where BlueMUSE would provide a more shallow ("higher") view above the dust clouds of embedded regions.

3.1 Key science case: ISM and HII regions in extreme starbursts

Low-metallicity starburst galaxies (blue compact dwarf galaxies - BCDs) provide a unique window in our understanding of galaxy formation, and fulfil several specific and irreplaceable roles in extragalactic astronomy and cosmology. They offer a unique opportunity to study galaxy formation under conditions approaching those of the first galaxies, prior to and during the epoch of reionisation (EoR). They: (1) are ideal laboratories in which to study at low intrinsic extinction the most rare, massive and extreme stars (Crowther and Bibby, 2009; Kehrig et al., 2015); (2) enable detailed studies of collective star formation and the associated feedback processes in the least chemically evolved local environments known (Kunth and Östlin, 2000; James et al., 2015); (3) are likely the sites of super-luminous supernova/hypernova explosions (Leloudas et al., 2015) and long-duration GRBs (Hashimoto et al., 2015); (4) have shallow gravitational potential wells which provide less resistance to galactic outflows, enabling material that is heated by the star formation process to escape into the galactic halo and beyond and enrich the intergalactic medium with metals. Additionally, chemical abundance patterns in BCDs (Roy and Kunth, 1995) can place valuable constraints on the timescales for dispersal and mixing of heavy elements in protogalaxies. (5) They may have more porous/disrupted ISM, which enhances the escape of Lyα radiation and ionising continua. They thereby allow us to understand how similar galaxies at high-redshift leak ionising photons, reionise the Universe, and maintain the meta-galactic ionising background; (6) they may be the closest analogues of some of the faint galaxies identified in high-z surveys, that dominate the star-formation budget at early times; and finally (7) several lines of evidence suggest that some of the most metal-poor – 12+log(O/H)<7.6 – local BCDs have experienced the dominant phase of their build-up at a late cosmic epoch. For this reason, they are convenient laboratories to explore the main processes driving dwarf galaxy formation, as long as their morphological and dynamical relics have not had time to be erased in the course of secular galactic evolution (Papaderos et al., 2008). For instance, some of these systems show a cometary morphology that might result from unidirectional star formation propagation, but other BCDs are clearly showing features of interactions and minor mergers (e.g. López-Sánchez 2010).

Observations of the interstellar medium (ISM) in the Milky Way and nearby galaxies have revealed supersonic gas velocity dispersions ($\sim 10-30$ km/s) in the ionized gas component, highlighting the pervasive role of turbulent motions (e.g. Krumholz and Burkhart, 2016). Turbulence appears even more significant at high redshifts, where galaxies display a shift in the balance between ordered and random motions. While rotationally dominated systems are observed up to at least redshift 2 and beyond (e.g. Lelli et al., 2023), the relative contribution of turbulence to the dynamical support of galaxies increases at earlier epochs (Übler et al., 2019). This evolution in velocity dispersion correlates with changes in several physical properties of galaxies, particularly those related to star formation and gas content. However, the physical mechanisms regulating turbulence in the ISM remain unclear. Two scenarios are typically considered, one relating to the stellar feedback which injects sufficient momentum to sustain the turbulence and another considering the release of the gravitational potential energy from radial inflows of gas through galactic disk. The balance between these two scenarios and their ability to explain galaxy properties across the Hubble time remains unresolved. A significant limitation of current studies is that most of what we know about turbulence in the ionised ISM comes from optical spectroscopic observations with spectral resolutions lower than required to probe the expected emission-line broadening. To advance our understanding of turbulence in nearby galaxies, it is essential to trace velocity dispersions at the ~ 15 km/s level.

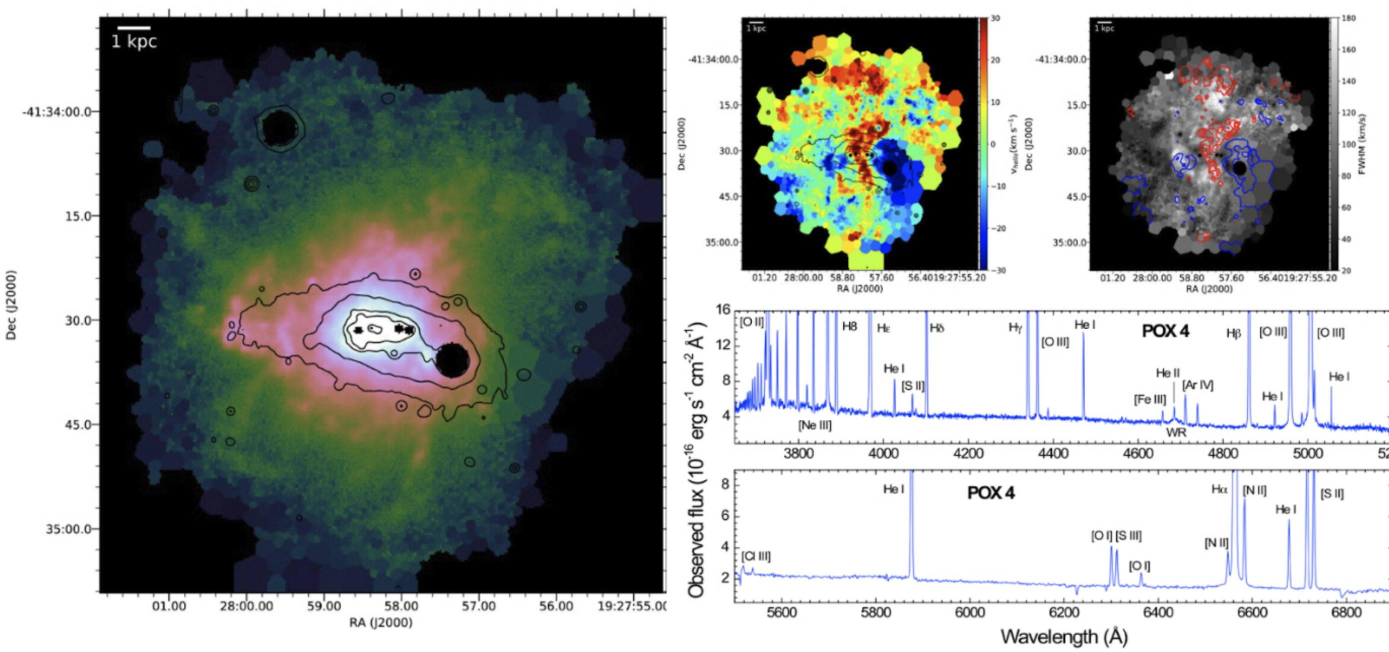

Figure 6: *Left*: MUSE Hα map of the local starburst galaxy ESO338-IG04, the nearest analogue of typical Lyman break galaxies at $z \gtrsim 2$. *Top right*: the derived velocity (left and velocity dispersion map (right) (Bik et al., 2018). Red and blue contours on the velocity dispersion maps show the gas velocities from the left map, receding and approaching motion, respectively. *Bottom right*: Blue and visual spectrum of the local starburst galaxy Pox 4 showing the rich emission-line spectrum expected for BlueMUSE observations of such systems (López-Sánchez and Esteban, 2009).

Why is BlueMUSE needed? Spatially resolved spectral synthesis studies of BlueMUSE data will offer a tremendous potential for reconstructing the assembly history of star forming galaxies and shedding light into the regulatory role of feedback produced by kpc-scale (or even down to a few pcs in the Local Volume) intense starburst episodes. In contrast to objects at $z \sim 2$ and beyond, such local starbursts can be studied in enormous detail and the physical properties determined exhaustively (Fig. 6). Most importantly is how feedback – both radiative and mechanical – from star-formation heats and disrupts the interstellar and circumgalactic gas, and how large-scale, enriched galaxy winds develop and evolve. In order to measure the thermal and kinetic energy in the gas phase we need accurate mapping of temperature and density to derive pressures, accurate masses, and ionisation states, and well-resolved lines to identify individual kinematic components of gas and measure the turbulent broadening. The goal is to reach velocity dispersions of ~ 30 km/s and characterise the full-width half-maximum (FWHM) of the line-spread function (LSF) of the spectrograph with an accuracy of a couple of percents. This capability should enable studies to probe dispersions at ~ 15 km/s or better allowing us to trace the dispersion of [O III] and Hβ emission-lines even in cold disks. Therefore, needed are the medium high-resolution optical spectroscopy, mainly focused at the blue end of the spectrum (covering key features such as [O II]$\lambda\lambda$3726,3729 and [O III]λ4363; Fig. 6), and a large FoV in order to capture the whole extended gaseous haloes. These parameters are offered by BlueMUSE, which will consequently be able to provide critical insights into the local physical drivers of turbulence in the ionized phases of the ISM and characterise the processes driving starburst phenomena.

Derived TLRs for the science case: physical properties of resolved nebulae. Characterising the physical processes (e.g. kinematics of emission-line gas, and accurate mapping of temperature, density, accurate masses and ionisation states), we need moderately high-resolution optical spectroscopy, in particular covering lines such as [O II]$\lambda\lambda$3726,3729 and [O III] λ4363. Large FoV is needed to encompass the full system, while relatively moderate spatial resolution is necessary to differentiate between SF regions and the diffuse ionised gas laying in between. A summary of TLRs for this science case is presented in Table 7.

TLR	Value	Comment
Wavelength range	350 - 580 nm	
Spectral resolution	3000	goal 4000
Field-of-View	≥ 1 arcmin^2	
Sensitivity	SN=5 for 5.41×10^{-18} ergs/s/cm^2/Å	[OII]3727, within 1h on source
Spatial sampling	$0.2'' <$ spaxel $< 0.3''$	sample seeing with ~ 2 spaxels
Spectral sampling	> 2 pixels	
Image quality	natural seeing	
Stability	0.1 pixels	

Table 7: TLR for the Key science case: ISM and HII regions in extreme sarbursts

3.2 Low surface brightness galaxies

Low Surface Brightness galaxies (LSBs) could represent a large fraction of local galaxies, up to 50% according to O'Neil and Bothun (2000). Despite this large fraction, their nature and origin have remained unknown: are they large spin disks (e.g., Boissier et al. 2003; Boissier et al. 2016) for instance, or the results of head-on collisions (Mapelli et al., 2008). Their exceedingly low surface brightness has been hindering in-depth studies (and in particular spectroscopy) of this important population, from which we could obtain a census, on crucial scientific questions. (1) A good constraint on the shape of the luminosity function of local galaxies can only be reached by taking into account the LSBs (Blanton et al., 2005). (2) LSBs bring crucial elements to understand the dark matter nature since they may be dark matter-dominated (Pickering et al., 1997). (3) LSBs allow the study of star formation in the low density regime, for which many issues are still debated such as lower efficiency, threshold, IMF variations, etc. This is directly comparable to the issues found in the discovered phenomenon of XUV galaxies (Gil de Paz et al., 2005; Thilker et al., 2007), with extended diffuse disks found around otherwise "normal" galaxies (see also Hagen et al. 2016). The study of LSBs and the star formation in their extended disks is thus of paramount importance for understanding galaxy evolution.

A full census of star formation regions, and a better determination of the dynamics in LSBs clearly call for large-IFU observations. Recent observation of Malin 1 (Fig. 7), a representative LSB, revealed strong Hα emission across numerous regions throughout the extended disk, but also a steep decline in star formation rate surface density (Junais et al., 2024). Malin 1 has a steep negative gas metallicity gradient, but the metallicity in the outer disk flattens and stays relatively constant at 0.6 $Z_{\odot}$, suggesting that the gas is not primordial. Furthermore, in comparison with other disk galaxies (Sánchez et al., 2014), the metallicity gradient in the outer disk of Malin 1 is an extreme, suggesting an existence of a particular mode of star formation at relatively low densities. BlueMUSE will allow key observations of many emission-lines that are of utmost importance to understand the nature and origin of gas and star formation in such galaxies. Oxygen lines will be used to determine the metallicity of the extended disk (e.g. Bresolin, Kennicutt, and Ryan-Weber, 2012; López-Sánchez et al., 2015), which will allow us to probe different formation scenarios of LSBs.

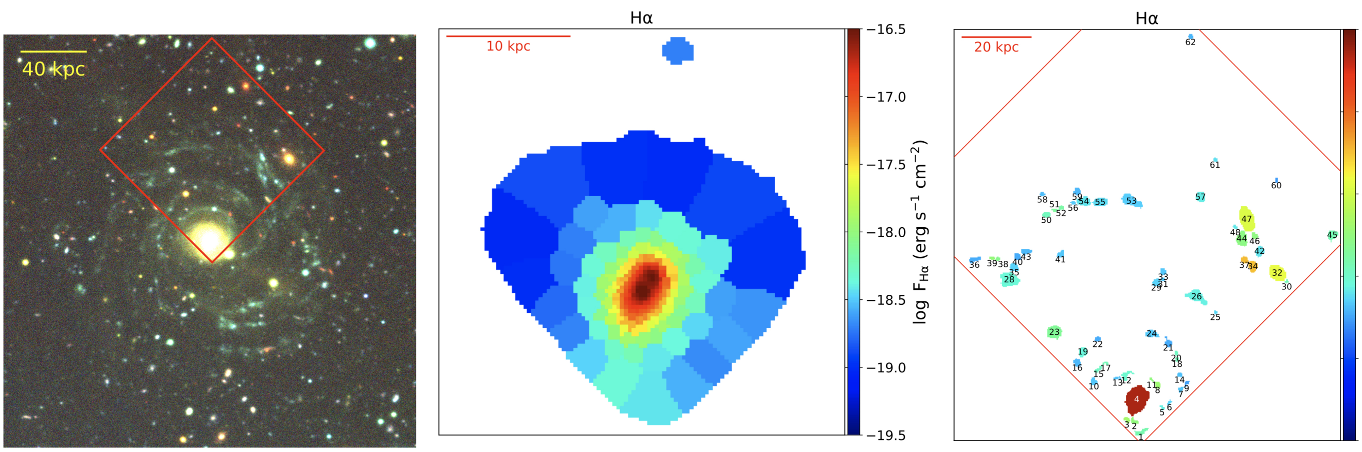

Figure 7: (Left) A composite image of Malin 1 with an over-plotted MUSE pointing. The image was obtained with Canda-French-Hawaii Telescope MegaCam NGCS survey (Ferrarese et al., 2012) and it is a composite of $u-$, $g-$ and $i-$band mages. (Middle): Emission-line flux map of the central region of Malin 1. (Right): Emission/line flux map of HII regions in Malin 1 covered by MUSE FoV. All panels are taken from Junais et al. (2024). BlueMUSE is expected to obtain a S/N = 5 for an extended emission equivalent of 26 mag/$''^2$ (or log $F_{[\mathrm{O\,II}]}$ (erg/s/m^2/Å/arcsec^2) = -18.5) in about 6h on source integration within modest $2 \times 2''$ apertures (based on BlueMUSE ETC).

The true nature of extended LSB galaxies, known as "Ultra-diffuse galaxies (UDGs)" (e.g. van Dokkum et al. 2018; Trujillo et al. 2019) is highly uncertain: they could be inflated regular dwarfs, tidally stripped satellites, tidal dwarf galaxies, or failed massive galaxies. The lack of information on the age and metallicity of their stellar populations, as well as on the kinematics of both the gaseous and stellar components, prevents us from having a definitive answer.

Why is BlueMUSE needed? BlueMUSE will be ideal to investigate the origin and structural properties of UDGs, giving simultaneous information on the diffuse stellar populations and associated globular clusters. BlueMUSE will revolutionise the study of LSBs and UDGs because, its wavelength coverage will provide the detections of age and metallicity indicator lines such as [O II]$\lambda\lambda$3727, only reachable in the blue, as well as Balmer absorption lines and Hβ emission allowing to probe the star formation history and activity of these galaxies. BlueMUSE, with its medium-high spectral resolution (with respect to MUSE), will allow us to determine the rotation curve of the star-forming gas-rich LSB galaxies and/or the dynamics of the globular cluster populations, together with the velocity dispersion of the diffuse stellar populations, thus testing previous hints on the DM content. Finally, its large FoV is well suited to the size of LSB/UDGs (e.g. Fig. 7) and the distribution of globular clusters.

Derived TLRs for the science case: physical properties of resolved nebulae. LSB galaxies are relatively large in the sky, making BlueMUSE an ideal instrument for efficiently investigating their properties. Investigating their stellar populations, ages and metallicities are strongly dependent on the [O II]$\lambda\lambda$3726,3729 and Balmer lines bluer than Hβ, together with a moderately high spectral resolution. Relatively high spatial resolution is necessary to be able to probe the inner (rising) part of the rotation curves to probe the central distribution of matter (e.g.

used to differentiate between the dark matter models). The main targets are the emission-lines, with similar properties as in § 3.1, but an attempt should be made at the stellar light. A summary of TLRs for this science case is presented in Table 8.

TLR	Value	Comment
Wavelength range	350 - 580 nm	
Spectral resolution	3000	
Field-of-View	≥ 1 arcmin^2	
Sensitivity	SN=5 for 26 mag/arcsec^2	for 6h (10x7 spatial and 2 spectral pixels binning)
Spatial sampling	$0.2'' <$ spaxel $< 0.3''$	sample seeing with ~ 2 spaxels
Spectral sampling	> 2 pixels	
Image quality	natural seeing	
Stability	0.1 pixels	

Table 8: TLR for the science case: low surface brightness galaxies

3.3 Environmental effects in local galaxy clusters

In the last decade it became increasingly clear that the environment plays a major role in shaping galaxy evolution (e.g. Peng et al. 2010). High-density regions are characterised by a large fraction of gas-poor, pressure-supported, quiescent objects compared to star forming, disk-like, rotating systems dominating the field. Different mechanisms have been proposed to explain the different evolution of galaxies in high-density regions which can be broadly divided into two main families, i.e. the gravitational perturbations and the hydrodynamical interactions of the cold ISM with the surrounding IGM, whose density and temperature increase in high-density regions (Boselli and Gavazzi, 2006). The relevance of these mechanisms in regions of different density (from clusters to compact and loose groups), for galaxies of different stellar mass (from dwarfs to giants), and at different epochs (local and high-z universe) remains a major challenge for galaxy formation theories.

The presence of prominent Balmer absorption lines indicates a violent mechanism able to drastically reduce the activity of star formation on short timescales ($\lesssim 0.5$ Gyr, ram pressure stripping) while smoothly declining star formation histories (SFH) are expected in milder mechanisms such as starvation. BlueMUSE will allow us to spatially reconstruct the recent SFH of all kind of systems, including dwarf ellipticals in local clusters, where the VLT collecting area allows medium resolution spectroscopic observations of the low surface brightness extended stellar disc (see § 3.2). The observed spectrum can be fitted with state-of-the-art pixel fitting codes which allow to reconstruct the star formation history of perturbed systems (e.g. Cappellari and Emsellem, 2004; Boselli et al., 2016; Fossati et al., 2018; Cappellari, 2023). This will enable an accurate reconstruction of the quenching timescale as a function of position in a galaxy, enabling, for example, detailed modelling of outside-in stripping as the galaxy moves into the cluster. The same Balmer absorption lines, including other main absorption features such as Ca H & K, G-band, and Mg, and several emission lines can be used to trace the stellar and gas kinematics of perturbed galaxies, also critical in the identification of the perturbing mechanism.

Of additional interest are kinematical properties of the stellar component of galaxies in clusters. While more massive galaxies have been studied extensively (e.g. Cappellari et al., 2011; Fogarty et al., 2014; Graham et al., 2019), status of the stellar angular momentum of dEs remains an open question. In particular, whether they are mainly fast rotators, as expected whenever their star formation activity has been quenched after a mild interaction with the hot and dense intra-cluster medium emitting in X-rays, or rather by more violent gravitational interactions with other cluster members (e.g., Toloba et al. 2011). In this respect, compact groups of galaxies offer valuable examples of interactions between galaxies and with the cluster (group) medium filling the space between the galaxies (see Fig. 8). With a high throughput, BlueMUSE will be able to study the properties of the stellar populations and kinematics within group memebr galaxies, but also detect emission-line emitting material between galaxies, and provide properties of the intercluster/group stellar light (e.g. stellar populations or kinematics).

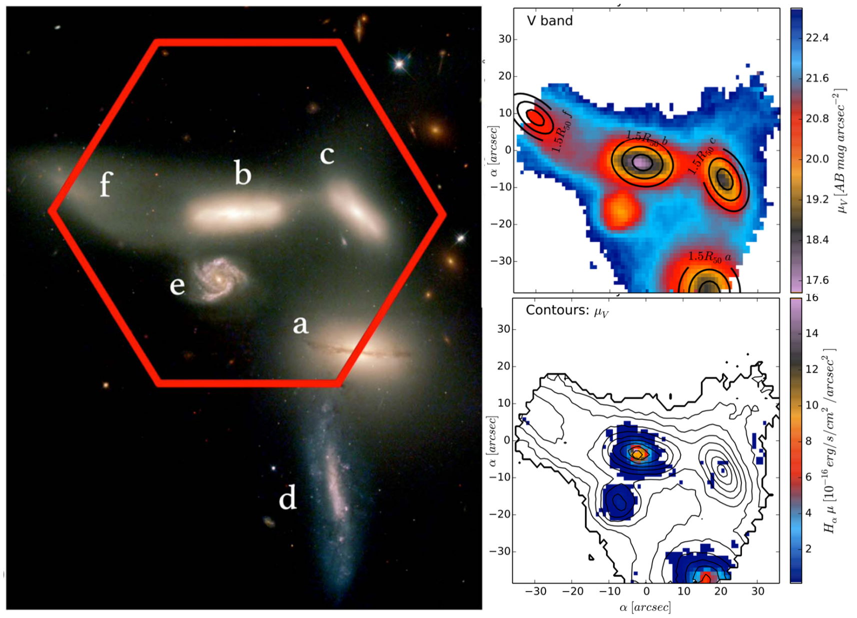

Figure 8: *Left*: An HST image of Seyfert Sextet compact group of galaxies with an overlay of the PPAK IFS, which has a similar size as BlueMUSE but covers the FoV with only 331 fiber spectra. *Right top*: continuum surface brightness achieved with PPAK within 0.75 hours on source exposure. *Bottom right*: surface brightness of the Hα emission within the same time. BlueMUSE is expected to reach 2 orders of magnitude fainter emission (and two magnitudes surface brightness level) within the same exposure time, allowing observation of the line emitting material between the galaxies. All panels are taken and adapted from López-Cruz et al. (2019).

Why is BlueMUSE needed? Integral-field spectroscopy with a large field of view on a 8-10 metre class telescope with a sufficient spectral resolution ($R \sim 3000$) in the blue spectral domain (350-580 nm) will offer a unique opportunity to unambiguously identify the dominant perturbing mechanisms in high-density regions. Indeed, this spectral range includes several age-sensitive Balmer absorption features inaccessible to MUSE which are crucial in the determination of the star formation histories and the quenching timescales, as well as [O II]$\lambda\lambda3726, 3729$ and [O III]$\lambda\lambda4363, 4959, 5007$, the most accurate indicators for density, temperature, and metallicity of the ionized gas. The high throughput of BlueMUSE will open a new observational window to search for the imprint of gravitational perturbations and merging episodes in low mass members of galaxy groups.

TLR	Value	Comment
Wavelength range	350 - 580 nm	
Spectral resolution	3000	
Field-of-View	≥ 1 arcmin^2	
Sensitivity	as for § 3.1 and 3.2	throughput of $> 30\%$
Spatial sampling	$0.2'' <$ spaxel $< 0.3''$	sample seeing with ~ 2 spaxels
Spectral sampling	> 2 pixels	
Image quality	natural seeing	
Stability	0.1 pixels	

Table 9: TLR for the science case: environmental effects in local galaxy clusters

Derived TLRs for the science case: physical properties of resolved nebulae. Probing the environment between galaxies in groups, and at the same time mapping the galaxies themselves is only possible with a panoramic IFS. The hope is that the inter-group environment is rich in ionised gas, which can be probed with emission-line diagnostics in the blue part of the optical spectrum. While observing the excited intra-galaxy gas, BlueMUSE will provide information of physical properties within galaxies. In particular, we want to look for the diagnostics of the possible quenching processes and of perturbing mechanisms. This will be done by investigating both gas (with-in and with-out galaxies) and stellar kinematics and star-formation histories. The necessary diagnostics are the [O II] and [O III] lines, Balmer lines, Ca H & K lines and the Mgb complex. As these are typically low mass galaxies, the stellar velocity dispersion is expected to be low, requiring a medium-high spectral resolution (comparable to § 3.1 and 3.2). A summary of TLRs for this science case is presented in Table 9.

3.4 Planetary nebulae as distance indicators and stellar population tracers

The Planetary Nebula Luminosity Function (PNLF) has been used as a distance indicator with a range of ~ 18 Mpc for more than 30 years (Jacoby, 1989) with the advantage over calibrators of the Hubble constant such as Cepheids, TRGB, SBF, JAGB that it is equally applicable to early-type and late-type galaxies. However, it has only been through the development of the MUSE-PNLF (Roth et al., 2023) that the range could be expanded out to 40 Mpc, to overlap with the 2nd rung of the distance ladder (Riess et al., 2022). It is thus capable to independently measure H_0 with galaxies outside of clusters and in the Hubble flow. The technique has been tested in a pilot study (Roth et al., 2018; Soemitro et al., 2023), technically developed and tested with three benchmark galaxies (Roth et al., 2021), and a proof-of-principle presented on the basis of archival data for 20 galaxies (Jacoby et al., 2024). Of that latter study, Fig. 9 illustrates how from two of the more distant galaxies a value of $H_0 = 74.2 \pm 7.2$ km/s/Mpc was derived, limited by less than ideal calibrations of the data taken for another purpose. Targeted BlueMUSE-PNLF observations will come with uncertainties comparable to the ones of Cepheids. Furthermore, recent progress with PNLF simulations based on stellar populations derived from cosmological models (Valenzuela et al., 2025), and empirical evidence for the universal invariance of the PNLF cut-off due to a self-regulating effect of circumstellar dust, based on the extinction – core mass relation (Jacoby & Ciardullo 2025, ApJ in press), provide physical evidence why the PNLF is indeed a precision standard candle.

Another source of extinction, directly affecting the ability of the PNLF as a distance estimator is the foreground dust, either from the galaxy in question or from the intervening medium. While the BlueMUSE (or MUSE, or even combined) wavelength can be used to derive the extinction, it is not possible to disentangle the contribution of the foreground from the intrinsic dust distribution. Therefore, observations of small areas in very dusty galaxies, where PNLF is limited to a low number of objects, can not yield reliable distance estimates (Jacoby et al., 2024). However, by mapping of larger areas (including outskirts) with a panoramic IFS, even of dusty spirals at low inclinations, should be able to provide accurate PNLFs. Crucial here is to be able to avoid the most obscure regions (e.g. NGC300 where the distance is in agreement with Cepheids or TRGB methods; Soemitro et al., 2023). Providing an independent distance indicator for the calibration of SN Ia distances can make a valuable contribution to the ongoing puzzle of the Hubble tension, but also the controversy about possible biases of classical calibrators.

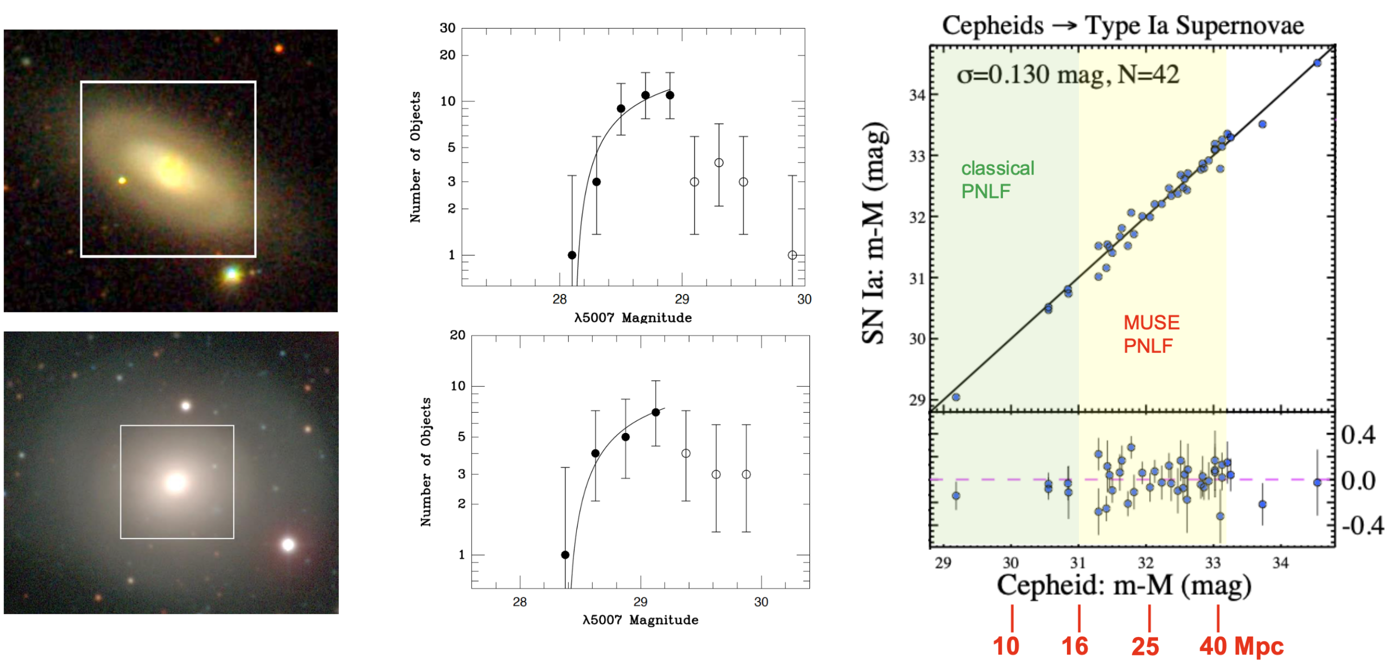

Figure 9: . Top: NGC 4418, D = 32.9 ± 1.3 Mpc determined from 24 PNe in top magnitude, exposure time of 6000 sec at 0.9″ seeing, H0 = 75.0 ± 9.6 km/s/Mpc. Bottom: NGC 6958, D = 36.2 ± 3.8 Mpc determined from 15 PNe in top magnitude, exposure time 1900 sec at 0.75″ seeing, H0 = 69.2 ± 11.0. The weighted average results in H0 = 74.2 ± 7.2. Right: these examples place the range of the MUSE-PNLF in the Cepheid regime of SN Ia calibrators (adapted from Riess et al., 2022). Obtained from less than ideal archival data by Jacoby et al. (2024).

The inner cores ($\lesssim$1 kpc) of massive elliptical galaxies harbour stellar populations that are of particular interest, as the likely descendants of very early starbursts now being unveiled by JWST. These regions have abundance patterns that are not found in the Milky Way (α and sodium enhancement at *high* metallicities), and peculiar spectral line strengths that seem to require a dwarf-rich IMF (e.g. Conroy and van Dokkum, 2012). Both the sodium enrichment and the IMF effects appear highly concentrated into the inner ~kpc (e.g. La Barbera et al., 2019). The detailed interpretation of integrated-light spectroscopy rests on the reliability and correctness of evolutionary models, which may not yet be assured in this metallicity/age regime.

The PN population provides an alternative window onto the evolved low-mass stellar content in elliptical galaxies, which is also intricately linked to the UV-excess light generated by hot/extreme HB stars (Buzzoni, Arnaboldi, and Corradi, 2006). Here the key observable is α_{PN}, the number of PNe (above some flux limit) generated per unit stellar mass or continuum luminosity. Some open possibilities for explaining the UV output include elevated helium abundance, which cannot be measured directly (e.g. Chung, Yoon, and Lee, 2011; Goudfrooij, 2018). Note that the high-temperature nucleosynthetic processes favouring sodium enhancement, which can be extreme in ellipticals, also tend generically to overproduce helium. Helium-rich stars evolve more rapidly, such that the initial masses of evolved stars at given age are smaller. Such stars are unlikely to ascend the AGB (affecting both M/L estimates and integrated-light spectra) or generate detectable PNe. A reliable measurement of α_{PN} in the cores of massive ellipticals would thus be relevant to several perplexing outstanding questions.

In NGC 3379 (distance ~11 Mpc), Hartke et al. (2023) found that the incidence of PN increases gently with radius in the galaxy halo, supporting a dependence on metallicity in the 5-30 kpc regime. In the inner kiloparsecs however, α_{PN} remains virtually unconstrained, due to the difficulty of detecting significant numbers of nebulae above the bright continuum light of the galaxy. MUSE has demonstrated the power of IFS observations to push much closer to the centre than the classical narrow-band imaging method, but BlueMUSE will exceed its capabilities significantly, thanks to its greater efficiency at 5000 Å and higher spectral resolution, which improves contrast over the continuum light.

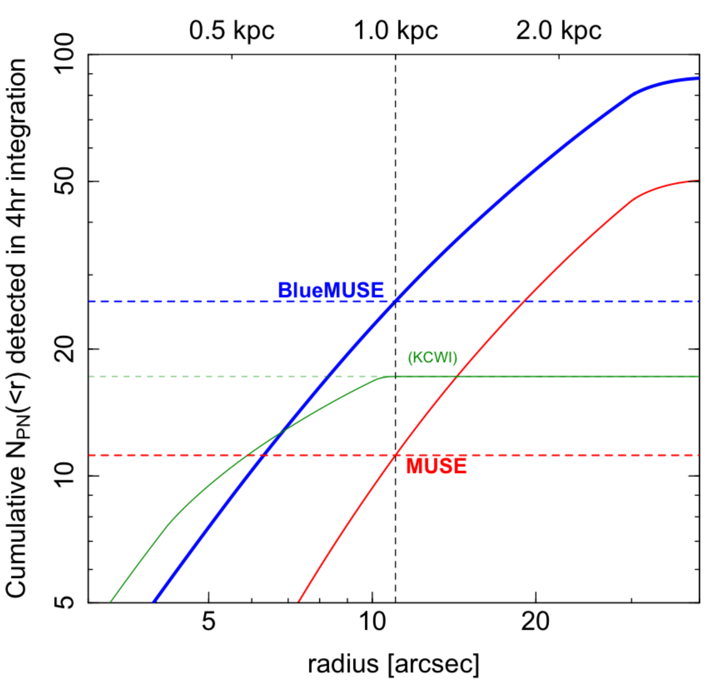

Figure 10: Comparison of predicted PN yield as function of radius for BlueMUSE (blue lines) versus MUSE (red lines) and KWCI (green lines). Assumed spectral resolution of BlueMUSE is R = 3500 at 500 nm. Horizontal dashed lines mark the number of PNe detected within 1 kpc, demonstrating the level to which BlueMUSE can over-perform other instruments.

Figure 10 shows a comparison between the expected yield of PNe from BlueMUSE observations for a massive elliptical galaxy at 18 Mpc. The calculations are based on the surface brightness profile of NGC 1404 in the Fornax cluster. We assume a constant specific incidence of PNe per unit continuum luminosity, distributed according to a standard PNLF. The PN limiting magnitude (for $S/N > 10$ in 4 hr total integration, with 20 min individual exposures, and 0.6 arcsec FWHM) is then computed as a function of continuum surface brightness, accounting for source, background and readout noise contributions. Considering PNe at radius <1 kpc, BlueMUSE (assumed

R=3500) outperforms existing MUSE (R=1750) by a factor of 2.3, due to its higher sensitivity and spectral resolution. The KCWI instrument on Keck can match the *sensitivity* of BlueMUSE, but yields fewer nebulae hour-for-hour, due to its much narrower field-of-view when configured suitably for PN detection (8×20 arcsec^2, with 0.35 arcsec slice-width and $\lambda/\Delta\lambda \approx 8000$). The MAVIS IFU mode will similarly be FoV-limited, as well as subject to large and uncertain aperture corrections from the AO-corrected PSF core. BlueMUSE will be unrivalled for such measurements.

Why is BlueMUSE needed? Effective mapping of large regions, including outskirts of dusty galaxies, crucially needed for derivation of PNLF, is possible with BlueMUSE. In addition, BlueMUSE provides two advances over MUSE to significantly enhance the precision and the distance range of PNLF measurements: (1) A factor of two or three smaller bandwidth per wavelength bin reduces the background continuum light by that factor, thus improving the completeness limit for the detection of more PNe in high surface brightness nuclei of galaxies, and (2) the efficiency of BlueMUSE is 27%, 50%, and 65% higher, respectively, than the one for MUSE at the wavelengths of [O III]λ5007, Hβ, and He IIλ4686. Other wavelengths such as [Ar IV]$\lambda\lambda$4711, 4740, [O III]λ4363, H$\gamma\lambda$4340, [Ne IV]λ4058, [Ne III]$\lambda\lambda$3967, 3869, He Iλ3888, and [O II]$\lambda\lambda$3727, 3729 are important plasma diagnostic lines that are needed to model the nebular emission and the central star mass, becoming accessible with BlueMUSE for the first time in more nearby galaxies beyond the Local Group (e.g., in the Sculptor group).

Derived TLRs for the science case: Planetary nebulae as distance indicators and stellar populations tracers. Key requirement for detecting PNe in the nuclei of ellipticals and disks is spectral resolution to enhance contrast against the continuum light. While there is no threshold that can not be overcome with longer exposures, significant gain over current capability would require $2-3\times$ the resolving power of MUSE. Nevertheless, the PNe emission will remain unresolved spectrally and, therefore, the continuum contrast is directly linked with detectability. Although mosaicking is a possibility, a large FoV would be advantageous to enhance the overall efficiency. Access to simultaneous guide star images as a science data product would strongly improve the accuracy of the photometry in terms of the PSF and derived aperture corrections, which are currently the major source of uncertainty with MUSE. A summary of TLRs for this science case is presented in Table 10.

TLR	Value	Comment
Wavelength range	350 - 580 nm	including [OIII] 495.5,500.7
Spectral resolution	> 3500	$2-3\times$ MUSE spectral resolution
Field-of-View	≥ 1 arcmin^2	
Sensitivity	3×10^{-18} erg/s/cm2 at 5000Å against galaxy continuum of 4×10^{-16} erg/s/cm2/A/arcsec2	S/N$\sim$ 5 achievable in 1h
Spatial sampling	$0.2'' <$ spaxel $< 0.3''$	sample seeing with ~ 2 spaxels
Spectral sampling	> 2 pixels	
Image quality	natural seeing	
Stability	0.1 pixels	

Table 10: TLR for the science case: planetary nebluae as distance indicators and stellar population tracers

3.5 Higher-order kinematics of cold stellar disks and dwarf galaxies

Detailed dynamical studies of stars in present-day galaxies provide a fossil record of their individual assembly history (de Zeeuw and Franx, 1991). The introduction of integral field spectroscopy has played a major role in developing a deeper understanding of the kinematic properties of the galaxy population as a whole (Emsellem et al., 2011; Cappellari, 2016; van de Sande et al., 2021b), revealing multiple kinematic sub-populations (e.g. fast and slow rotator galaxies). One of the most important discovery has been that for early-type galaxies, visual morphology can be misleading for predicting kinematic structure, with the majority of elliptical galaxies being classified as fast rotators (Emsellem et al., 2011; van de Sande et al., 2021a).

High-order kinematic moments, i.e. the skewness ($\sim h_3$) and kurtosis ($\sim h_4$) of the line-of-sight velocity distribution, reveal complex stellar orbital structures that go undetected when measuring the velocity and velocity dispersion alone (van der Marel and Franx, 1993; Gerhard, 1993; Krajnović et al., 2006; Krajnović et al., 2011; van de Sande et al., 2017). High-order kinematic measurements have been utilised to detect bars in edge-on galaxies (Chung and Bureau, 2004; Guérou et al., 2016; Fraser-McKelvie et al., 2024), distinguish between different merger pathways (Naab et al., 2014; van de Sande et al., 2017), and are essential parameters to constrain orbit-superposition Schwarzschild dynamical models (e.g. Poci et al., 2019; Santucci et al., 2022). However, relatively low spectral resolution of recent IFS has limited the application of high-order kinematics to the central regions of intermediate to high-mass galaxies ($\log(M_\star/M_\odot) > 10$; van de Sande et al., 2017).

In the last decade, two key areas have emerged where high-order kinematic measurements will be essential to provide a deeper understanding. First, recent results indicate that both low-mass ($\log(M_\star/M_\odot) < 9.5$) spirals and spheroidals have unusually low ratios of V/σ as compared to more massive galaxies (Falcón-Barroso et al., 2019; Scott et al., 2020). These galaxies break away from fundamental galaxy scaling relations (e.g., Faber-Jackson, $M_\star$-$S_{0.5}$; Barat et al., 2019; Barat et al., 2020), and the reason for their higher velocity dispersion remains unclear. High-order kinematic measurement will be crucial for revealing the origin of these galaxies, giving insight into the stellar orbital distribution and thereby its assembly history.

Secondly, Galactic archaeology surveys are currently revealing that the Milky Way's disk is shaped through minor collisions with satellite galaxies leaving measurable stellar kinematic signatures (Bland-Hawthorn et al., 2019; Xiang and Rix, 2022). To place our Milky Way in a cosmological context, high-precision measurements of the stellar orbits in galactic disks are required to understand how minor mergers impact the formation and evolution of galaxy structure. Recent high-spatial resolution observations of Milky Way-mass disk galaxies with VLT/MUSE (e.g. TIMER Gadotti et al. 2019; PHANGS Emsellem et al. 2022; GECKOS van de Sande et al. 2024) are starting, but MUSE's limiting spectral resolution has proven challenging for determining accurate high-order moments (Fraser-McKelvie et al., 2024).

Why is BlueMUSE needed? Determining the physical cause for low-mass galaxies to be outliers as well as understanding the impact of minor mergers on Milky Way-like disks is currently restricted by the limited spectral resolution of the largest IFS surveys (e.g., CALIFA Sánchez et al. 2012; SAMI Croom et al. 2012; MaNGA Bundy et al. 2015) as well as VLT/MUSE. High-order kinematic measurements require an instrumental spectral resolution that is greater than the measured velocity dispersion, but an $R \sim 2000 - 3000$ ($\sigma \sim 45 - 65$ km s$^-1$) limits us to higher mass galaxies $\log(M_\star/M_\odot) < 9.5$) and the inner regions of galaxies like our Milky Way. A high spatial resolution similar to MUSE is essential for resolving galaxy sub-kpc stellar structures in galaxies, such as nuclear disks and seperating the thin and thick disk in edge-on galaxies. Excellent througput is essential for detecting low surface brightness stellar continuum light in the outer disk in face-on galaxies and above the plane in edge-on galaxies.

TLR	Value	Comment
Wavelength range	375 - 575 nm	
Spectral resolution	4000	
Field-of-View	≥ 1 arcmin^2	
Sensitivity	SN=40; 23.5 mag/arcsec (g-band)^2	$10 \times 10 - 30 \times 30$ binning, 4.8h on source
Spatial sampling	$0.2'' <$ spaxel $< 0.3''$	sample seeing with ~ 2 spaxels
Spectral sampling	> 2 pixels	
Image quality	natural seeing	
Stability	0.1 pixel	

Table 11: TLR for the science case: Higher-order kinematics of cold stellar disks and dwarf galaxies

Derived TLRs for the science case: higher-order kinematics of cold stellar disks and dwarf galaxies. Understanding the complex kinematic structure of Milky Way-like disks and low-mass galaxies requires integral field spectroscopy, with a large-field of view, high throughput, and high spectral resolution. Specifically, the high-order kinematic measurements would benefit from the highest achievable spectral resolution (i.e., $R \sim 4000$, $\sigma \sim 30$ km/s), a Gaussian line spread function with its parameters known to 5% accuracy, over a wavelength region that contains the key stellar absorption lines (Hθ at 379.7 nm to Mgb at 517.7 nm). A summary of TLRs for this science case is presented in Table 11.

4 Science cases - The Distant Universe

Observations of deep extragalactic fields performed with MUSE (HDFS, Bacon et al. 2015; UDF, Bacon et al. 2017; CDFS, Urrutia et al. 2019; MUDF, Lusso et al. 2019; MXDF, Bacon et al. 2021) have demonstrated how a wide-field optical IFU is a game-changer for the study of distant galaxies. BlueMUSE has a similar potential, but also some advantages over MUSE due to its blue wavelength and higher spectral resolution. Here we outline several science cases that BlueMUSE will enable:

- A wide-field optical IFS producing high quality spectra for all sources within FoV at a high sensitivity to emission-lines is a game-changer for the study of distant galaxies. With its blue/UV spectral coverage BlueMUSE will be a complementary and even more powerful facility compared to MUSE in the study of deep extragalactic fields. The current MUSE redshift desert ($1.5 < z < 3$) will be largely filled down to z = 1.88, and the large population of [OII] emitters will be probed down to z = 0. In addition, the cosmological surface brightness dimming at $z \sim 2-3$ is a factor ~ 4 lower in comparison to $z \sim 3-5$ with MUSE, we therefore expect a similar gain in the ability of BlueMUSE to detect Lyα emission from diffuse gas around galaxies, which will allow us to detect emission from gas all the way out into the intergalactic medium

- Despite the impressive success of recent large-scale cosmological simulations at reproducing the bulk of galaxy properties across cosmic time, the fundamental questions about how galaxies acquire gas from the intergalactic medium, and how they regulate their growth through galactic winds or other pre-emptive processes, are mostly unconstrained from observations or theory. Observations with BlueMUSE in the redshift range $2 < z < 3$ will be key in constraining galaxy formation because they cover the peak of cosmic star formation. Among the factors that drive this turn-over in the cosmic SFR, we may expect a change in the form of accretion flows and their interactions with galactic winds, which marks the beginning of the transition from the early Universe – where cold and collimated gas flows onto galaxies, and the late Universe – where star formation is sustained by cooling-regulated accretion from hot coronae. Observing the evolution of the circum-galactic medium (CGM) through this epoch will be a key in discriminating between the various competing theoretical models.

- The nature of the first luminous sources responsible for reionising the predominantly neutral intergalactic medium remains so far totally unknown due to the increasing opacity of the intergalactic medium with redshift which renders direct Lyman continuum (LyC) detections impossible (or extremely inefficient) at $z > 4$. BlueMUSE will be able to directly probe the LyC from sources at $z \sim 3-5$ and it will allow for the first time to collect a statistical sample of LyC emitters as part of blind surveys. We expect most detections to fall in the redshift range $z = 3-4$ where Lyα can be used to assess the spectroscopic redshift, and where the IGM transmission remains reasonably high. We expect BlueMUSE to be particularly efficient at detecting the faintest population of $z \sim 3$ galaxies which are potentially strong leakers and may correspond to the analogues of the sources of reionisation.

- Through the observation of massive galaxy cluster cores, we can study gravitationally magnified low luminosity galaxies that would otherwise be undetectable. Compared to current MUSE studies, BlueMUSE will fill in the redshift space between $2 < z < 4$ increasing the number of background lensed sources. We expect a significant increase of giant arcs as we will be able to detect them a lower redshifts ($z \sim 2$). BlueMUSE will provide the unique opportunity to study the massive stellar content and the conditions of the ionised gas around these systems. Mapping a significant fraction of the surroundings of the critical lines with BlueMUSE has a potential of further improving the mass distribution models of the clusters.

- BlueMUSE appears as the best means to discover and characterise giant Lyα nebulae that now we know are widespread in the early generation of galaxy groups and clusters. The presence of such nebulae demonstrates that cold gas is co-existing with hot gas inside the deep potential well of these structures, but the origin, powering mechanism and fate of the cold gas is still unclear and a matter of debate. BlueMUSE will uniquely allow us to discover Lyα emitting nebulae in the first generation of forming clusters including the critical redshift range $z = 1.8 - 3$ where we expect cold accretion to massive haloes to peak.

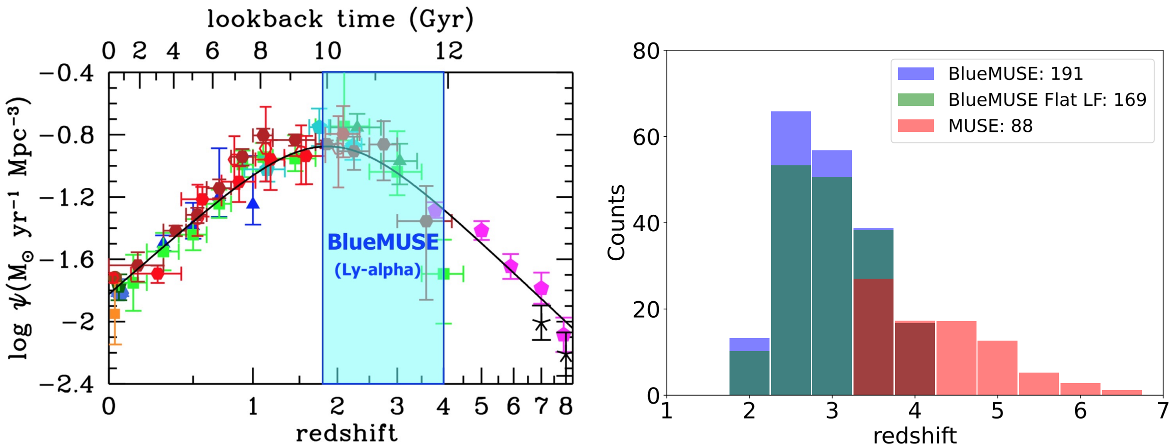

Figure 11: (Left) Evolution of the cosmic SFR (from Madau and Dickinson 2014) and redshift range probed in Lyman-α with BlueMUSE. (Right) Estimated LAE counts as function of redshift for a single BlueMUSE 10 hrs depth exposure (in blue) and a 5σ detection limit. In green the LAE number counts is shown when the LAE luminosity function is assumed to flatten below $10^{41.2}$ erg s^{-1}. MUSE counts (in red) for the same depth and SNR limit, is given for comparison.

4.1 Deep fields

Two features of MUSE instrument stand out to explain its impact in observations of deep extragalactic fields. First, MUSE provides a *comprehensive spectroscopic view of the sky*, i.e. high quality spectra for all sources in the FoV with no prior selection. This approach has produced an order of magnitude increase in the number of spectroscopic redshifts measured in these deep fields (Herenz et al., 2017; Inami et al., 2017). The second feature, which really makes MUSE a transformative instrument, is its *unprecedented and unique sensitivity to emission lines*. This has led to an impressive revision of the census of distant star-forming galaxies (e.g. Maseda et al. 2018). Perhaps uniquely, this ability to detect line emission has led MUSE to open a new window on the physics of the CGM, and there exists no rival technique. With its blue spectral coverage and large FoV, BlueMUSE will be a complementary and even more powerful facility. The current MUSE redshift desert ($1.5 < z < 3$, corresponding to the redshift of [O II] emitters at the red end and of Lyα emitters (LAEs) at the blue end) will be largely filled down to $z = 1.88$, and the large population of [O II] emitters will be probed down to $z = 0$. BlueMUSE will observe LAEs and their CGM in the $1.9 < z < 3.8$ redshift range. Extrapolating from current Deep-Field numbers, we expect to find 191 LAEs for a single 10-hour pointing, that is 2.2 times larger than MUSE observations at the same depth in the UDF (88 LAEs, Bacon et al. 2017, see right panel of Fig. 11).

The cosmological surface brightness dimming at $z \sim 2 - 3$ is a factor ~ 4 lower in comparison to $z \sim 3 - 5$ with MUSE, we therefore expect a similar gain in the ability of BlueMUSE to detect Lyman-α emission from diffuse gas around galaxies, which may allow us to detect emission from gas all the way out into the intergalactic medium (IGM, §4.2.1). More than this significantly improved efficiency, the redshift range where BlueMUSE will see Lyα covers a key period of cosmic history, also known as "cosmic noon", when the cosmic star formation rate (SFR) peaks and a large fraction of the stellar mass in galaxies is built up (left panel of Fig. 11). It also coincides with the period when both the quasar activity and galaxies mergers peak, and it is the epoch of formation of the first large cosmic structures, which will evolve into large galaxy clusters. By allowing us to build a complete and homogeneous census of star-forming galaxies and galaxy groups throughout this epoch, and to survey the evolution of their circum-galactic medium (CGM), BlueMUSE will show these major transitions (SFR, mergers) and structure formations as they happen and help understand the emergence of strong cosmological accretion shocks, the conditions for survival of cold streams, and the effect of galactic winds (§4.2, 4.5).

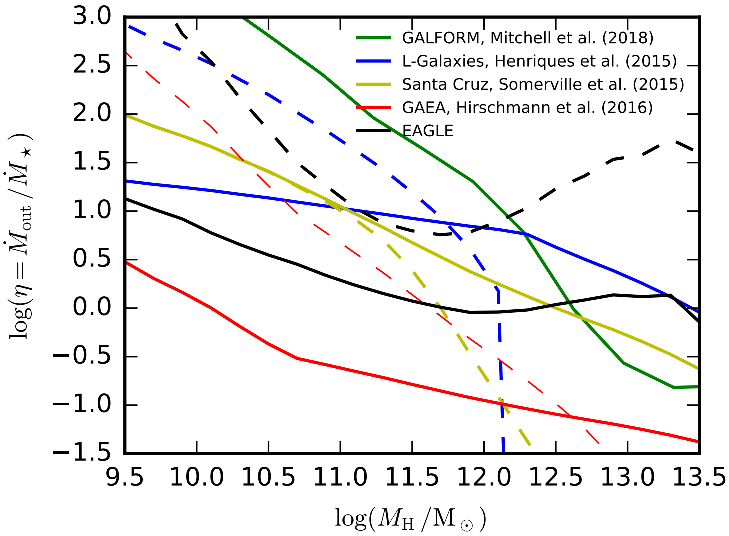

Figure 12: The efficiency of galactic outflows, expressed as the dimensionless ratio of outflow rate per unit star formation rate, and plotted as a function dark matter halo mass (from Mitchell et al., 2020). Different colours show different contemporary theoretical models, with solid lines indicating how much gas is removed from the interstellar medium of galaxies, and dashed lines indicating how much gas is then ejected through the halo virial radius. Discrepancies spanning multiple orders of magnitude exist between different models, despite the fact that each model is able to reproduce the observed stellar properties of galaxies. Observations of gas flows around galaxies are vital to constrain the otherwise degenerate picture represented by this figure.

4.2 Key science case: Gas flows around and between galaxies

Despite the impressive success of recent large-scale cosmological simulations at reproducing the bulk of galaxy properties across cosmic time, the fundamental questions about how galaxies acquire gas from the intergalactic medium, and how they regulate their growth through galactic winds or other preemptive processes, are mostly unconstrained from observations or theory. Figure 12 illustrates this by showing predictions of outflow rates from different state-of-the-art simulations, all extremely well calibrated to reproduce the stellar properties of galaxies. These predictions differ by orders of magnitudes! It is therefore clear that observing the CGM and constraining the flows of gas that traverse it would be a radically new constraint on galaxy formation.

MUSE has spectacularly demonstrated its ability to observe the CGM through its emission in the Lyα line of hydrogen (e.g., Wisotzki et al. 2016). Observations with BlueMUSE in the redshift range $2 < z < 3$ will be no less spectacular, but more importantly, they will be key in constraining galaxy formation because they cover the peak of cosmic star formation (Fig. 11, left). Among the factors that drive this turn-over in the cosmic SFR, we may expect a change in the form of accretion flows and their interactions with galactic winds, which marks the beginning of the transition from the early Universe – where gas flows cold and collimated onto galaxies, and the late Universe – where star formation is sustained by cooling-regulated accretion from hot coronae. Observing the evolution of the CGM through this epoch will be a key in discriminating between the various competing theoretical models. Fig. 13 shows a schematic collage of various phases of CGM which will be possible to detect with BlueMUSE.

4.2.1 Imaging the Intergalactic Medium at $z \sim 2-3$

A fundamental prediction of ΛCDM is that galaxies form in overdensities that are connected by a network of filaments, which compose the cosmic web (e.g. background of Fig. 13). For successful direct images of this cosmic web at $z \sim 1.8-3$, the epoch when galaxy formation was at its peak, one needs to map it over large areas, and BlueMUSE sensitivity will be well suited to do this. Specifically, the experience with MUSE showed (Bacon et al., 2021) that mosaicking is required to highlight the faint signal, which is often subtracted in a single field. The true signal from the inter-galactic medium (IGM) can get recovered, however, only when mapping across large scales. This is reachable to BlueMUSE with deep (tens of hours) integrations.

Why is BlueMUSE needed? In the redshift range z $\sim 2-3$ probed by BlueMUSE the cosmological surface brightness dimming is a factor of four lower (on average) compared to z $\sim 3-5$ covered by MUSE. For a fixed

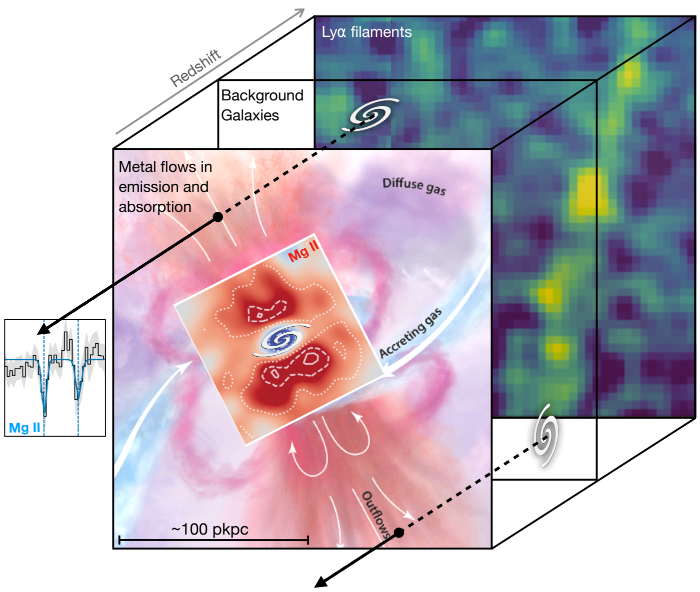

Figure 13: BlueMUSE will probe gas flows using both emission and absorption lines techniques. The foreground image showcases gas flows in the CGM from Tumlinson, Peeples, and Werk (2017), with metallic outflows imaged in Mg II emission by MUSE (Guo et al., 2023) extending over tens of kiloparsecs. BlueMUSE will detect gas at even greater distances using absorption features in background galaxies (Leclercq et al., 2022), leveraging the complementarity between emission and absorption techniques. The background image shows a mock BlueMUSE Lyα observations of an IGM region demonstarting the flourescent emission from halos connected by a filament illuminated by the UV background and local sources. The mock image is based on EAGLE simulation snapshot at $z \sim 2$ (James et al., 2015). BlueMUSE will be able to detect cosmic filaments in the young universe (z=2-3) more than 16 times faster than MUSE, thanks to reduced surface brightness dimming.

S/N and background limited exposures, this will make BlueMUSE $\sim 16\times$ faster at mapping the IGM compared to the current MUSE. This means that BlueMUSE will be able to construct large mosaics of the IGM in emission in reasonable exposure times. At the same time, several galaxies will be detected with a data quality that is sufficient to reconstruct a tomographic map of the cosmic web in absorption against the galaxy continuum on scales of ~ 200 kpc, complementing measurements in emission. Finally, a detection of the cosmic web in emission will enable a direct determination of the amplitude of the ionizing background at $z \sim 2-3$.

4.2.2 The Circumgalactic Medium of star-forming galaxies in Lyα emission

Narrowband Lyman-α images have suggested for many years that Lyα emitters are "fuzzy", and image stacks have revealed significantly extended emission (Hayashino et al., 2004; Matsuda et al., 2012; Momose et al., 2014; Xue et al., 2017). Thanks to MUSE we know now that Lyα haloes are ubiquitous around even low-mass galaxies at redshifts $z > 3$ (Wisotzki et al., 2016; Leclercq et al., 2017), with halo scale lengths typically $10\times$ larger than the UV sizes of the hosting galaxies (e.g., Fig. 13). Stacking some of the deepest MUSE data reveals that these haloes extend out to the virial radius, matching the incidence rates of high column density H I absorbers (Wisotzki et al., 2018). This extended Lyα emission thus holds unique clues about the spatial distribution and potentially also kinematics of circumgalactic hydrogen, but due to the resonant nature of the Lyα transition it is a huge challenge to decode this information.

Why is BlueMUSE needed? BlueMUSE will allow us to investigate the motions of gas in the CGM of galaxies and thus obtain crucial constraints on the balance of inflows and outflows. Due to the large FoV of BlueMUSE, there will be several galaxies in each observed field bright enough to be used as background sources for absorption line spectroscopy. Thus it will be possible to infer H I or metal line column densities for a significant number of foreground Lyα emitters and connect this information to the detected extended emission (e.g. Fumagalli et al., 2017; Lofthouse et al., 2019). While this experiment is in principle also conceivable with MUSE, the almost total dearth of sufficiently bright background galaxies at $z > 3$ makes it practically impossible. Therefore, the move to $z \sim 2$ afforded by BlueMUSE will imply an almost complete change.

4.2.3 Tomography of the Circumgalactic Medium with metal absorption lines

Up to now, the state-of-the-art CGM studies are limited to either single galaxy-quasar pairs (Bouché et al. 2013; Rahmani et al. 2018; Péroux et al. 2019; Zabl et al. 2019a) on small samples or to stacking techniques with large samples of pairs (e.g., Lan and Mo 2018; Bordoloi et al. 2014). Examples in individual pairs (Rubin et al.,

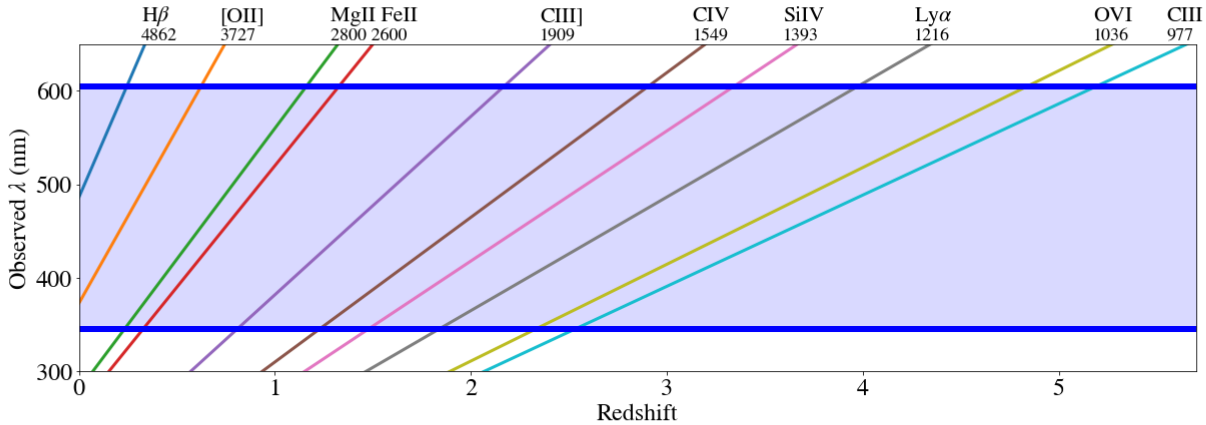

Figure 14: Main nebular lines available to BlueMUSE as a function of redshift. Rest-frame wavelengths are provided for each line in Angstroms. In particular metal lines in the rest-frame UV (Mg II, Fe II, O VI) will help probe the CGM in emission.

2018; Zabl et al., 2019b) show the promise of extending this technique to the use of background galaxies as probes of foreground ones. However, in order to understand the exact nature of gas flows around galaxies, the CGM kinematics can only be mapped using multiple background sources (quasars or galaxies) as in Zabl et al. (2019b). This is fortunately within reach with background galaxies (e.g. Fig. 13), but not feasible with MUSE for the following reasons: (a) the spectral range (480-930 nm) does not allow to study UV absorption lines below $z = 0.85$, whereas $z = 0.6 - 0.7$ is a sweet spot for group selections as background galaxies and (b) the spectral resolution of MUSE at 5000 Å is too low (R=1800 or 160 km s^{-1}; see Fig. 22).

Why is BlueMUSE needed? With BlueMUSE, we will reach many more extended background galaxies to spatially resolve absorption and address metal mixing on small scales (e.g., Péroux et al. 2018). It will become possible to study the spatial and kinematics properties of the CGM around *individual* galaxies at intermediate redshifts $z = 0.4 - 0.8$. This redshift range is particularly well suited as (i) this corresponds to the regime where the source density of background galaxies (24 mag) is now becoming $> 10/\text{arcmin}^2$ as groups are predominantly found at $\lesssim 0.7$ (Kudritzki et al., 2012); and (ii) this corresponds to the wavelength range ($<$ 500nm) necessary to observe the low-ionisation lines Fe II and Mg II at redshifts $\lesssim 0.8$, currently inaccessible with MUSE.

4.2.4 Probing the Circumgalactic Medium in emission with metal lines

Metal emission lines are significantly fainter than Lyα, with characteristic surface brightness predicted around $10^{-21} - 10^{-20}$ erg s^{-1} cm^{-2} arcsec^{-2} at $z \sim 2$ (Bertone and Schaye 2012, Augustin et al. 2019). Due to the cosmological surface brightness dimming, detection at $z > 3$ with MUSE is almost prohibitive and thus limited to only extreme environments, making the case for low-redshift/shorter-wavelength observations obvious. The detection of such low surface brightness signal will require deep exposures, but is expected to yield a tremendous return (Zabl et al., 2021; Leclercq et al., 2022; Pessa et al., 2024). Indeed, while Lyα traces the bulk of the gas mass, metal transitions become key traces to map the spatial extent of the multiphase CGM. Low and moderate ions will yield maps of the relatively cool ($T \lesssim 10^5$ K) CGM, with ions at higher ionisation states tracing the warm-hot medium at $T \gtrsim 10^5$ K. Combined together, these traces will enable a complete reconstruction of the multiple phases of the CGM.

Why is BlueMUSE needed? With BlueMUSE, we will have access to a plethora of rest-frame UV lines in the redshift range $\sim 0 - 2.5$ (Fig. 14), opening up a completely new way to map the CGM directly. Focusing on $z < 3.5$ the increase in the surface brightness and the large FoV of BlueMUSE will enable effective coverage or large area providing a large number of targets.

4.2.5 Circumgalactic Medium around AGNs

While MUSE has greatly advanced our knowledge of extended Lyα emitting gas around AGN at $z > 3$ (e.g., Borisova et al. 2016), an important limitation has been the general rarity of detections of extended emission from other UV lines. BlueMUSE will provide a quantum leap in our ability to study Lyα halos and the CGM around AGN, by proving the wavelength coverage and sensitivity to detect the faint UV emission lines that are crucial to characterise the kinematic, ionisation and chemical enrichment properties of AGN–photoionised Ly-α halos and CGM, in the redshift range $1.9 < z < 3.6$. Non-resonant lines such as He II 1640 and C III] will allow more reliable gas kinematics to be derived, free from the potential complications of Ly-α line transfer effects, and the inclusion of metal lines such as N V λ1239,1243 and C IV λ1548,1551 will allow the ionisation properties and chemical enrichment history of the gas to be derived (e.g., Villar-Martín et al. 2003; Humphrey et al. 2019). Mapped in two spatial dimensions thanks to the IFU technique, this information will afford detailed study of AGN feedback, the dispersion of metals via outflows, and accretion of gas in/around massive galaxies near the peak in the star formation and AGN activity histories.

Why is BlueMUSE needed? The main benefit of using BlueMUSE is the focus (in terms of detectability of emission-lines) on the epoch when the AGN activity peaks and less dramatic effects of the cosmological surface brightness dimming, which affects MUSE observations.

TLR	Value	Comment
Wavelength range	350 - 580 nm	
Spectral resolution	2800 < R < 3700	
Field-of-View	$\geq$ 1 arcmin^2	
Sensitivity		
Spatial sampling	0.2 < spaxel < 0.3	sample seeing with $\sim$ 2 spaxels
Spectral sampling	$\geq$ 2 pixels	
Image quality	natural seeing	
Stability	0.1 pixels	

Table 12: TLR for the Key science case: gas flows around and between galaxies

Derived TLRs for the science case: Gas flows around and between galaxies. The constraints on the BlueMUSE requirements is driven by the importance of covering the currently inaccessible redshift range (with MUSE) setting up the ideal wavelength range between 350 and 580 nm. A further extension to even bluer wavelengths (i.e. within the extended range down to 330nm) will also be beneficial. The various science cases listed above do not make a strong requirement at the spectral resolution of BlueMUSE, as long as it is better then MUSE and the [OII] doublet is resolvable, setting a lower limit to about R$\sim$ 2800. On the other hand, high sensitivity, especially for detection of extended low-surface brightness features, is considered an important requirement. In this respect the pixels size is actually desirable to be large, to minimise the readout noise and be sky-noise limited in the empty regions (no targets). This leads to TLRs for the above science cases listed in Table 12.

4.3 Lyman Continuum Emitters

Cosmic reionisation corresponds to the period in the history of theUniverse during which the predominantly neutral intergalactic medium was ionized by the emergence of the first luminous sources. Although star-forming galaxies in the early Universe are thought to be the main sources of reionisation, the nature of these objects remains so far totally unknown due to the increasing opacity of the intergalactic medium with redshift which renders direct LyC detections impossible (or extremely inefficient) at $z \gtrsim 4$. However, LyC Emitters can be observed at lower redshifts, even though these observations have proven difficult: so far, only 14 detections have been reported in the low-z Universe (< 0.4, Bergvall et al. 2006; Leitet et al. 2013; Borthakur et al. 2014; Izotov et al. 2016b; Izotov et al. 2016a; Izotov et al. 2018a; Izotov et al. 2018b), and more candidates at high

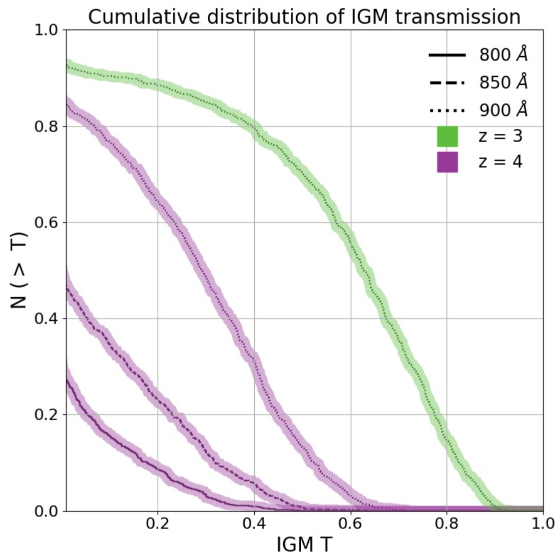

Figure 15: Distribution of IGM transmissions for different redshifts and rest wavelengths. At $z \sim 3$ (green curve), 80% of the lines of sight have a transmission higher than 40%; at $z \sim 4$ (purple curves), the IGM is still not completely opaque to ionizing radiation: even at 800Å rest-frame, 10% of the lines of sight have a transmission higher than 20%.

redshift (de Barros et al. 2016; Vanzella et al. 2016; Shapley et al. 2016; Bian et al. 2017; Vanzella et al. 2018; Steidel et al. 2018; Fletcher et al. 2019). Indirect methods are the only probes of LyC leakage in the epoch of reionization. Lyman-α escape from galaxies is expected to correlate with LyC escape (Verhamme et al., 2015; Dijkstra, Gronke, and Venkatesan, 2016). By investigating the links between LyC emission and the Lyman-α spectral/spatial shapes, one can provide unique and robust tests to probe ionizing sources during the epoch of reionization.

Why is BlueMUSE needed? BlueMUSE will be able to directly probe the Lyman continuum from sources at $z \sim 3$ to 5 and, unlike previous targeted observations, it will allow us to collect a statistical sample of LyC emitters as part of blind surveys. Nevertheless, due to the IGM opacity increasing rapidly towards higher redshifts, we expect most detections to fall in the redshift range $z = 3 - 4$ where Lyman-α can be used to assess the spectroscopic redshift, and where the IGM transmission ($T_{\rm IGM}$) remains reasonably high: at $z \sim 3$, 80% of the lines of sights have a transmission higher than 40%, as shown on Fig. 15. We expect BlueMUSE to be particularly efficient at detecting the faintest population of $z \sim 3$ galaxies (Drake et al., 2017; Hashimoto et al., 2017). These low mass objects are plausibly strong leakers according to previous observations (Izotov et al., 2018a) and simulations (Wise et al., 2014; Trebitsch et al., 2017; Kimm et al., 2019), and may correspond to the analogues of the sources of reionisation.

Valuable information on the nature of LyC emitters could also be extracted from BlueMUSE spectra. In the red, the rest-frame far-UV emission ($\sim$ 1400 Å) can be detected up to $z = 3.5$, while at the blue end, BlueMUSE will probe ionising emission from the Lyman limit (912 Å) down to 780 Å to add new constraints on the typical shape of the Lyman continuum. In addition, we can expect to detect Lyman-series absorption lines to get insight into the H I content of galaxies (column density, covering fraction) and its link with LyC escape. Detecting these lines at $z \sim 3$ with BlueMUSE will be outstanding since such observations are usually limited to galaxies at much lower redshift.

Derived TLRs for the science case: Lyman Continuum Emitters. Similarly to the previous set of science cases, the main requirement on the instrument is focusing on the blue coverage and moderate spectral resolution, while the spaxel size as well as the FoV are favoured to be large. The derived TLRs are outlined in Table 13.

4.4 Gravitational lensing in clusters

Massive galaxy clusters locally curve Space-Time and thus stretch and magnify the light of background galaxies. Within the central square arcminute, distant sources are generally multiply imaged by the lensing effect and the magnification of these images is generally larger than a factor of a few but can reach factors of hundreds for gravitational arcs straddling the critical lines. Thanks to the lensing magnification we can study lower luminosity/mass galaxies that would otherwise be undetectable. The identification of the multiple images and

TLR	Value	Comment
Wavelength range	350 - 600	
Spectral resolution	R< 3500	
Field-of-View	$\geq$ 1 arcmin^2	
Sensitivity		
Spatial sampling	$\geq$ 0.3	
Spectral sampling	> 2 pixels	
Image quality	natural seeing	
Stability	0.1 pixel	

Table 13: TLR for the science case: Lyman continuum emitters

the precise determination of their redshifts offer a unique opportunity to map the total mass distribution of the cluster cores including the unknown dark matter. In the best cases, such as for the Hubble Frontier Field Clusters, the precision of the mass determination is better than the percent level (e.g., Jauzac et al. 2014). However, this is only possible if a large number of multiple images have measured precise redshifts (Richard et al., 2015). IFUs are able to measuring a large number of redshifts over their FoV without the a priori knowledge of the galaxy locations, thus revolutionising the cluster lensing modelling power (e.g., Lagattuta et al. 2017), with potential further application to put constraints on the properties of dark matter cross-section (e.g., Harvey et al. 2017) or cosmological parameters (e.g., Jullo et al. 2010). Using these precise models of the cluster lensing, we can then correct for the lensing magnification of distant sources, thus extracting their full properties.

There are several key science questions which can be addressed using gravitational lensing of massive clusters:

- **Multiple images and faint LAEs:** The redshift distribution of lensed background galaxies is dominated by the population of LAEs, as currently seen in MUSE surveys (Fig. 16). We expect with BlueMUSE a much larger number of background sources (a factor ~ 5 based on the LAE luminosity function, see "deep fields" science case §4.1) and therefore multiple images.

- **Giant arcs:** because they require an almost-perfect alignment between a large background galaxy and the center of a lens, highly magnified giant arcs are quite unique. By moving to $z = 2$ the number of such high redshift giant arcs increases significantly, allowing us to probe very small scales in the source plane ($<$ 1 kpc,Patrício et al. 2016, Johnson et al. 2017, Claeyssens et al. 2019). These giant arcs are perfect laboratories to study the mechanisms of Lyman-α and UV emission, and their high continuum level make them unique background sources for resolved CGM absorption studies (e.g., Lopez et al. 2018, see also the gas flows science case §4.2.3)

- **GC progenitors:** Thanks to gravitational lensing we will be able to get FUV rest-frame spectroscopy of very compact star-forming regions ($<$ 50 pc, e.g. Vanzella et al. 2017; Rivera-Thorsen et al. 2019) that are thought to be the birth place of GCs. GC formation peaks at similar redshift as the cosmic star formation history. As introduced in §2.3 GCs have peculiar chemical patterns in their stars, that make them unique. Direct FUV spectroscopy of GC progenitors will be a unique chance to address whether GC formation is confined to special physical conditions of high-redshift galaxies or is still possible in local galaxies.

- **Critical line mapping:** The identification of new multiple images with spectroscopic redshifts along the critical lines will help further improve the mass distribution models of the clusters. The spectroscopic identification of several multiple images at different redshifts allows us to constrain the cosmological parameters (e.g., Jullo et al. 2010). Compared to blank fields, isolated emission lines in strong-magnification regions can be easily classified as either high-z or low-z interlopers through multiple-imaging considerations.

Why is BlueMUSE needed? BlueMUSE will fill in the redshift space between $2 < z < 4$ increasing the number of backround lensed sources by a factor of ~ 2.5. In particular, we expect a significant increase of giant arcs as

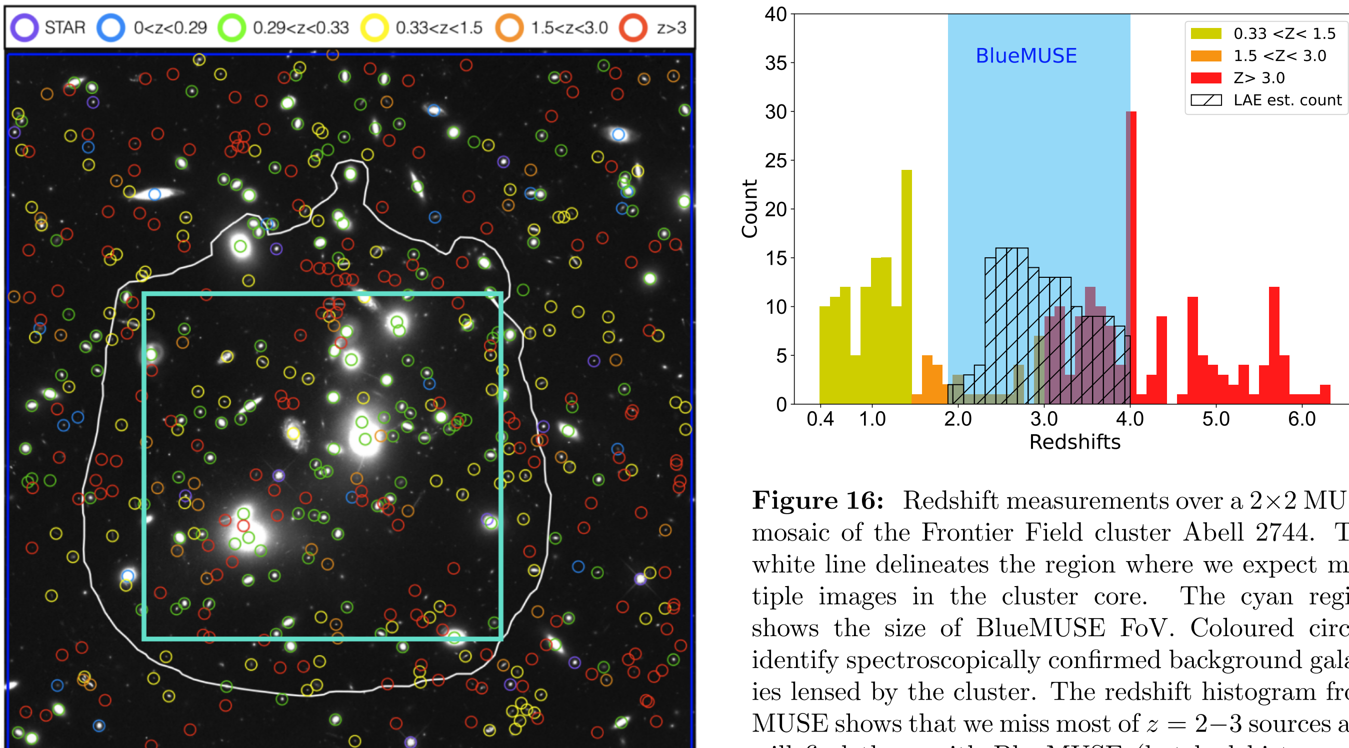

Figure 16: Redshift measurements over a 2×2 MUSE mosaic of the Frontier Field cluster Abell 2744. The white line delineates the region where we expect multiple images in the cluster core. The cyan region shows the size of BlueMUSE FoV. Coloured circles identify spectroscopically confirmed background galaxies lensed by the cluster. The redshift histogram from MUSE shows that we miss most of $z = 2-3$ sources and will find them with BlueMUSE (hatched histogram). Adapted from Mahler et al. (2018).

we will be able to detect them a lower redshifts (z $\sim$ 2). BlueMUSE will provide the unique opportunity to study the massive stellar content and the conditions of the ionised gas around some of these systems. For a typical massive cluster at $z \sim 0.3$ the Einstein radius (characterising the scale of strong lensing) is $\sim$50$''$ and the area of high magnification fits perfectly the FoV of BlueMUSE or within a small mosaic (Fig. 16). Mapping a significant fraction of the surroundings of the critical lines with BlueMUSE has a potential of further improving the mass distribution models of the clusters.

TLR	Value	Comment
Wavelength range	350 - 380 nm	goal: 330 - 600 nm
Spectral resolution	2500 <R< 4500	
Field-of-View	$\geq$ 1 arcmin^2	
Sensitivity		
Spatial sampling	$0.2'' <$ spaxel $< 0.3''$	sample seeing with $\sim$ 2 spaxels
Spectral sampling	$>$ 2 pixels	
Image quality	natural seeing	
Stability	0.1 pixels	

Table 14: TLR for the science case: gravitational lensing in clusters

Derived TLRs for the science case: gravitational lensing in clusters. Blue wavelength range is the key asset and the key requirement for BlueMUSE for this science case. Here an extension to even lower blue cutoff (330 nm) is welcome, in order to increase the number of multiple images of $z \sim 2$ galaxies and improve on the lensing mass models. Requirements on the spectral resolution, size of the spaxels and the FoV are similar to other science cases within this set investigating the distant Universe. The derived TLRs are outlined in Table 14.

4.5 The emergence of the first galaxy clusters

BlueMUSE clearly appears as the best means to discover and characterise giant Lyman-α nebulae that now we know are widespread in the early generation of galaxy groups and clusters (Valentino et al., 2016; Daddi et al., 2021; Daddi et al., 2022a; Daddi et al., 2022b; Li et al., 2021; Umehata et al., 2019; Travascio et al., 2024; Herwig et al., 2024). Following the initial discoveries in the dense core of a prototypical galaxy cluster progenitor, CL J1449+0856 at $z = 1.995$ ((Valentino et al., 2016; Gobat et al., 2011; Gobat et al., 2013; Strazzullo et al., 2013)), KCWI at Keck (in collaboration with Michael Rich at the University of California) has later revealed giant Ly-α nebulae inside several more $z > 2$ structures (Daddi et al., 2022a). This included the most distant X-ray detected cluster known (CL J1001+0220 at $z = 2.506$; Wang et al., 2016) and the most spectacular detection is in a radio-selected forming cluster core at $z = 2.9$ (Daddi et al., 2021). The presence of these nebulae clearly demonstrates that cold gas is co-existing with hot gas inside the deep potential well of these structures (Valentino et al., 2016; Wang et al., 2016). The origin, powering mechanism and fate of the cold gas is still unclear and a matter of debate: the lack of strong AGN photo-ionization sources suggests it might be related to cold-stream accretion and/or arise from feedback between galaxy activity and the intra-cluster medium (Daddi et al., 2021).

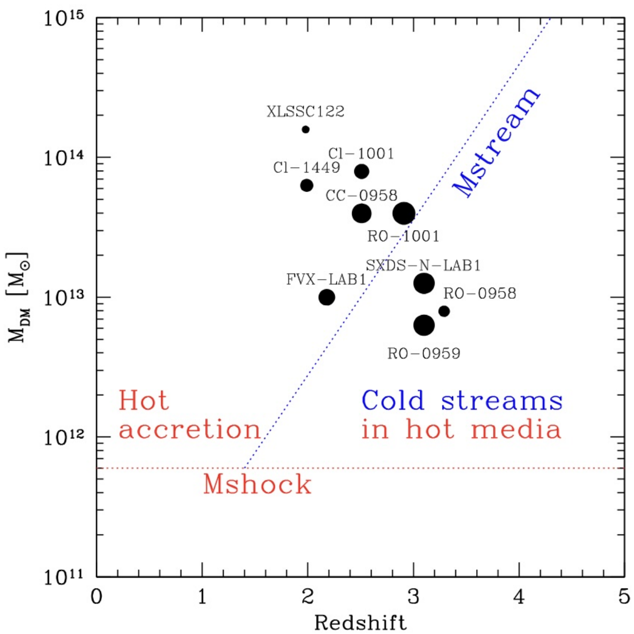

Figure 17: Theory prediction (Dekel et al., 2009) on the region of the redshift-dark matter mass parameter space where cold accretion versus hot haloes are expected (adapted from Daddi et al. 2022a). Typical structures currently investigated are shown, including RO-1001, the clusters in which we observed and detected giant Lyα nebula with prominent filamentary structure suggesting accretion (Daddi et al., 2021).

Why is BlueMUSE needed? At the redshift range of $z \sim 1.5-3$, enabled by BlueMUSE, simulations predict that massive $\sim 10^{13-14}$ $M_\odot$ dark matter haloes should become less efficiently shielded by this hot atmosphere, thus permitting large-scale infall of cold gas into their cores (Dekel et al., 2009, Fig. 17). This process is however still not well constrained and observations from BlueMUSE will crucially enable us to trace the epoch and duration of this transition (Daddi et al., 2022a) that might be also related to star-formation (and quenching) in galaxies (Daddi et al., 2022b). BlueMUSE will uniquely allow us to discover Lyα emitting nebulae in the first generation of forming clusters down to $z = 1.87$, thus allowing exploration of the critical redshift range 1.8-3 where we expect cold accretion to massive haloes to peak due to the competing effects of hierarchical mass assembly of clusters (increasing the number density of massive structures towards lower redshifts) and cosmic evolution of accretion rates (rapidly increasing with redshift at fixed structure mass). BlueMUSE will be able to statistically investigate these competing processes for the first time. This will be primarily possible because of the large FoV of BlueMUSE, which will enable efficient observing of large nebulae at a given redshift range, as well as provide information on the sky background. Further constraints are a high spectral resolution, expected stability of the flat-fielding (at least at the level of MUSE) and a high image quality (at the level of a well behaved natural seeing), all which are expected from BlueMUSE. There are great prospects for assembling large samples of very suitable targets the future: Euclid is already able to identify massive $z > 1.8$ groups and clusters even from its shallower, wide coverage, promising the identification of order of thousands of candidates over

$1.87 < z < 3$. While IFS observations of giant nebulae will continue before BlueMUSE becomes operational, its capabilities place it as the unique instrument for surveying the giant nebulae and first galaxy clusters in the 'cosmic noon' epoch.

Derived TLRs for the science case: the emergence of the first galaxy clusters. As for most science cases in this section, the possibility to efficiently probe blue wavelength regions is a key drivers. In this respect, BlueMUSE blue cut off should be as low as possible and its throughput at 330 - 350 nm of the order of 15-20%. A large pixel scale will limit the effect of read-out noise in the blue. Together with high flat-fielding stability, this will improve sensitivity

TLR	Value	Comment
Wavelength range	350 - 580 nm	down to 330 nm
Spectral resolution		
Field-of-View	> 1 arcmin^2	
Sensitivity		$15 - 20\%$ through put at 350 nm
Spatial sampling	> 0.3	
Spectral sampling	> 2 pixels	
Image quality	natural seeing	
Stability	0.1 pixel	

Table 15: TLR for the science case: the emergence of the first galaxy clusters

5 BlueSi: preparing for science with BlueMUSE

Successful operations of BlueMUSE depends on three aspects: the quality of the instrument, the availability of the data reduction software, and the readiness of the scientific team to use the instrument. Preparation of the scientific team to use BlueMUSE data needs to happen before the first photons are taken, the first data are reduced and science-ready. Crucially, as the MUSE experience showed, availability of a software simulating the data products of the instrument are extremely valuable and often necessary for an effective preparation of science cases. BlueSi (Wendt et al., 2024) is an end-to-end simulation software, which is able to provide realistic BlueMUSE data products. It utilises the technical specifications of BlueMUSE based on the defined TLRs, and therefore it can be also used to assess certain tradeoffs regarding instrument capabilities.

Worth mentioning is that BlueSi is not envisioned as a software dedicated for the BlueMUSE consortium, but accessible to a broader science community, which could also use it for preparation of their observations. The accessibility of the software to the wider audience is ensured by its well defined interface, and a separation of the simulation core and the parts that define inputs and specify individual science cases. BlueSi inputs are divided between the *scene config* and *simulation config* ASCII files. The *scene config* contains the information specific to the science content of the simulated cube, such as the type of scene, a FoV, the main input catalog as well as numerous optional parameters (i.e. radial velocities, extinction correction or vacuum-to-air correction, and information about the simulated object(s)). The *simulation config* provides all the details relating to the instrument and the simulated observation, such as the technical specifications of the simulated instrument (i.e. BlueMUSE, but MUSE baseline is also implemented), the environmental conditions (seeing, airmass) and the observation setup (number of exposures and exposure time per exposure). Furthermore, the telluric emission and absorption is referenced from the full Cerro Paranal Advanced Sky Model Version (Noll et al., 2012; Jones et al., 2013). Based on these config files, BlueSi first sets up a raw cube with proper dimensions, and then applies the instrumental (e.g. LSF) and observational (e.g. PSF) conditions and prepares an output BlueMUSE data cube.

While not yet ready for a wider distribution, the current implantation of BlueSi is used by the BlueMUSE science team to test the instrumental effects on desired science cases. These efforts are described in more detail in Wendt et al. (2024). For example, the team tested the effects of the rectangular spaxels on the PSF properties (e.g. Section 6.2) and effects of including covariance in the data analysis. BlueSi prepared BlueMUSE data cubes emulating observations of several science cases (e.g., Fig. 18) outlined in this work such as globular cluster, massive stars, faint Lyα emitters, while data cubes for other science cases are in production (e.g. stellar kinematics of nearby galaxies of various masses as well as a Milky Way analogue), as well as the inclusion of the ISM in the datacubes.

BlueSi is an important tool developed to assists the Science Team in devising the optimal science cases for BlueMUSE. It will also be a useful tool for the broader scientific community at the time of completion of BlueMUSE.

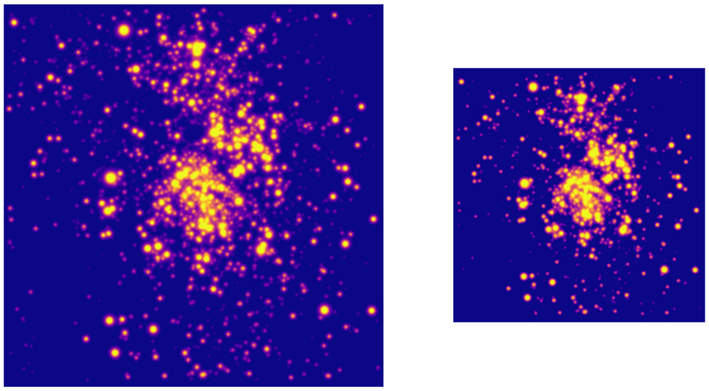

Figure 18: "White light" reconstructed images of the 30 Doradus inspired object at different distances. *Left*: natural, spanning about 30 parsec at the distance of 49 kpc. *Right*: projected to a distance of 75 kpc. Intensities on both images are shown with a logarithmic scale stretch. As the distance increases the number of stars that can be uniquely extracted decreases, but 72% of the stars from the more distant (right) BlueMUSE cube could still be robustly extracted, with respect to the closer (left) BlueMUSE cube.

6 Uniqueness and Synergies

6.1 Instrumental landscape

BlueMUSE is a well placed instrument to tackle the science cases presented in this document, as well as numerous other ideas advocated by the community[4]. As an IFS with a large FoV it will continue in the steps of MUSE, which pioneered the "spectroscopy of everything", essentially providing spectra of all detected objects within the FoV, without a necessary preselection by imaging, as is the case when using multi-object spectroscopy. BlueMUSE FoV will be the same as that of MUSE, but its spectral resolution will be a factor of two larger, while the wavelength coverage is shifted into the blue. In these respects, BlueMUSE will perform well both as a suitable alternative and a support instrument to the existing and planned facilities. In Fig. 19 we show the landscape of existing and planned instruments and their comparison with BlueMUSE in two well defined parameters: the size of the FoV and the covered wavelength range. Of these instruments, a few that are on a similar class telecopes (6-10m) are worth highlighting. Some of them are already operational and will have a long history of operations by the time BlueMUSE is ready, while others are still in the development stage.

- **MUSE** by construction, BlueMUSE has a very similar architecture to MUSE and the two instruments overlap in wavelength in the range 480-580 nm (465-600 nm using extended wavelength coverage for both instruments). However, even in this overlap region BlueMUSE provides a much higher sensitivity and twice the spectral resolution of MUSE, making it at least twice as efficient (e.g. Section 3.4).

- **KCWI:** the Keck Cosmic Web Imager (KCWI, Martin et al. 2010) is a slicer based IFU with broadly similar characteristics (wavelength range, spectral resolution) as BlueMUSE. However there is a strong difference in FoV between BlueMUSE and KCWI. Indeed, at the same spectral range and spatial / spectral resolution as BlueMUSE, the FoV from KCWI is $8.2 \times 20.4''$, which is more than a factor of 20 smaller. This makes KCWI unsuitable to cover large areas to a high depth and underlines its main purpose as a single-target instrument, unlike BlueMUSE. BlueMUSE is also optimised to a single mode of operation and we expect its transmission to be 1.5-2$\times$ higher than KCWI. Furthermore, while BlueMUSE will also have rectangular spaxels, there is a large difference in the aspect ratios, which is 1.5 for BlueMUSE and up to 4.6 for KCWI, and therefore the ability to resample the observations into square pixels.

[4]For general community interests in BlueMUSE, please see the talks presented at the meeting held at ESO 18-22 November 2024 A decade of discoveries with MUSE and beyond.

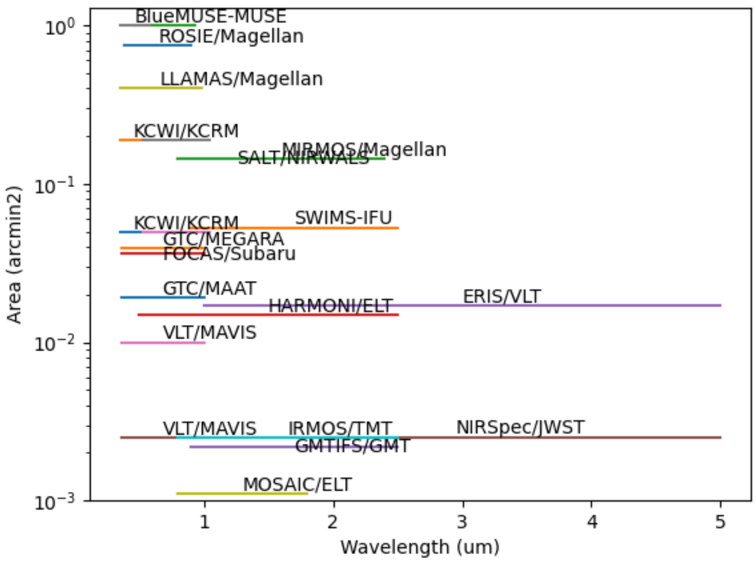

Figure 19: Comparison of existing and planned IFS on 6 – 39 m size telescopes, both ground- and space-based, focusing on their FoV and wavelength coverage.

- **MEGARA:** the MEGARA instrument recently commissioned at GTC (Carrasco et al. 2018) has a fiber-based IFU with similar characteristics (wavelength range, spectral resolution) as BlueMUSE, but its 25 times smaller FoV ($12.5 \times 11.3''$), its low end-to-end throughput (<7% at 350 nm) and smaller simultaneous spectral range will not be able to target the science cases proposed for BlueMUSE.

- **VIRUS:** Hobby-Eberly Telescope Dark Energy Experiment (HETDEX) is using a *Visible Integral-Field Replicable Unit Spectrographs* (VIRUS), which is an IFU made of 156 spectrograph linked with 78 bundles of optical fibres with each bundle containing 448 filers, with almost 35000 fibers that observe the sky over an are of 90 deg^2 (Hill et al., 2021). This is by far the largest area covered by an IFS based instrument, and it is located on the 10 m Hobby-Eberly Telescope. The wavelength range (350 - 550 nm) is very similar to that of BlueMUSE. Its resolution is, however, much smaller (R $\sim$ 800), with significant gaps between the IFUs on the sky and the HETDEX survey is relatively shallow with only 6 min observations per pointing to reach the large survey area of 540 deg^2 (Gebhardt et al., 2021). In this respect, VIRUS is not a direct competitor, but could be used to guide and preselect interesting field and objects that could be followed up with BlueMUSE.

- **ROSIE:** with $50'' \times 54''$ FoV *Reformatting Optically-Sensitive IMACS Enhancing IFU* (ROSIE), a proposed instrument for the Magellan -Baade telescope at Las Campanas Observatory, is the the most similar in size with BlueMUSE (McGurk et al., 2020). It offers three spectral ranges of which one overlaps with that of BlueMUSE (390- 565 nm), and its maximum spectral resolution is given as R =1800.

- **LLAMAS:** or *Large Lenslet Array Magellan Spectrograph* is another IFS in development for the Las Campanas Observatory. Its FoV is almost a factor of 3 smaller than of BlueMUSE ($37'' \times 37''$) covered with micro-lens array splitting the light in about 2560 pupils, which is dispersed through 8 spectrographs. Its spectral resolution is expected to be R=1300, and it will cover the optical wavelength range (350 - 970 nm), with a possibility of increasing the micro-lens array to cover the same area as BlueMUSE (with 7680 lenslets).

While similar types of science can be pursued with above mentioned instruments, and in some aspects they might be seen as a competitors, none of them is as versatile as BlueMUSE. Furthermore, KWCI and MEGARA are on the northern hemisphere and should be considered also as providers of valuable synergetic coverage of targets or fields.

6.2 Uniqueness

When taken separately, each characteristic of BlueMUSE can be matched, or surpassed, by other instruments. When taken together, BlueMUSE characteristics, such as the blue wavelength range, large FoV IFS, high spectral resolution, high throughput, 8m telescope, and well chosen samplings in both spectral and spatial directions, define BlueMUSE as a truly unique instrument.

Single mode, seeing-limited, large FoV: The single mode of operation simplifies the use of BlueMUSE, but it imposes certain constraints on selecting suitable science cases. The absence of adaptive optics capabilities is a limitation, making BlueMUSE a seeing-limited instrument. This, however, does not impose significant restrictions to science cases presented here, as they are benefiting from other characteristics, such as the large FoV, larger spaxels, blue wavelengths and, especially, higher spectral resolution.

BlueMUSE architectural design is well adapted to the natural seeing, as its rectangular pixels ($\sim 0.2'' \times 0.3''$), are able to sample the best expected natural seeing. Our BlueSi based tests (Fig. 20; Wendt et al., 2024), confirm that a point source would have a nearly circular shape in the reconstructed images as long as the natural seeing is larger than $0.3''$ (FWHM). Relatively large spaxels are also preferred by extragalactic science cases, especially those targeting low surface brightness regions and focusing on deep observations (see also Section 8.4).

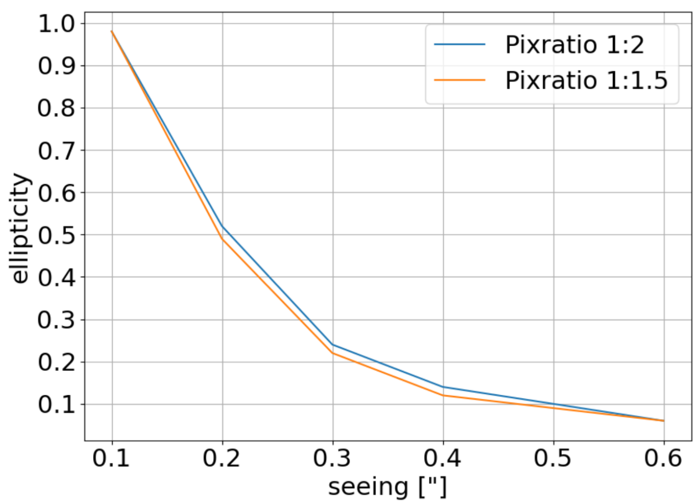

Figure 20: Ellipticity change with increasing natural seeing (FWHM) of a point source obtained with a BlueSi simulations (see Section 5). BlueSi reproduces realistic BlueMUSE cubes, including the rectangular spaxels, which could infuence the regularity and the shape of the point-spread function (PSF) of BlueMUSE observations. As the plot shows, only at unrealistically good seeing of $< 0.3''$ the image of the point source is significantly elongated. At seeings $> 0.6''$ that can be expected at blue wavelengths on Paranal, ellipticities are typically smaller than 0.05, ensuring that exposures of stars will appear round, even with rectangular sampling.

BlueMUSE will also have a higher end-to-end transmission than MUSE at wavelengths $\lambda < 540$ nm, which helps compensate for the lack of AO correction: as an example, at 500nm, the image quality of MUSE in WFM-AO is expected to be typically 20% better than BlueMUSE in NOAO, while the end-to-end transmission of BlueMUSE is 40% higher. This makes BlueMUSE in NOAO and MUSE-AO reach similar sensitivities for point source detection at this wavelength, in less on-source time (see also *High spectral resolution* below).

As a further test of the influence of seeing limited observations with BlueMUSE compared with MUSE-AO assisted observations, we produced two mock data cubes using BlueSi. The first one emulated MUSE in the AO mode, and the second BlueMUSE in natural seeing observations. In both cases the inputs were the same: a 30Dor-like stellar cluster populated with various types of stars (see Fig. 18 for the description of the scene Castro et al., 2021). The BlueSi mock data cubes reflected all respective properties of the two instruments (e.g. spaxel shapes and sizes, wavelength range and resolution, FoV, throughput, etc), as well as imposed the same observational constraints, where the natural seeing was set to $0.8''$(FWHM). This seeing was translated to the BlueMUSE data cube PSF, while the PSF FWHM for the MUSE data cube was set to $0.6''$, imitating a respectable GLAO correction. Both data cubes were subsequently analysed in the same way, starting first with extraction of stars using PampelMUSE (Kamann, Wisotzki, and Roth, 2013). A remarkable results is that the number of extracted stars is the same on both data cubes. From the mock MUSE datacube it is possible to extract 89.7% of targets, and 99.4% of those with S/N$>$ 50. The same numbers for the mock BlueMUSE data cube are 89.7% and 99.3%, respectively. This is understandable as the selection of sources in both data cubes is based on the same high resolution HST image.

In addition to the number of sources extracted from a crowded region, the key consideration is the precision

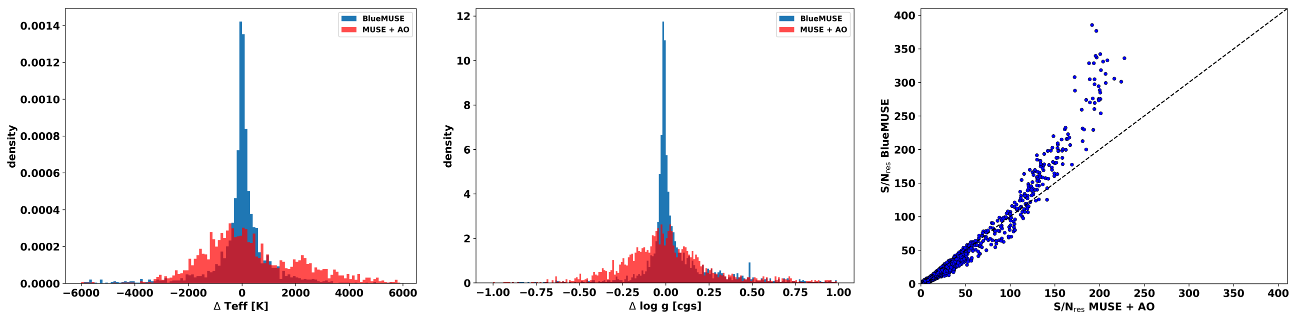

Figure 21: Comparison of extracted parameters from mock BlueMUSE and MUSE-AO data cubes of a 30Dor-like system. Both data cubes were simulated by BlueSi software (Section 5), accounting for all reciprocal instrumental properties (e.g. rectangular spaxels for BlueMUSE) and the same observing conditions, where BlueMUSE was limited by the natural seeing (FWMH=0.8″), while MUSE was assisted by GLAO (PSF FWMH improved to 0.6″). Stellar spectra were first extracted from both cubes using the same method and subsequently analysed to extract stellar parameters: effective temperature and surface gravity (see text for details). The extracted values were compared with the original values fed into BlueSi and used for the construction of the data cubes. *From left to right*: histograms of the differences in effective temperature and surface gravity, followed by the signal-to-residual noise ratio (S/N$_{res}$) where the noise represents the dispersion of the residuals obtained by fitting the spectra with stellar models. The first two plots show the increase in the precision of the stellar parameters when using BlueMUSE, which can be attributed to the larger information content in the blue part of the spectra. Spectra from the MUSE-AO data show somewhat larger S/N$_{res}$, as AO provides more flux. However, as the S/N$_{res}$ increases, BlueMUSE spectra provide better fits to stellar models primarily because there are even more fainter absorption lines in the blue part of the spectra that can be used in the fitting process.

with which the physical properties of those sources can be determined. We test this using the same BlueSi simulation of BlueMUSE and MUSE-AO data cubes, taking as examples two stellar properties: the effective temperature and the surface gravity. Extracted spectra were analysed using ULYSS software (Koleva et al., 2009) together with two set of stellar templates (Lanz and Hubeny, 2007; Husser et al., 2013). The same templates were used for the construction of the input scene simulated with BlueSi. In Fig. 21 we show the difference between the input and derived parameters as histograms. BlueMUSE parameters are typically more similar to the input parameters, showing a significantly smaller dispersion in the histograms compared to the MUSE-AO data. The reason for this is in the blue part of the spectrum where there are many absorption lines, useful for deriving the physical parameters of stars. The advantage of MUSE-AO data is in somewhat larger and more centrally concentrated flux. However, BlueMUSE higher spectral resolution and the wavelength range compensates, as can be seen on the right panel in Fig. 21. Here we show the comparison between the BlueMUSE and MUSE-AO estimated signal-to-residual noise ratios (S/N$_{res}$), where N$_{res}$ is the standard deviation of the residuals of the ULYSS fit. For low S/N$_{res}$, BlueMUSE and MUSE-AO provide spectra of similar quality (with respect to the fit), but for high S/N$_{res}$ BlueMUSE spectra are noticeably better. This is also a consequence of many fainter lines below 500 nm that become more prominent and useful for fitting in the high S/N spectra.

The large FoV will allow BlueMUSE to effectively map extended targets, especially in the Local Volume, where resolved nebulae and globular clusters require substantial mosaicking, e.g. the 6×5 mosaic of M42 or the 8×8 mosaic of N180 by respectively Weilbacher et al. (2015) and McLeod et al. (2019). Some nearby galaxies, LSB galaxies and high redshift nebulae require large FoV or moderate mosaics (e.g. Guérou et al., 2016; Daddi et al., 2021; Junais et al., 2024). Even for smaller targets, which do not fill the FoV, a large observing area is of critical importance as it can be used to correctly reduce the sky background. Observing such targets in the blue is not possible now and will not be possible until BlueMUSE is operational. Furthermore, observing the outer regions of systems (e.g. GC, UFD), where the surface brightness is low, requires a large FoV to sample a significant fraction of stars needed for analysis of abundances, SFHs, kinematics and to constrain their dark matter content.

Blue spectral range: BlueMUSE, with its 350 - 580 nm optimised spectrum, will open a new range in the wavelength space, only partially accessible at this moment for large IFS. For the studies targeting the distant Universe the blue wavelength range translates into a specific redshift range, depending on the targeted

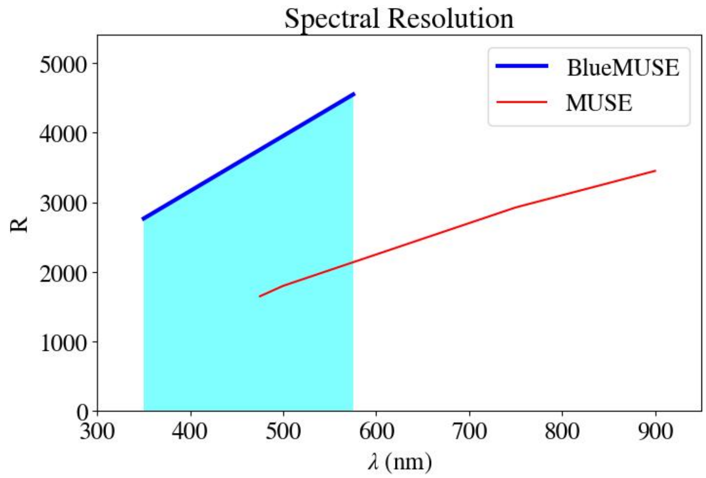

Figure 22: Comparison of BlueMUSE (blue curve) and MUSE (red curve) spectral resolution as a function of wavelength.

emission- or absorption-lines (Fig. 14). As outlined at various places in Section 4, BlueMUSE will open access to the "cosmic noon". For studies of nearby galaxies, resolved nebulae and individual stellar spectra, the blue wavelength range will cover the region below 500nm, which is very rich in spectral lines, allowing estimates of elemental abundances and various physical properties (temperature, density, etc). This is especially true for low metallicity stars, regions and galaxies, where the metal indicators are hardly found in the red part of the spectra. The potential new satellites of the Milky Way, which could be efficiently observed with BlueMUSE to obtain spectra, are also expected to be rather metal poor and therefore will need a blue optimised panoramic IFS to survey them. BlueMUSE will be uniquely positioned to do this efficiently.

High spectral resolution: BlueMUSE spectral resolution varies with wavelength, starting from R$\sim$ 2600 at 350nm, crossing R$\sim$ 3000 at 400nm and the average value of R$\sim$ 3500 at the mid-wavelength range of 465nm, and reaching R$\sim$ 4350 at 580nm (Fig 22). It is at any common wavelength at least a factor of 2 higher than the spectral resolution of MUSE, which allows BlueMUSE to address several science cases in a more efficient way, or even be uniquely suited for them, as emphasised in the previous sections. The fact that the spectral resolution is the highest at the reddest part of the spectrum is not a significant issue for the presented science cases. For studies of emission-lines, it is the local spectral resolution that matters, and the science cases are adapted for the expected variation. An example, based on the calculations with the public BlueMUSE ETC[5], shows that in case of a point-like, spectrally-unresolved emission line at 500 nm (such as the [O III] for PNe, Sect. 3.4), BlueMUSE will typically be 3× faster than MUSE-AO to reach the same 5σ line sensitivity. For absorption-lines studies, such as determination of the RV, or extraction of unresolved stellar kinematics, where the fit is across the full spectral range, significant is the average spectral resolution, where BlueMUSE excels among large IFS.

High sensitivity: One of the main characteristics of the BlueMUSE design is a very high sensitivity, with a throughput reaching up to ∼35% at the peak (end-to-end including atmosphere and telescope) and an average of 30% within the nominal range (350 - 580 nm). A precursor blue-sensitive integral field spectrograph for technology transfer from astronomy to medicine (Schmälzlin et al., 2014; Schmälzlin et al., 2018) based on the MUSE spectrograph layout, was developed by the manufacturer Winlight System (France). This instrument has demonstrated that the expected level of efficiency in the blue is feasible (Moralejo et al., 2016). This makes MUSE and BlueMUSE unique instruments, having the highest sensitivity of all optical spectrographs on VLT at their respective wavelength (Fig. 23). Note also that BlueMUSE+VLT combination will have a larger effective aperture in the blue-UV area than the ELT and any of its instruments[6].

Serendipitous science: Discoveries in astronomy are closely related to the unexplored parameter space opened

[5]BlueMUSE ETC

[6]For example the seeing-limited HARMONI bluest limit is 500 nm with an efficiency of 12% (excluding atmosphere), which is already a factor 3.7 less than BlueMUSE at the same wavelength (44%). Given the telescope aperture difference this translate to a factor 6 in favor of the ELT. The corresponding HARMONI field of view is $9''\times6''$, which is a factor 66 less than the 1 arcmin^2 BlueMUSE field of view. Neglecting possible readout noise impact that might affect the HARMONI seeing limited mode with its tiny spaxels ($0.03''\times0.06''$), BlueMUSE will be approximately 11 times more efficient than HARMONI. Note than HARMONI will not be competitive for any field larger than $17''\times17''$.

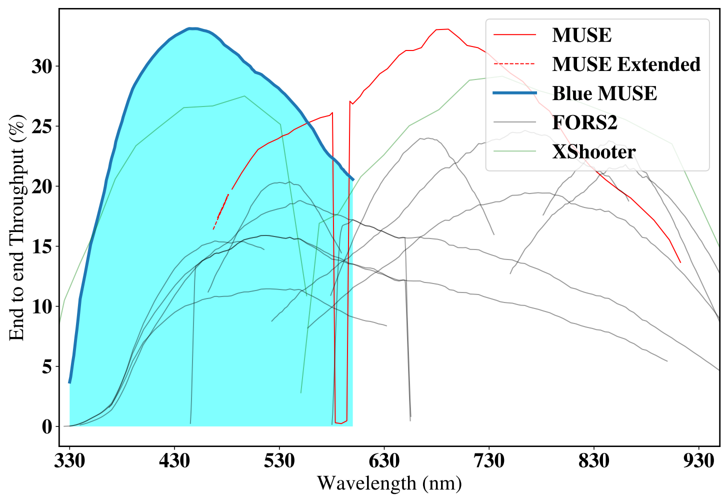

Figure 23: Comparison between the expected BlueMUSE transmission curve (end-to-end, including instrument, telescope and atmosphere) compared to the same transmissions for other spectrographs currently on VLT and working at similar wavelengths and resolution. A 15% slit loss has been included in all slit spectrograph transmissions when compared to the MUSE and BlueMUSE IFUs. We plot the extended wavelength range (330 – 600 nm) for BlueMUSE.

by new instrumentation. Like MUSE, a single BlueMUSE observation provides 60000 spectra over 1700 spectral resolution elements covering one square arcminute in one go. Spectra of all detected objects (stars, distant galaxies) or structures (e.g. giant emission-line nebulae, galaxy disk, bulge, ISM, CGM, IGM) will become available for further analysis. Thanks to its 256 million voxels (volume pixels), each BlueMUSE data cube produced by a single pointing observation is extremely rich in information. Some good examples of the potential richness of the BlueMUSE information content are given in the recent papers by Collier, Smith, and Lucey (2018), Johnston, Puzia, and Eigenthaler (2018), Johnston et al. (2019) and Smith (2020) which report discoveries of rare objects such as low-redshift gravitational lenses, high-redshift dwarf-dwarf pairs, or novae outbursts, all identified from a systematic search of archival MUSE observations. The probability of serendipitous discovery being proportional to the probed volume, BlueMUSE will have at least the same discovery potential as MUSE, but covering a different wavelength range poorly explored by previous and current IFUs. Compared to other MOS instruments or small field IFUs, like KCWI which can only perform pointed observations, BlueMUSE is expected to have a two orders of magnitude higher chance of making serendipitous discoveries.

6.3 Synergies

With an expected first light around 2032, BlueMUSE will be at the telescope at a time when all other major facilities (ELT, JWST in particular) will focus on red and near-infrared wavelengths (see the schematic view Fig. 24). By providing a complement at shorter wavelengths, BlueMUSE will have strong synergies with these facilities, and will be the perfect follow-up spectroscopic instrument at short wavelengths at a time when HST will, presumably, no longer exist. All the science cases presented have synergies with future major facilities, in particular SKA at longer wavelengths, and will benefit from all the targets identified by Euclid, Roman and the Legacy Survey of Space and Time (LSST) in large field imaging. The ALMA Deep Fields are also important as they provide a large number of targets with an overlapping redshift with BlueMUSE. In this respect, BlueMUSE can be viewed as both a “discovery” and a “follow-up” machine. In the former role it will provide targets to other instruments to be observed at higher spatial resolution or at other wavelengths, while in the latter role it will provide spectroscopic coverage in the sense of “spectroscopy of everything” within the FoV. Some examples are provided below.

The unique survey capability and discovery potential of BlueMUSE will be able to provide numerous targets to ELT. At $z = 2$, BlueMUSE and ELT’s first light instrument HARMONI will provide unprecedented science. Indeed, BlueMUSE will provide access to large populations of faint Lyman-alpha emitters whose resolved ionized gas dynamics are currently inaccessible, but will be possible with HARMONI, which is more efficient than JWST/NIRSPEC in the K-band for resolved kinematics (from Hα) at $z = 2$. Similarly, BlueMUSE will be able to provide targets in the range $\sim 2 < z < 3.7$ for MOSAIC and its NIR multiple-IFU mode, to study their CGM and dark matter distribution.

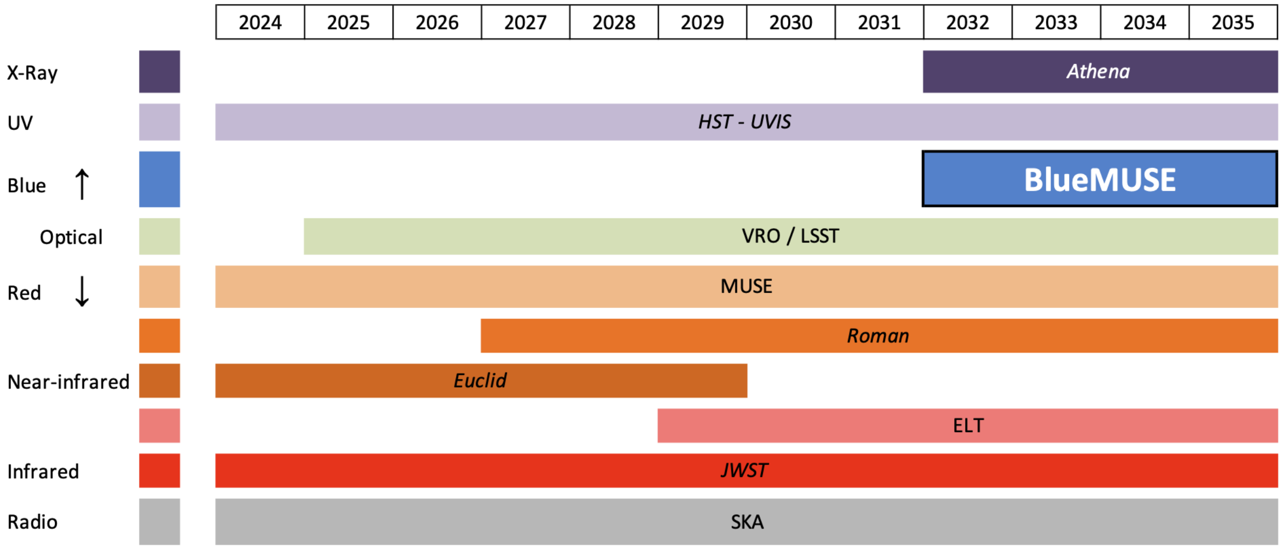

Figure 24: Overview of the BlueMUSE operation timeline in the context of other major future facilities, colour-coded as a function of their main wavelength domain. BlueMUSE will largely complement future facilities focusing on red and near-infrared wavelengths. Note that, given the limited life time of JWST and Euclid, an early availability of BlueMUSE will be an asset for the European community.

Based on the information gathered using the ESO Telescope Bibliography[7], data from different VLT instruments are often used together. This is the case for MUSE as well, with about 33% of papers presenting MUSE data have also used other data sources, where 21% of papers used at least one other instrument. Similar practice can be expected for BlueMUSE. MUSE is certainly the most likely "collaboration" instrument, but among the next generation of VLT instrumentation, MAVIS (IFU) (McDermid et al., 2020) and the long-slit spectrograph CUBES (Genoni et al., 2024) in particular provide ample opportunities for synergies with BlueMUSE. MAVIS has a much smaller FoV ($2.5'' \times 3.6''$), but broader wavelength coverage (370 - 720 nm) and higher resolution (R=5900), with very high spatial resolution, allowing for high spatial resolution followups of BlueMUSE targets. Next to not being an IFS, CUBES' main difference is a very high spectral resolution (R$>$ 20000) and a spectral coverage down to 305 nm, offering a tool for further spectroscopic followup of BlueMUSE targets.

Finally, the synergy between BlueMUSE and MUSE should not be forgotten. BlueMUSE offers a natural extension into the blue spectral region for any field that was already targeted with MUSE, but one can clearly devise combined observations of a specific (new) target, such as a starbursting galaxy, AGN, "jellyfish" galaxy or a galaxy merger, with both instruments, providing a large wavelength base line and an IFU coverage. Some of these targets are characterised by large dust content and significant extinction across large parts of the body, making the observations in the blue more challenging. This is also why some of the related science cases are not included in this work. Nevertheless, BlueMUSE could provide significant contribution assisting observations at red wavelengths in regions where low opacity channels are opened (e.g. Antennae galaxy as an example of a merging systems with a significant Lyman-continuum escape fraction; Weilbacher et al., 2018). Furthermore, a combination of BlueMUSE and MUSE spectra is well suited for investigating the distribution of dust in galaxies and its effects on the observed physical processes. The concatenated long wavelength range will allow the observations of the full Balmer series and in this way provide a powerful measure of the extinction. BlueMUSE is, however, designed as a stand-alone instrument, which does not need other instruments to deliver scientific discoveries. Crucially, it is primarily designed to open a parameters space previously not sufficiently, or not at all, covered with a panoramic IFS.

[7] `https://telbib.eso.org` accessed on 22.01.2025

7 Community Engagement

With its high performance and unique capabilities, BlueMUSE is attractive to a very wide science community, with a large variety of science cases going from Solar System to very distant galaxies. Previous experience has shown how an instrument like MUSE allows very diverse science cases, many of them which were not expected originally. The scientific production rate of MUSE makes it one of the most productive instruments on the planet (recently with more than 200 refereed publications per year[8], see Fig. 25). The most remarkable aspect of the bibliographical statistics is that even after 10 years of operation the number of MUSE papers published per year keeps growing, contrary to a typical experience with all other instruments. We expect BlueMUSE to reach similar levels. We have started to engage the community beyond the consortium while defining the first series of science cases where BlueMUSE will have a strong impact, in the form of a scientific white paper (Richard et al., 2019). The result was very productive, with about 50% of the original white paper contributors (28/61) not being affiliated with BlueMUSE consortium institutes.

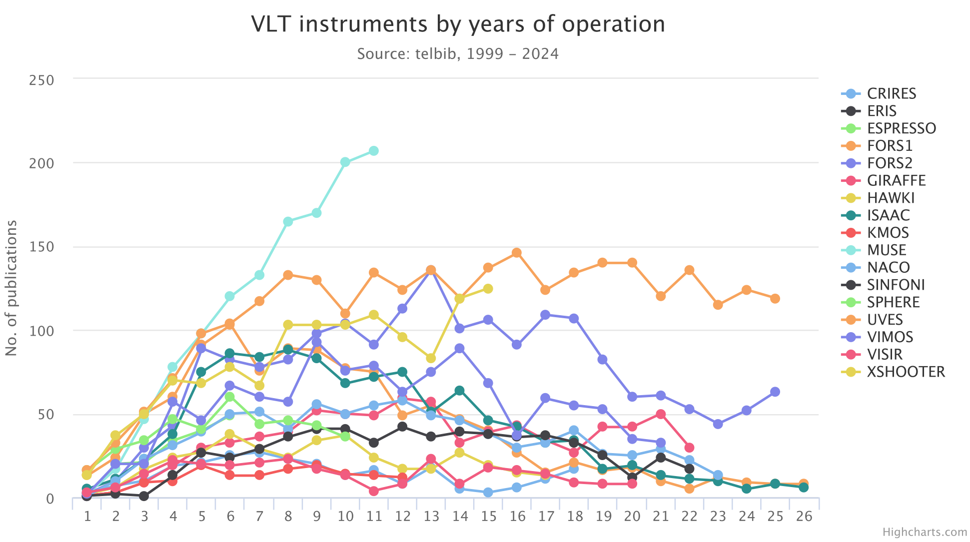

Figure 25: MUSE publication statistics, taken from ESO Telescope Bibliography, showing the number of publications per year based for various ESO instruments. Since the commissioning in 2014 MUSE publication productivity has kept rising without any noticeable saturation. Since 2020 MUSE is the most productive VLT (and ESO) instrument.

This effort has been maintained beyond the white paper through an organisation of two scientific (online) workshops in 2020 about the science that BlueMUSE will achieve and inviting the community to showcase their science ideas[9]. The workshops included a large majority of time dedicated to individual contributions and scientific discussions. Our aim was to bring together the scientific community and discuss the key science cases in relation with the top level requirements and capabilities of BlueMUSE. Furthermore, between 23 - 25. April 2024, we organised a BlueMUSE Science Team meeting[11], inviting as well speakers from the wider community to address some science cases not covered by the consortium, but potentially important for Top Level Requirements specification. Finally, we would like to mention again the very positive feedback from the community of primarily MUSE users that gathered at the ESO conference dedicated to the 10 years of MUSE operations (see footnote 4). The consortium was invited to present BlueMUSE, but it was remarkable to see a number of talks considering BlueMUSE as the next step in investigation of the presented science cases and phenomena. This is not surprising as the breakdown scientific topics addressed by MUSE (Fig. 26) is very similar to those expected by BlueMUSE.

We plan to continue these efforts during all development phases of the instrument, which will include the organisation of workshops, advertising the project to the community through various media channels, while keeping an eye on new or strongly evolving science cases for BlueMUSE. We are determined to reach a diverse community, making BlueMUSE an accessible instrument, both in terms of (computation) resource and a socially inclusive meta-space where members of under-represented groups in science are welcomed and encouraged to contribute. This will be achieved through our outreach efforts, openness to collaborations and a code of conduct accepted by the consortium members.

[8] `http://www.eso.org/sci/php/libraries/telbibstats/vlt-startyear.php`

[9] The first one was scheduled on Mar 30-Apr 1st for the European time zones [10] and the second one on Sep 16-18 for the Australian

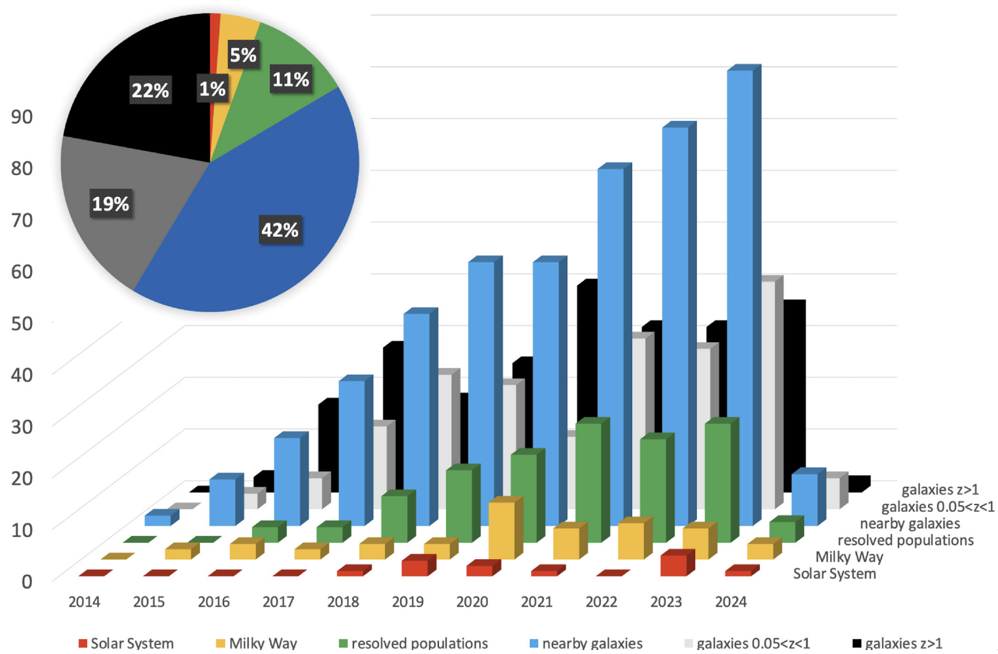

Figure 26: Break down of the MUSE publications by scientific category, highlighting the Solar System, Milky Way, resolved stellar populations, nearby galaxies and redshift regions less or greater than z=1. The main science cases which are studied by the community with MUSE are nearby galaxies, distant galaxies and resolved stellar populations. BlueMUSE can expect a similar distribution, but with a higher emphasis on cases based on the blue wavelength regions, such as resolved stellar populations, star burst and star forming nearby galaxies, and galaxies between $2 < z < 3$. Taken from Roth (2024).

8 Top Level Requirements Analysis

From the science case detailed in the previous sections we have derived a set of top level requirements, which define the main characteristics of BlueMUSE. The performance TLRs are listed in Table 1 at the beginning of the document, and here we summarise them in a decreasing priority.

8.1 Blue wavelength range

The highest priority for BlueMUSE is to provide integral field spectroscopy at blue wavelengths below the 480 nm blue cut-off of MUSE in nominal mode. While the bluest possible wavelength is desirable from the science case, there are other aspects to be taken into consideration. The Paranal atmospheric absorptions (Fig. 27) is the first obvious limitation, it falls below 60% and 40% at respectively 350 and 320 nm. There are also technical limitations due to glass absorption which impact the instrument throughput and cost. The red limit should be as high as possible considering the spectral resolution and sampling, with a minimum value to cover the strong 557.7 nm skyline for improved wavelength calibration and a maximum value below the strong Laser Guide Star (LGS) Na line at 589 nm. The trade-off converge to a spectral range of 350-580 nm, which will be covered on all detectors. We call this the *common* wavelength range. The positions of the slices on detectors, however, allow also for an *extended* wavelength range, such that every third slice will cover the following ranges: 330 - 580 nm, 340 - 590 nm and 350 - 600 nm. These potentially allow some science cases to reach further desirable wavelengths. While in some cases the LGS light will be covered by the BlueMUSE extended wavelength region, the contamination impact is expected to be very limited, and can be masked in the output data, while in the case of required observation for $\lambda > 589$ nm, there are observational procedures in place to avoid crossing the laser beams.

The nominal wavelength range gives access to specific spectral lines in the local Universe, such as the K&H absorption lines and the 4000Å break in the stellar continuum, important diagnostic absorption lines of hot massive stars, and the combination of [O II]λ3727 and [O III]λ5007, as well as the temperature-sensitive auroral line [O III]λ4363 (§3.1) for ionized nebulae. In the distant Universe, blue wavelengths allow to observe Ly-α (121.6

time zones.

[11] https://bluemuse.univ-lyon1.fr/index.php/science-team-meeting-2024/

nm) already at $z = 2$, near the peak of the cosmic SFR, with an advantageous reduction in surface brightness dimming (§4.2)

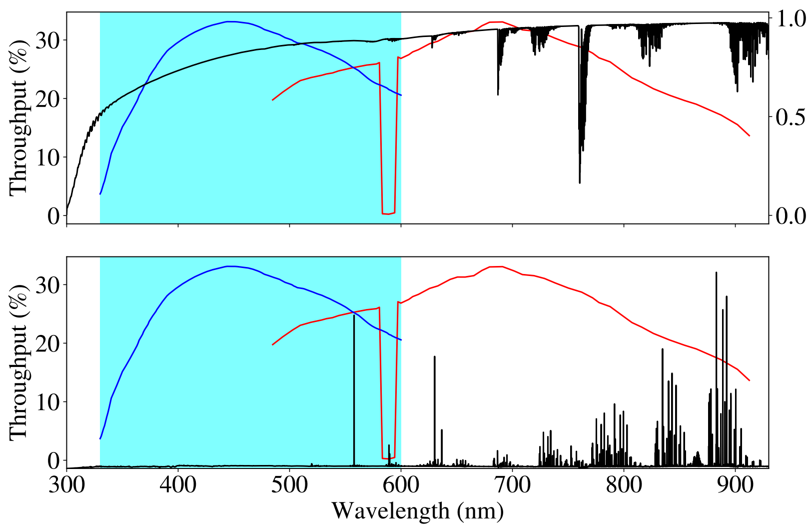

Figure 27: Comparison between the end-to-end (including telescope and atmosphere) BlueMUSE (blue curve) and MUSE (red curve) sensitivities, plotted together with the atmospheric transmission (top panel) and sky emission (bottom panel). We plot the extended wavelength (330 - 600 nm) coverage for BlueMUSE.

8.2 Spectral resolution, line spread function, sampling and calibration accuracy

The spectral resolution is the second highest priority. MUSE achieved a resolving power of 2700 at 700 nm, but only 1700 at 480 nm. For BlueMUSE we aim at a spectral resolution which is at least twice that of MUSE in the same wavelength region. Such resolution ensure the measurements of small velocity shifts and velocity dispersions, which is important in particular for the stellar science cases (§2.1, 2.3, 3.4 and 3.5). It also provides more precise spectral line profiles, which allows for a more precise physical modelling of the emission or absorption, resolve line doublets, as well as study variations of line shapes across an object (§3.1,4.3).

The spectra will be dispersed on the detector such that at least two pixels in the spectral directions cover the LSF and the Nyquist sampling condition is fulfilled. As the sampling of the LSF is expected to vary across the FoV, and to ensure the Nyquist sampling, the FWHM of the LSF sampled will be sampled with at least 2.1 – 2.2 pixels. In the spectral dimension each pixel will sample the wavelength at 0.66 Å, so the FWHM of the LSF can be expected to be about $\sim 1.32 - 1.45$ Å.

The trade-off between spectral resolution, spectral range, spectral sampling and detector size leads to a spectral resolution of $R = 2600 - 4350$ across the wavelength range, with an average of $R = 3500$, which is twice the one from MUSE in the region of overlap (Fig. 22). Shortening the spectral wavelength (e.g. the red cutoff) would increase the resolution, but a significant increase (i.e average $R \sim 5000$) would require a drastic cut (below 500 nm) and impair desired BlueMUSE capabilities.

The quality of observations also depends on the accuracy at which the wavelength solution is calibrated. This is in particular important for kinematical and dynamical studies and sciences cases investigating the properites of resolved gas in galaxies (e.g. §2.2, 3.1 or 3.5). BlueMUSE will follow the example of MUSE and achieve a precision of 3 – 6 km/s (or 1/20 of the spectral resolution element).

8.3 Throughput and limiting magnitude

Throughput is very important for the overall survey speed, as already seen with the MUSE instrument. Furthermore, at blue wavelengths, the instrument throughput has to maintain a high value to compensate for the decrease in atmospheric transmission, in particular at $\lambda < 400$ nm (Fig. 27). Last, but not least, given the cost and pressure of 8m-class telescope time, high throughput in practice makes the difference between feasible and non-feasible observations.

Based on the end-to-end MUSE transmission curve, taking into account state-of-the art CCD QE, VPH grating, optimised optical design, we aim to an overall end-to-end BlueMUSE average throughput within the nominal wavelength range of $\sim 30\%$ (including telescope and atmosphere; Fig. 27). With such a throughput, BlueMUSE will be the most efficient instrument in the blue on an 8m-class telescope. Furthermore, the minimum throughout, including the blue end (350 nm) will be higher than 15% across the common wavelength range.

A number of science cases are ambitions in terms of the faintness of their targets. In order to make these observations realistic BlueMUSE will be able to provide observations of S/N of 5 for a point source of 22.9 V-mag (AB) within 1h of on-source observations. This will be achieved at the reference wavelength of 400 nm, airmass of 1.2 and Moon FLI of 0 (dark). For extended targets, the same S/N will be achieved for targets of V(AB) = 23.4 mag/$''^2$, within the same observing conditions.

8.4 Field of view and spatial sampling

BlueMUSE will have a FoV similar to MUSE (1 arcmin^2). Large observing area is crucial for survey speed, and BlueMUSE will be able to maintain the efficiency delivered by MUSE in this respect. In addition, a large area will always be beneficial for expanding the discovery space and the number of serendipitous discoveries, even when the main target of interest does not cover the entire FoV. Many astrophysical sources (e.g., extended nearby galaxies § 3.2, lensing cluster cores § 4.4) have physical sizes well suited to the BlueMUSE FoV and will require only minimal mosaicking.

BlueMUSE will operate as a seeing limited instrument and its spatial sampling will be adapted to the typical seeing conditions at Paranal. At 580 nm the best expected seeing conditions are 0.6$''$ FWHM and should be sampled by at least 2 pixels. Pursuing a cost effective design, BlueMUSE will feature rectangular spaxels, with size defined through the geometrical mean $\mu = \sqrt{s_1 \times s_2}$, where s_1 and s_2 are the two respective dimensions of the rectangular spaxel. The spatial sampling across the BlueMUSE FoV will then be $0.2 < \mu < 0.3$. Such definition ensures sufficient size of the BlueMUSE spaxels across the full FoV with $0.18'' < s_1 < 0.22''$ and $0.3'' < s_2 < 0.35''$. Crucially, while rectangular spaxels provide a cost effective design, as Fig. 28 shows, their larger spaxel area also ensures that BlueMUSE will be background limited for execution times longer than 15-20 min, allowing efficient observations of deep fields.

Typical observations with BlueMUSE will consists of several rotations by 90 degrees (as is the case for MUSE) in order to minimise instrumental effects. The individual exposures will be combined during the data reduction, and the original rectangular spaxels resampled onto a grid of square spaxels (for example of a size of $0.25'' \times 0.25''$), allowing for an easier scientific analysis and high image quality.

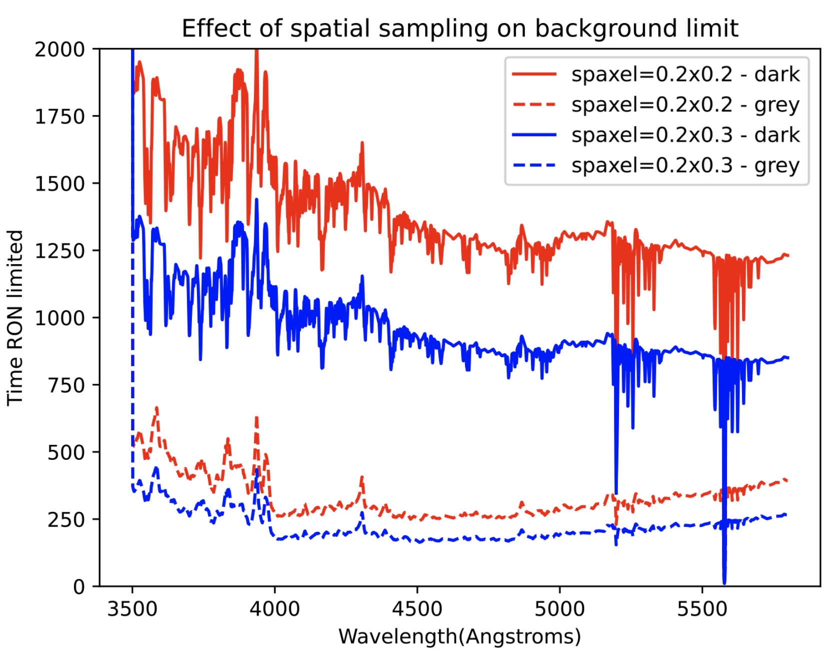

Figure 28: BlueMUSE exposure time needed to reach equivalent noise contributions between detector readout noise (RON) and Poisson noise generated by the background sky. The exposure time assumes a faint source (negligible photon noise contribution) and $3e^-$ RON per pixel. The red and blue curves show MUSE-like 0.2$''$ square spaxels and the selected BlueMUSE $0.2'' \times 0.3''$ rectangular spaxels respectively, under two background levels (grey or dark conditions). With 0.2$''$ square spaxels we would always be readout noise-limited in the blue for exposures shorter than 1500 sec, which would limit the performance in deep fields. The use of rectangular spaxels strongly mitigates this effect.

8.5 Image quality and stability

The instrument image quality (IQ) requirement has been defined to minimise its contribution to the final image quality taking into account Paranal atmospheric parameters, but not the telescope. The main contributor to the deteriorate image quality are the “wobble” of the derotator and the differential atmospheric dispersion. The former effect is most prominent when observations are done close to the zenith (high airmass), while the latter are dominant when the observations are at low inclination (low airmass). This effect is well known and measurable for MUSE observations, which can be used to put constraints on the image quality that BlueMUSE will be able to provide. In order not to degrade the input image quality by more than 25%, the intrinsic BlueMUSE image quality (instrument point-spread function) needs to have a FWHM lower than $0.42''$.

As mentioned above, even though BlueMUSE has rectangular spaxels, based on our simulations (see Section 5 and Wendt et al., 2024) we do not expect any deterioration of the final PSF (Fig 20) even in excellent observing conditions. This is due to the fact that the aspect ratio of the sides of the rectangle is small (1:1.5) and that BlueMUSE is a seeing limited instrument; even at the best natural seeng the BlueMUSE PSF of an unresolved point source is approximately circular.

Stability is key for long integration. On the other hand, the experience with MUSE shows that there are rarely exposures longer than 30 min. Nevertheless, the science cases require a certain level of stability, in both the spatial and spectral dimensions. This means that we will aim to have calibrated reduced data to be accurate to 0.1 pixel (spatial and spectral) based solely on calibrations taken during daytime, with an illumination difference within 10% over the full FoV (during the night-time observations). This aspect of the instrument, including the thermal stability will be studied during the subsequent phases, using MUSE for tests and as a template.

9 Conclusion

In this document, we have presented a selection of science cases where we believe BlueMUSE will have a very strong impact due to its unique capabilities. They were selected as cases that push and define the capabilities of the instrument (as specified through TLRs), and they represent only a fraction of the science allowed by a blue-optimised wide-field monolithic IFU. We do not address investigations of merging galaxies, active galactic nuclei, tidal dwarfs, star formation in massive disks, stellar populations of rejuvenating early-type galaxies, galactic winds and outflows, or follow-ups of gravitational wave emitting events. They all make obvious science cases for BlueMUSE, but including them is beyond the purpose of this document. Indeed, we expect BlueMUSE to be a transformative instrument for many science cases, anticipating a number of new science cases that will arise by the time of the first light. By focusing on the blue/UV wavelength range, at a time where many new facilities will be operating at red/IR wavelengths, BlueMUSE will open up new discovery space, while allowing more MUSE-like science for the benefit of the community.

During the last three years of the pre-phase and Phase A development, the science cases for BlueMUSE have well matured. They have enabled us to derive ambitious top level requirements with prioritisation of certain instrumental characteristics. We have assembled a strong consortium science team that is eager to start preparing the general science cases towards well a defined set of observations design to answer specific questions. Furthermore, the enthusiastic feedback we get from the large and diverse user community reinforces our will to proceed and deliver a world class instrument capable of new discoveries.

A Appendix: A

References

[1] R. Augustin et al. "Emission from the circumgalactic medium: from cosmological zoom-in simulations to multiwavelength observables". In: MNRAS 489.2 (Oct. 2019), pp. 2417–2438. arXiv: 1909.02575 [astro-ph.GA].

[2] R. Bacon et al. "The MUSE 3D view of the Hubble Deep Field South". In: A&A 575, A75 (Mar. 2015), A75. arXiv: 1411.7667.

[3] R. Bacon et al. "The MUSE Extremely Deep Field: The cosmic web in emission at high redshift". In: A&A 647, A107 (Mar. 2021), A107. arXiv: 2102.05516 [astro-ph.CO].

[4] R. Bacon et al. "The MUSE Hubble Ultra Deep Field Survey. I. Survey description, data reduction, and source detection". In: A&A 608, A1 (Nov. 2017), A1. arXiv: 1710.03002.

[5] R. Bacon et al. "The MUSE second-generation VLT instrument". In: *Ground-based and Airborne Instrumentation for Astronomy III*. Vol. 7735. Proc. SPIE. July 2010, p. 773508.

[6] D. Barat et al. "SHαDE: survey description and mass-kinematics scaling relations for dwarf galaxies". In: MNRAS 498.4 (Nov. 2020), p. 5885. arXiv: 2009.04453 [astro-ph.GA].

[7] D. Barat et al. "The SAMI Galaxy Survey: mass-kinematics scaling relations". In: MNRAS 487.2 (Aug. 2019), p. 2924. arXiv: 1905.12637 [astro-ph.GA].

[8] N. Bastian and C. Lardo. "Multiple Stellar Populations in Globular Clusters". In: ARA&A 56 (Sept. 2018), pp. 83–136. arXiv: 1712.01286 [astro-ph.SR].

[9] V. Belokurov. "Galactic Archaeology: The dwarfs that survived and perished". In: New Astr. Rev. 57 (Sept. 2013), pp. 100–121. arXiv: 1307.0041.

[10] N. Bergvall et al. "First detection of Lyman continuum escape from a local starburst galaxy. I. Observations of the luminous blue compact galaxy Haro 11 with the Far Ultraviolet Spectroscopic Explorer (FUSE)". In: A&A 448 (Mar. 2006), pp. 513–524.

[11] Serena Bertone and Joop Schaye. "Rest-frame ultraviolet line emission from the intergalactic medium at $2 \leq z \leq 5$". In: MNRAS 419.1 (Jan. 2012), pp. 780–798. arXiv: 1008.1791 [astro-ph.CO].

[12] F. Bian et al. "High Lyman Continuum Escape Fraction in a Lensed Young Compact Dwarf Galaxy at z = 2.5". In: ApJ 837, L12 (Mar. 2017), p. L12. arXiv: 1702.06540.

[13] A. Bik et al. "Super star cluster feedback driving ionization, shocks and outflows in the halo of the nearby starburst ESO 338-IG04". In: A&A 619, A131 (Nov. 2018), A131. arXiv: 1809.03597.

[14] J. Bland-Hawthorn and K. C. Freeman. "Galaxy Genesis - Unravelling the Epoch of Dissipation in the Early Disk". In: PASA 21 (2004), pp. 110–120. eprint: astro-ph/0403700.

[15] Joss Bland-Hawthorn et al. "The GALAH survey and Gaia DR2: dissecting the stellar disc's phase space by age, action, chemistry, and location". In: MNRAS 486.1 (June 2019), pp. 1167–1191. arXiv: 1809.02658 [astro-ph.GA].

[16] M. R. Blanton et al. "The Properties and Luminosity Function of Extremely Low Luminosity Galaxies". In: ApJ 631 (Sept. 2005), pp. 208–230. eprint: astro-ph/0410164.

[17] S. Boissier et al. "Chemical and spectrophotometric evolution of low surface brightness galaxies". In: MNRAS 343 (Aug. 2003), pp. 653–664. eprint: astro-ph/0304313.

[18] S. Boissier et al. "The properties of the Malin 1 galaxy giant disk. A panchromatic view from the NGVS and GUViCS surveys". In: A&A 593, A126 (Oct. 2016), A126. arXiv: 1610.00918.

[19] R. Bordoloi et al. "The Dependence of Galactic Outflows on the Properties and Orientation of zCOSMOS Galaxies at z ˜ 1". In: ApJ 794, 130 (Oct. 2014), p. 130. arXiv: 1307.6553.

[20] E. Borisova et al. “Ubiquitous Giant Lyα Nebulae around the Brightest Quasars at $z \sim 3.5$ Revealed with MUSE”. In: ApJ 831, 39 (Nov. 2016), p. 39. arXiv: 1605.01422.

[21] S. Borthakur et al. “A local clue to the reionization of the universe”. In: *Science* 346 (Oct. 2014), pp. 216–219. arXiv: 1410.3511.

[22] A. Boselli et al. “Quenching of the star formation activity in cluster galaxies”. In: A&A 596, A11 (Nov. 2016), A11. arXiv: 1609.00545.

[23] Alessandro Boselli and Giuseppe Gavazzi. “Environmental Effects on Late-Type Galaxies in Nearby Clusters”. In: PASP 118.842 (Apr. 2006), pp. 517–559. arXiv: astro-ph/0601108 [astro-ph].

[24] N. Bouché et al. “Signatures of Cool Gas Fueling a Star-Forming Galaxy at Redshift 2.3”. In: *Science* 341 (July 2013), pp. 50–53. arXiv: 1306.0134 [astro-ph.CO].

[25] F. Bresolin et al. “Extragalactic Chemical Abundances: Do H II Regions and Young Stars Tell the Same Story? The Case of the Spiral Galaxy NGC 300”. In: ApJ 700 (July 2009), pp. 309–330. arXiv: 0905.2791 [astro-ph.CO].

[26] Fabio Bresolin, Robert C. Kennicutt, and Emma Ryan-Weber. “Gas Metallicities in the Extended Disks of NGC 1512 and NGC 3621. Chemical Signatures of Metal Mixing or Enriched Gas Accretion?” In: ApJ 750.2, 122 (May 2012), p. 122. arXiv: 1203.0956 [astro-ph.CO].

[27] James S. Bullock and Michael Boylan-Kolchin. “Small-Scale Challenges to the ΛCDM Paradigm”. In: ARA&A 55.1 (Aug. 2017), pp. 343–387. arXiv: 1707.04256 [astro-ph.CO].

[28] Kevin Bundy et al. “Overview of the SDSS-IV MaNGA Survey: Mapping nearby Galaxies at Apache Point Observatory”. In: ApJ 798.1, 7 (Jan. 2015), p. 7. arXiv: 1412.1482 [astro-ph.GA].

[29] Alberto Buzzoni, Magda Arnaboldi, and Romano L. M. Corradi. “Planetary nebulae as tracers of galaxy stellar populations”. In: MNRAS 368.2 (May 2006), pp. 877–894. arXiv: astro-ph/0602458 [astro-ph].

[30] Michele Cappellari. “Full spectrum fitting with photometry in PPXF: stellar population versus dynamical masses, non-parametric star formation history and metallicity for 3200 LEGA-C galaxies at redshift z $\approx$ 0.8”. In: MNRAS 526.3 (Dec. 2023), pp. 3273–3300. arXiv: 2208.14974 [astro-ph.GA].

[31] Michele Cappellari. “Structure and Kinematics of Early-Type Galaxies from Integral Field Spectroscopy”. In: ARA&A 54 (Sept. 2016), pp. 597–665. arXiv: 1602.04267 [astro-ph.GA].

[32] Michele Cappellari and Eric Emsellem. “Parametric Recovery of Line-of-Sight Velocity Distributions from Absorption-Line Spectra of Galaxies via Penalized Likelihood”. In: PASP 116.816 (Feb. 2004), pp. 138–147. arXiv: astro-ph/0312201 [astro-ph].

[33] Michele Cappellari et al. “The ATLAS^{3D} project - VII. A new look at the morphology of nearby galaxies: the kinematic morphology-density relation”. In: MNRAS 416.3 (Sept. 2011), pp. 1680–1696. arXiv: 1104.3545 [astro-ph.CO].

[34] E. Carrasco et al. “MEGARA, the R=6000-20000 IFU and MOS of GTC”. In: Proc. SPIE. Vol. 10702. Society of Photo-Optical Instrumentation Engineers (SPIE) Conference Series. July 2018, p. 1070216.

[35] N. Castro et al. “Mapping the core of the Tarantula Nebula with VLT-MUSE. I. Spectral and nebular content around R136”. In: A&A 614, A147 (June 2018), A147. arXiv: 1802.01597.

[36] N. Castro et al. “Mapping the core of the Tarantula Nebula with VLT-MUSE. II. The spectroscopic Hertzsprung-Russell diagram of OB stars in NGC 2070”. In: A&A 648, A65 (Apr. 2021), A65. arXiv: 2102.03372 [astro-ph.SR].

[37] N. Castro et al. “The spectroscopic Hertzsprung-Russell diagram of Galactic massive stars”. In: A&A 570, L13 (Oct. 2014), p. L13. arXiv: 1410.3499 [astro-ph.SR].

[38] D. Ceverino and A. Klypin. “The Role of Stellar Feedback in the Formation of Galaxies”. In: ApJ 695 (Apr. 2009), pp. 292–309. arXiv: 0712.3285.

[39] Aeree Chung and M. Bureau. “Stellar Kinematics of Boxy Bulges: Large-Scale Bars and Inner Disks”. In: AJ 127.6 (June 2004), pp. 3192–3212. arXiv: astro-ph/0403232 [astro-ph].

[40] Chul Chung, Suk-Jin Yoon, and Young-Wook Lee. “The Effect of Helium-enhanced Stellar Populations on the Ultraviolet-upturn Phenomenon of Early-type Galaxies”. In: ApJ 740.2, L45 (Oct. 2011), p. L45. arXiv: 1109.3463 [astro-ph.GA].

[41] A. Claeyssens et al. “Spectral variations of Lyman α emission within strongly lensed sources observed with MUSE”. In: MNRAS 489.4 (Nov. 2019), pp. 5022–5029. arXiv: 1909.01692 [astro-ph.GA].

[42] W. P. Collier, R. J. Smith, and J. R. Lucey. “A new strong-lensing galaxy at z= 0.066: another elliptical galaxy with a lightweight IMF”. In: MNRAS 478 (Aug. 2018), pp. 1595–1600. arXiv: 1803.07082.

[43] Charlie Conroy and Pieter G. van Dokkum. “The Stellar Initial Mass Function in Early-type Galaxies From Absorption Line Spectroscopy. II. Results”. In: ApJ 760.1, 71 (Nov. 2012), p. 71. arXiv: 1205.6473 [astro-ph.CO].

[44] Edvige Corbelli et al. “From molecules to young stellar clusters: the star formation cycle across the disk of M 33”. In: A&A 601, A146 (May 2017), A146. arXiv: 1703.09183 [astro-ph.GA].

[45] Scott M. Croom et al. “The Sydney-AAO Multi-object Integral field spectrograph”. In: MNRAS 421.1 (Mar. 2012), pp. 872–893. arXiv: 1112.3367 [astro-ph.CO].

[46] P. A. Crowther. “Physical Properties of Wolf-Rayet Stars”. In: ARA&A 45 (Sept. 2007), pp. 177–219. eprint: astro-ph/0610356.

[47] P. A. Crowther and J. L. Bibby. “On the massive star content of the nearby dwarf irregular Wolf-Rayet galaxy IC 4662”. In: A&A 499 (May 2009), pp. 455–464. arXiv: 0903.2288.

[48] E. Daddi et al. “Evidence for Cold-stream to Hot-accretion Transition as Traced by Lyα Emission from Groups and Clusters at 2 ¡ z ¡ 3.3”. In: ApJ 926.2, L21 (Feb. 2022), p. L21. arXiv: 2202.03715 [astro-ph.CO].

[49] E. Daddi et al. “The bending of the star-forming main sequence traces the cold- to hot-accretion transition mass over 0 ¡ z ¡ 4”. In: A&A 661, L7 (May 2022), p. L7. arXiv: 2203.10880 [astro-ph.CO].

[50] E. Daddi et al. “Three Lyman-α-emitting filaments converging to a massive galaxy group at z = 2.91: discussing the case for cold gas infall”. In: A&A 649, A78 (May 2021), A78. arXiv: 2006.11089 [astro-ph.GA].

[51] S. de Barros et al. “An extreme [O III] emitter at z = 3.2: a low metallicity Lyman continuum source”. In: A&A 585, A51 (Jan. 2016), A51. arXiv: 1507.06648.

[52] Tim de Zeeuw and Marijn Franx. “Structure and dynamics of elliptical galaxies.” In: ARA&A 29 (Jan. 1991), pp. 239–274.

[53] A. Dekel et al. “Cold streams in early massive hot haloes as the main mode of galaxy formation”. In: Nature 457 (Jan. 2009), pp. 451–454. arXiv: 0808.0553.

[54] Lorenza Della Bruna et al. “Stellar feedback in M 83 as observed with MUSE. II. Analysis of the H II region population: Ionisation budget and pre-SN feedback”. In: A&A 666, A29 (Oct. 2022), A29. arXiv: 2206.09741 [astro-ph.GA].

[55] Lorenza Della Bruna et al. “Studying the ISM at ∼10 pc scale in NGC 7793 with MUSE. II. Constraints on the oxygen abundance and ionising radiation escape”. In: A&A 650, A103 (June 2021), A103. arXiv: 2104.08088 [astro-ph.GA].

[56] Lorenza Della Bruna et al. “Studying the ISM at ∼10 pc scale in NGC 7793 with MUSE. II. Constraints on the oxygen abundance and ionising radiation escape (Corrigendum)”. In: A&A 663, C2 (July 2022), p. C2.

[57] M. Dijkstra, M. Gronke, and A. Venkatesan. “The Lyα-LyC Connection: Evidence for an Enhanced Contribution of UV-faint Galaxies to Cosmic Reionization”. In: ApJ 828, 71 (Sept. 2016), p. 71. arXiv: 1604.08208.

[58] G. Dorman, D. M. Pierce, and A. L. Cochran. “The Spatial Distribution of C_2, C_3, and NH in Comet 2P/Encke”. In: ApJ 778, 140 (Dec. 2013), p. 140.

[59] A. B. Drake et al. "The MUSE Hubble Ultra Deep Field Survey. VI. The faint-end of the Lyα luminosity function at $2.91 < z < 6.64$ and implications for reionisation". In: A&A 608, A6 (Nov. 2017), A6. arXiv: 1711.03095.

[60] A. Drlica-Wagner et al. "Eight Ultra-faint Galaxy Candidates Discovered in Year Two of the Dark Energy Survey". In: ApJ 813, 109 (Nov. 2015), p. 109. arXiv: 1508.03622.

[61] Eric Emsellem et al. "The ATLAS^{3D} project - III. A census of the stellar angular momentum within the effective radius of early-type galaxies: unveiling the distribution of fast and slow rotators". In: MNRAS 414.2 (June 2011), pp. 888–912. arXiv: 1102.4444 [astro-ph.CO].

[62] Eric Emsellem et al. "The PHANGS-MUSE survey. Probing the chemo-dynamical evolution of disc galaxies". In: A&A 659, A191 (Mar. 2022), A191. arXiv: 2110.03708 [astro-ph.GA].

[63] Santiago Erroz-Ferrer et al. "The MUSE Atlas of Disks (MAD): resolving star formation rates and gas metallicities on <100 pc scales†". In: MNRAS 484.4 (Apr. 2019), pp. 5009–5027. arXiv: 1901.04493 [astro-ph.GA].

[64] C. Esteban et al. "Carbon and oxygen abundances from recombination lines in low-metallicity star-forming galaxies. Implications for chemical evolution". In: MNRAS 443.1 (Sept. 2014), pp. 624–647. arXiv: 1406.3986 [astro-ph.GA].

[65] César Esteban et al. "Keck HIRES Spectroscopy of Extragalactic H II Regions: C and O Abundances from Recombination Lines". In: ApJ 700.1 (July 2009), pp. 654–678. arXiv: 0905.2532 [astro-ph.CO].

[66] C. Evans et al. "The VLT-FLAMES Survey of Massive Stars". In: *The Messenger* 122 (Dec. 2005), pp. 36–38.

[67] C. Evans et al. "The VLT FLAMES Tarantula Survey". In: *The Messenger* 145 (Sept. 2011), pp. 33–38.

[68] C. J. Evans et al. "The VLT-FLAMES survey of massive stars: Observations in the Galactic clusters NGC 3293, NGC 4755 and NGC 6611". In: A&A 437 (July 2005), pp. 467–482. eprint: astro-ph/0503655.

[69] C. J. Evans et al. "The VLT-FLAMES Tarantula Survey. I. Introduction and observational overview". In: A&A 530, A108 (June 2011), A108. arXiv: 1103.5386 [astro-ph.SR].

[70] J. Falcón-Barroso et al. "The CALIFA view on stellar angular momentum across the Hubble sequence". In: A&A 632, A59 (Dec. 2019), A59. arXiv: 1910.06236 [astro-ph.GA].

[71] X. Fang and X.-W. Liu. "Very deep spectroscopy of the bright Saturn nebula NGC 7009 - I. Observations and plasma diagnostics". In: MNRAS 415 (July 2011), pp. 181–198. arXiv: 1103.1705 [astro-ph.SR].

[72] L. Ferrarese et al. "The Next Generation Virgo Cluster Survey (NGVS). I. Introduction to the Survey". In: ApJS 200, 4 (May 2012), p. 4.

[73] Thomas J. Fletcher et al. "The Lyman Continuum Escape Survey: Ionizing Radiation from [O III]-strong Sources at a Redshift of 3.1". In: ApJ 878.2, 87 (June 2019), p. 87. arXiv: 1806.01741 [astro-ph.GA].

[74] L. M. R. Fogarty et al. "The SAMI Pilot Survey: the kinematic morphology-density relation in Abell 85, Abell 168 and Abell 2399". In: MNRAS 443.1 (Sept. 2014), pp. 485–503. arXiv: 1406.3899 [astro-ph.GA].

[75] M. Fossati et al. "A Virgo Environmental Survey Tracing Ionised Gas Emission (VESTIGE). II. Constraining the quenching time in the stripped galaxy NGC 4330". In: A&A 614, A57 (June 2018), A57. arXiv: 1801.09685.

[76] A. Fraser-McKelvie et al. "The GECKOS Survey: Identifying kinematic sub-structures in edge-on galaxies". In: *arXiv e-prints*, arXiv:2411.03430 (Nov. 2024), arXiv:2411.03430. arXiv: 2411.03430 [astro-ph.GA].

[77] Michele Fumagalli et al. "Witnessing galaxy assembly in an extended z$\approx$3 structure". In: MNRAS 471 (Nov. 2017), pp. 3686–3698. arXiv: 1707.07003 [astro-ph.GA].

[78] Dimitri A. Gadotti et al. "Time Inference with MUSE in Extragalactic Rings (TIMER): properties of the survey and high-level data products". In: MNRAS 482.1 (Jan. 2019), pp. 506–529. arXiv: 1810.01425 [astro-ph.GA].

[79] Miriam Garcia et al. “Massive stars in extremely metal-poor galaxies: a window into the past”. In: *Experimental Astronomy* 51.3 (June 2021), pp. 887–911.

[80] J. García-Rojas et al. “Faint emission lines in the Galactic HII regions M16, M20 and NGC 3603*”. In: MNRAS 368.1 (May 2006), pp. 253–279. arXiv: `astro-ph/0601595 [astro-ph]`.

[81] Karl Gebhardt et al. “The Hobby-Eberly Telescope Dark Energy Experiment (HETDEX) Survey Design, Reductions, and Detections”. In: ApJ 923.2, 217 (Dec. 2021), p. 217. arXiv: `2110.04298 [astro-ph.IM]`.

[82] Matteo Genoni et al. “CUBES, the Cassegrain U-Band Efficient Spectrograph: towards final design review”. In: *Ground-based and Airborne Instrumentation for Astronomy X*. Ed. by Julia J. Bryant, Kentaro Motohara, and Joël. R. D. Vernet. Vol. 13096. Society of Photo-Optical Instrumentation Engineers (SPIE) Conference Series. July 2024, 130967T. arXiv: `2412.03460 [astro-ph.IM]`.

[83] O. E. Gerhard. “Line-of-sight velocity profiles in spherical galaxies: breaking the degeneracy between anisotropy and mass.” In: MNRAS 265 (Nov. 1993), p. 213.

[84] B. Giesers et al. “A detached stellar-mass black hole candidate in the globular cluster NGC 3201”. In: MNRAS 475 (Mar. 2018), pp. L15–L19. arXiv: `1801.05642 [astro-ph.SR]`.

[85] A. Gil de Paz et al. “Discovery of an Extended Ultraviolet Disk in the Nearby Galaxy NGC 4625”. In: ApJ 627 (July 2005), pp. L29–L32. eprint: `astro-ph/0506357`.

[86] R. Gobat et al. “A mature cluster with X-ray emission at z = 2.07”. In: A&A 526, A133 (Feb. 2011), A133. arXiv: `1011.1837`.

[87] R. Gobat et al. “WFC3 GRISM Confirmation of the Distant Cluster Cl J1449+0856 at z = 2.00: Quiescent and Star-forming Galaxy Populations”. In: ApJ 776, 9 (Oct. 2013), p. 9. arXiv: `1305.3576`.

[88] Paul Goudfrooij. “Dissolved Massive Metal-rich Globular Clusters Can Cause the Range of UV Upturn Strengths Found among Early-type Galaxies”. In: ApJ 857.1, 16 (Apr. 2018), p. 16. arXiv: `1804.00668 [astro-ph.GA]`.

[89] Mark T. Graham et al. “Complete census of massive slow rotators in ten large galaxy clusters”. In: *arXiv e-prints*, arXiv:1911.06103 (Nov. 2019), arXiv:1911.06103. arXiv: `1911.06103 [astro-ph.GA]`.

[90] A. Guérou et al. “Exploring the mass assembly of the early-type disc galaxy NGC 3115 with MUSE”. In: A&A 591, A143 (July 2016), A143. arXiv: `1605.07667 [astro-ph.GA]`.

[91] Yucheng Guo et al. “Bipolar outflows out to 10 kpc for massive galaxies at redshift z $\approx$ 1”. In: Nature 624.7990 (Dec. 2023), pp. 53–56. arXiv: `2312.05167 [astro-ph.GA]`.

[92] Vasilii V. Gvaramadze et al. “Two Circumstellar Nebulae Discovered with the Wide-field Infrared Survey Explore and Their Massive Central Stars”. In: AJ 157.2, 53 (Feb. 2019), p. 53. arXiv: `1812.00007 [astro-ph.SR]`.

[93] Maximilian Häberle et al. “Author Correction: Fast-moving stars around an intermediate-mass black hole in ω Centauri”. In: Nature 634.8032 (Oct. 2024), E1–E1.

[94] L. M. Z. Hagen et al. “On the Classification of UGC 1382 as a Giant Low Surface Brightness Galaxy”. In: ApJ 826, 210 (Aug. 2016), p. 210. arXiv: `1607.02147`.

[95] J. Hartke et al. “Planetary nebulae populations in the haloes of nearby massive early-type galaxies”. In: *arXiv e-prints*, arXiv:2312.02587 (Dec. 2023), arXiv:2312.02587. arXiv: `2312.02587 [astro-ph.GA]`.

[96] D. Harvey et al. “A detection of wobbling brightest cluster galaxies within massive galaxy clusters”. In: MNRAS 472 (Dec. 2017), pp. 1972–1980. arXiv: `1703.07365`.

[97] T. Hashimoto et al. “The MUSE Hubble Ultra Deep Field Survey. X. Lyα equivalent widths at 2.9 < z < 6.6”. In: A&A 608, A10 (Nov. 2017), A10. arXiv: `1711.01747`.

[98] T. Hashimoto et al. “The Star Formation Rate and Metallicity of the Host Galaxy of the Dark GRB 080325 at z=1.78”. In: ApJ 806, 250 (June 2015), p. 250. arXiv: `1411.3357`.

[99] Tomoki Hayashino et al. “Large-Scale Structure of Emission-Line Galaxies at z=3.1”. In: AJ 128.5 (Nov. 2004), pp. 2073–2079.

[100] E. C. Herenz et al. “The MUSE-Wide survey: A first catalogue of 831 emission line galaxies”. In: A&A 606, A12 (Sept. 2017), A12. arXiv: 1705.08215.

[101] Eileen Herwig et al. “QSO MUSEUM: II. Search for extended Lyα emission around eight z $\sim$ 3 quasar pairs”. In: A&A 691, A210 (Nov. 2024), A210. arXiv: 2408.16826 [astro-ph.GA].

[102] E. R. Higgins and J. S. Vink. “Massive star evolution: rotation, winds, and overshooting vectors in the mass-luminosity plane. I. A calibrated grid of rotating single star models”. In: A&A 622, A50 (Feb. 2019), A50. arXiv: 1811.12190 [astro-ph.SR].

[103] Gary J. Hill et al. “The HETDEX Instrumentation: Hobby-Eberly Telescope Wide-field Upgrade and VIRUS”. In: AJ 162.6, 298 (Dec. 2021), p. 298. arXiv: 2110.03843 [astro-ph.IM].

[104] K. Hollyhead et al. “Evidence for multiple populations in the intermediate-age cluster Lindsay 1 in the SMC”. In: MNRAS 465 (Feb. 2017), pp. L39–L43. arXiv: 1609.01302.

[105] A. Humphrey et al. “Photoionization models for extreme Lyα λ1216 and HeII λ1640 line ratios in quasar halos, and PopIII vs. AGN diagnostics”. In: A&A 621, A10 (Jan. 2019), A10. arXiv: 1810.04463.

[106] T. O. Husser et al. “A new extensive library of PHOENIX stellar atmospheres and synthetic spectra”. In: A&A 553, A6 (May 2013), A6. arXiv: 1303.5632 [astro-ph.SR].

[107] T.-O. Husser et al. “MUSE crowded field 3D spectroscopy of over 12 000 stars in the globular cluster NGC 6397. I. The first comprehensive HRD of a globular cluster”. In: A&A 588, A148 (Apr. 2016), A148. arXiv: 1602.01649 [astro-ph.SR].

[108] H. Inami et al. “The MUSE Hubble Ultra Deep Field Survey. II. Spectroscopic redshifts and comparisons to color selections of high-redshift galaxies”. In: A&A 608, A2 (Nov. 2017), A2. arXiv: 1710.03773.

[109] Y. I. Izotov et al. “Detection of high Lyman continuum leakage from four low-redshift compact star-forming galaxies”. In: MNRAS 461 (Oct. 2016), pp. 3683–3701. arXiv: 1605.05160.

[110] Y. I. Izotov et al. “Eight per cent leakage of Lyman continuum photons from a compact, star-forming dwarf galaxy”. In: Nature 529 (Jan. 2016), pp. 178–180. arXiv: 1601.03068.

[111] Y. I. Izotov et al. “J1154+2443: a low-redshift compact star-forming galaxy with a 46 per cent leakage of Lyman continuum photons”. In: MNRAS 474 (Mar. 2018), pp. 4514–4527. arXiv: 1711.11449.

[112] Y. I. Izotov et al. “Low-redshift Lyman continuum leaking galaxies with high [O III]/[O II] ratios”. In: MNRAS 478 (Aug. 2018), pp. 4851–4865. arXiv: 1805.09865.

[113] George H. Jacoby. “Planetary Nebulae as Standard Candles. I. Evolutionary Models”. In: ApJ 339 (Apr. 1989), p. 39.

[114] George H. Jacoby et al. “Toward Precision Cosmology with Improved Planetary Nebula Luminosity Function Distances Using VLT-MUSE. II. A Test Sample from Archival Data”. In: ApJS 271.2, 40 (Apr. 2024), p. 40.

[115] B. L. James et al. “Uncovering blue diffuse dwarf galaxies”. In: MNRAS 448 (Apr. 2015), pp. 2687–2703. arXiv: 1411.7371.

[116] M. Jauzac et al. “Hubble Frontier Fields: a high-precision strong-lensing analysis of galaxy cluster MACSJ0416.1-2403 using ~200 multiple images”. In: MNRAS 443 (Sept. 2014), pp. 1549–1554. arXiv: 1405.3582.

[117] A. P. Ji et al. “R-process enrichment from a single event in an ancient dwarf galaxy”. In: Nature 531 (Mar. 2016), pp. 610–613. arXiv: 1512.01558.

[118] T. L. Johnson et al. “Star Formation at z = 2.481 in the Lensed Galaxy SDSS J1110+6459: Star Formation Down to 30 pc Scales”. In: ApJ 843, L21 (July 2017), p. L21. arXiv: 1707.00706.

[119] Evelyn J. Johnston, Thomas H. Puzia, and Paul Eigenthaler. “The Serendipitous Detection of a Second Einstein Ring behind the Fornax Cluster”. In: *Research Notes of the American Astronomical Society* 2.4, 235 (Dec. 2018), p. 235.

[120] Evelyn J. Johnston et al. "The Next Generation Fornax Survey (NGFS). V. Discovery of a Dwarf-Dwarf Galaxy Pair at z = 0.30 and Its Characterization Using Deep VLT/MUSE Observations". In: ApJ 873.1, 59 (Mar. 2019), p. 59. arXiv: 1902.02360 [astro-ph.GA].

[121] A. Jones et al. "An advanced scattered moonlight model for Cerro Paranal". In: A&A 560, A91 (Dec. 2013), A91. arXiv: 1310.7030 [astro-ph.IM].

[122] E. Jullo et al. "Cosmological Constraints from Strong Gravitational Lensing in Clusters of Galaxies". In: *Science* 329 (Aug. 2010), pp. 924–927. arXiv: 1008.4802 [astro-ph.CO].

[123] Junais et al. "MUSE observations of the giant low surface brightness galaxy Malin 1: Numerous HII regions, star formation rate, metallicity, and dust attenuation". In: A&A 681, A100 (Jan. 2024), A100. arXiv: 2310.11872 [astro-ph.GA].

[124] S. Kamann, L. Wisotzki, and M. M. Roth. "Resolving stellar populations with crowded field 3D spectroscopy". In: A&A 549, A71 (Jan. 2013), A71. arXiv: 1211.0445 [astro-ph.IM].

[125] S. Kamann et al. "A stellar census in globular clusters with MUSE: The contribution of rotation to cluster dynamics studied with 200 000 stars". In: MNRAS 473 (Feb. 2018), pp. 5591–5616. arXiv: 1710.07257.

[126] S. Kamann et al. "Cluster kinematics and stellar rotation in NGC 419 with MUSE and adaptive optics". In: MNRAS 480 (Oct. 2018), pp. 1689–1695. arXiv: 1807.10612.

[127] S. Kamann et al. "How stellar rotation shapes the colour-magnitude diagram of the massive intermediate-age star cluster NGC 1846". In: MNRAS 492.2 (Feb. 2020), pp. 2177–2192. arXiv: 2001.01731 [astro-ph.SR].

[128] C. Kehrig et al. "The Extended He II λ4686-emitting Region in IZw 18 Unveiled: Clues for Peculiar Ionizing Sources". In: ApJ 801, L28 (Mar. 2015), p. L28. arXiv: 1502.00522.

[129] T. Kimm et al. "Understanding the escape of LyC and Lyα photons from turbulent clouds". In: MNRAS 486 (June 2019), pp. 2215–2237. arXiv: 1901.05990.

[130] M. Koleva et al. "ULySS: a full spectrum fitting package". In: A&A 501.3 (July 2009), pp. 1269–1279. arXiv: 0903.2979 [astro-ph.IM].

[131] D. Krajnović et al. "Kinemetry: a generalization of photometry to the higher moments of the line-of-sight velocity distribution". In: MNRAS 366 (Mar. 2006), pp. 787–802. eprint: astro-ph/0512200.

[132] D. Krajnović et al. "The ATLAS^{3D} project - II. Morphologies, kinemetric features and alignment between photometric and kinematic axes of early-type galaxies". In: MNRAS 414 (July 2011), pp. 2923–2949. arXiv: 1102.3801.

[133] K. Kreckel et al. "Mapping Metallicity Variations across Nearby Galaxy Disks". In: ApJ 887.1, 80 (Dec. 2019), p. 80. arXiv: 1910.07190 [astro-ph.GA].

[134] J. M. Diederik Kruijssen et al. "Fast and inefficient star formation due to short-lived molecular clouds and rapid feedback". In: Nature 569.7757 (May 2019), pp. 519–522. arXiv: 1905.08801 [astro-ph.GA].

[135] Mark R. Krumholz and Blakesley Burkhart. "Is turbulence in the interstellar medium driven by feedback or gravity? An observational test". In: MNRAS 458.2 (May 2016), pp. 1671–1677. arXiv: 1512.03439 [astro-ph.GA].

[136] R. P. Kudritzki et al. "A Spectroscopic Study of Blue Supergiant Stars in the Sculptor Galaxy NGC 55: Chemical Evolution and Distance". In: ApJ 829, 70 (Oct. 2016), p. 70. arXiv: 1607.04325.

[137] R.-P. Kudritzki et al. "Quantitative Spectroscopy of Blue Supergiant Stars in the Disk of M81: Metallicity, Metallicity Gradient, and Distance". In: ApJ 747, 15 (Mar. 2012), p. 15. arXiv: 1112.3643.

[138] D. Kunth and G. Östlin. "The most metal-poor galaxies". In: A&A Rev. 10 (Jan. 2000), pp. 1–79. arXiv: astro-ph/9911094 [astro-ph].

[139] F. La Barbera et al. "IMF radial gradients in most massive early-type galaxies". In: MNRAS 489.3 (Nov. 2019), pp. 4090–4110. arXiv: 1909.01382 [astro-ph.GA].

[140] D. J. Lagattuta et al. "Lens modelling Abell 370: crowning the final frontier field with MUSE". In: MNRAS 469 (Aug. 2017), pp. 3946–3964. arXiv: 1611.01513.

[141] T.-W. Lan and H. Mo. “The Circumgalactic Medium of eBOSS Emission Line Galaxies: Signatures of Galactic Outflows in Gas Distribution and Kinematics”. In: ApJ 866, 36 (Oct. 2018), p. 36. arXiv: 1806.05786.

[142] N. Langer. “Presupernova Evolution of Massive Single and Binary Stars”. In: ARA&A 50 (Sept. 2012), pp. 107–164. arXiv: 1206.5443 [astro-ph.SR].

[143] Thierry Lanz and Ivan Hubeny. “A Grid of NLTE Line-blanketed Model Atmospheres of Early B-Type Stars”. In: ApJS 169.1 (Mar. 2007), pp. 83–104. arXiv: astro-ph/0611891 [astro-ph].

[144] F. Leclercq et al. “The MUSE Hubble Ultra Deep Field Survey. VIII. Extended Lyman-α haloes around high-z star-forming galaxies”. In: A&A 608, A8 (Nov. 2017), A8. arXiv: 1710.10271.

[145] Floriane Leclercq et al. “The MUSE eXtremely deep field: first panoramic view of an Mg II emitting intragroup medium”. In: A&A 663, A11 (July 2022), A11. arXiv: 2203.05614 [astro-ph.GA].

[146] E. Leitet et al. “Escape of Lyman continuum radiation from local galaxies. Detection of leakage from the young starburst Tol 1247-232”. In: A&A 553, A106 (May 2013), A106. arXiv: 1302.6971.

[147] Federico Lelli et al. “Cold gas disks in main-sequence galaxies at cosmic noon: Low turbulence, flat rotation curves, and disk-halo degeneracy”. In: A&A 672, A106 (Apr. 2023), A106. arXiv: 2302.00030 [astro-ph.GA].

[148] G. Leloudas et al. “Spectroscopy of superluminous supernova host galaxies. A preference of hydrogen-poor events for extreme emission line galaxies”. In: MNRAS 449 (May 2015), pp. 917–932. arXiv: 1409.8331.

[149] Qiong Li et al. “Discovery of a Protocluster Core Associated with an Enormous Lya Nebula at z = 2.3”. In: ApJ 922.2, 236 (Dec. 2021), p. 236. arXiv: 2111.01384 [astro-ph.GA].

[150] T. S. Li et al. “Farthest Neighbor: The Distant Milky Way Satellite Eridanus II”. In: ApJ 838, 8 (Mar. 2017), p. 8. arXiv: 1611.05052.

[151] X.-W. Liu. “Optical recombination lines as probes of conditions in planetary nebulae”. In: *Planetary Nebulae in our Galaxy and Beyond*. Ed. by M. J. Barlow and R. H. Méndez. Vol. 234. IAU Symposium. 2006, pp. 219–226. eprint: astro-ph/0605082.

[152] Emma K. Lofthouse et al. “MUSE Analysis of Gas around Galaxies (MAGG) - I: Survey design and the environment of a near pristine gas cloud at z $\approx$ 3.5.” In: MNRAS (Nov. 2019), p. 2667. arXiv: 1910.13458 [astro-ph.GA].

[153] S. Lopez et al. “A clumpy and anisotropic galaxy halo at redshift 1 from gravitational-arc tomography”. In: Nature 554 (Feb. 2018), pp. 493–496. arXiv: 1801.10175.

[154] Omar López-Cruz et al. “Secondary Infall in the Seyfert’s Sextet: A Plausible Way Out of the Short Crossing Time Paradox”. In: ApJ 886.1, L2 (Nov. 2019), p. L2. arXiv: 1910.12533 [astro-ph.GA].

[155] Á. R. López-Sánchez. “Massive star formation in Wolf-Rayet galaxies. V. Star-formation rates, masses and the importance of galaxy interactions”. In: A&A 521, A63 (Oct. 2010), A63. arXiv: 1005.0659 [astro-ph.CO].

[156] A. R. López-Sánchez and C. Esteban. “Massive star formation in Wolf-Rayet galaxies. II. Optical spectroscopy results”. In: A&A 508.2 (Dec. 2009), pp. 615–640. arXiv: 0910.1578 [astro-ph.CO].

[157] Á. R. López-Sánchez et al. “Eliminating error in the chemical abundance scale for extragalactic H II regions”. In: MNRAS 426.4 (Nov. 2012), pp. 2630–2651. arXiv: 1203.5021 [astro-ph.CO].

[158] Á. R. López-Sánchez et al. “Ionized gas in the XUV disc of the NGC 1512/1510 system”. In: MNRAS 450.4 (July 2015), pp. 3381–3409.

[159] M. Lorenzo et al. “A new reference catalogue for the very metal-poor Universe: +150 OB stars in Sextans A”. In: MNRAS 516.3 (Nov. 2022), pp. 4164–4179. arXiv: 2207.09700 [astro-ph.GA].

[160] E. Lusso et al. “The MUSE Ultra Deep Field (MUDF) - I. Discovery of a group of Lyα nebulae associated with a bright z $\approx$ 3.23 quasar pair”. In: MNRAS 485.1 (May 2019), pp. L62–L67. arXiv: 1903.00483 [astro-ph.GA].

[161] Piero Madau and Mark Dickinson. "Cosmic Star-Formation History". In: ARA&A 52 (Aug. 2014), pp. 415–486. arXiv: `1403.0007 [astro-ph.CO]`.

[162] G. Mahler et al. "Strong-lensing analysis of A2744 with MUSE and Hubble Frontier Fields images". In: MNRAS 473 (Jan. 2018), pp. 663–692. arXiv: `1702.06962`.

[163] M. Mapelli et al. "Are ring galaxies the ancestors of giant low surface brightness galaxies?" In: MNRAS 383 (Jan. 2008), pp. 1223–1231. arXiv: `0710.5354`.

[164] P. Marchant et al. "A new route towards merging massive black holes". In: A&A 588, A50 (Apr. 2016), A50. arXiv: `1601.03718 [astro-ph.SR]`.

[165] C. Martin et al. "The Keck Cosmic Web Imager". In: *Ground-based and Airborne Instrumentation for Astronomy III*. Vol. 7735. Proc. SPIE. July 2010, p. 77350M.

[166] F. Martins. "Quantitative spectral classification of Galactic O stars". In: A&A 616, A135 (Aug. 2018), A135. arXiv: `1805.08267 [astro-ph.SR]`.

[167] F. Martins et al. "The MiMeS survey of magnetism in massive stars: CNO surface abundances of Galactic O stars". In: A&A 575, A34 (Mar. 2015), A34. arXiv: `1411.4420 [astro-ph.SR]`.

[168] M. V. Maseda et al. "MUSE Spectroscopic Identifications of Ultra-faint Emission Line Galaxies with $M_{UV} \sim -15$". In: ApJ 865, L1 (Sept. 2018), p. L1. arXiv: `1809.01142`.

[169] P. Massey, K. F. Neugent, and B. M. Smart. "A Spectroscopic Survey of Massive Stars in M31 and M33". In: AJ 152, 62 (Sept. 2016), p. 62. arXiv: `1604.00112 [astro-ph.SR]`.

[170] Y. Matsuda et al. "Diffuse Lyα haloes around Lyα emitters at z=3: do dark matter distributions determine the Lyα spatial extents?" In: MNRAS 425 (Sept. 2012), pp. 878–883. arXiv: `1204.4934`.

[171] A. W. McConnachie. "The Observed Properties of Dwarf Galaxies in and around the Local Group". In: AJ 144, 4 (July 2012), p. 4. arXiv: `1204.1562`.

[172] Richard M. McDermid et al. "Phase A Science Case for MAVIS – The Multi-conjugate Adaptive-optics Visible Imager-Spectrograph for the VLT Adaptive Optics Facility". In: *arXiv e-prints*, arXiv:2009.09242 (Sept. 2020), arXiv:2009.09242. arXiv: `2009.09242 [astro-ph.IM]`.

[173] Rosalie C. McGurk et al. "Development of the ROSIE integral field unit on the Magellan IMACS spectrograph". In: *Ground-based and Airborne Instrumentation for Astronomy VIII*. Ed. by Christopher J. Evans, Julia J. Bryant, and Kentaro Motohara. Vol. 11447. Society of Photo-Optical Instrumentation Engineers (SPIE) Conference Series. Dec. 2020, p. 1144769. arXiv: `2012.12293 [astro-ph.IM]`.

[174] A. F. McLeod et al. "Feedback from massive stars at low metallicities: MUSE observations of N44 and N180 in the Large Magellanic Cloud". In: MNRAS 486.4 (July 2019), pp. 5263–5288. arXiv: `1810.01433 [astro-ph.GA]`.

[175] A. F. McLeod et al. "The Pillars of Creation revisited with MUSE: gas kinematics and high-mass stellar feedback traced by optical spectroscopy". In: MNRAS 450.1 (June 2015), pp. 1057–1076. arXiv: `1504.03323 [astro-ph.SR]`.

[176] Anna F. McLeod et al. "The impact of pre-supernova feedback and its dependence on environment". In: MNRAS 508.4 (Dec. 2021), pp. 5425–5448. arXiv: `2109.08703 [astro-ph.GA]`.

[177] K. J. Meech et al. "Deep Impact, Stardust-NExT and the behavior of Comet 9P/Tempel 1 from 1997 to 2010". In: Icarus 213 (May 2011), pp. 323–344.

[178] Matteo Messa et al. "Looking for Obscured Young Star Clusters in NGC 1313". In: ApJ 909.2, 121 (Mar. 2021), p. 121. arXiv: `2011.09392 [astro-ph.GA]`.

[179] G. Meynet and A. Maeder. "Stellar evolution with rotation. V. Changes in all the outputs of massive star models". In: A&A 361 (Sept. 2000), pp. 101–120. eprint: `astro-ph/0006404`.

[180] Peter D. Mitchell et al. "Galactic outflow rates in the EAGLE simulations". In: MNRAS 494.3 (May 2020), pp. 3971–3997. arXiv: `1910.09566 [astro-ph.GA]`.

[181] R. Momose et al. “Diffuse Lyα haloes around galaxies at z = 2.2-6.6: implications for galaxy formation and cosmic reionization”. In: MNRAS 442 (July 2014), pp. 110–120. arXiv: 1403.0732.

[182] B. Moralejo et al. “The Potsdam MRS spectrograph: heritage of MUSE and the impact of cross-innovation in the process of technology transfer”. In: *Advances in Optical and Mechanical Technologies for Telescopes and Instrumentation II*. Vol. 9912. Proc. SPIE. July 2016, p. 991222. arXiv: 1607.01269 [astro-ph.IM].

[183] Thorsten Naab et al. “The ATLAS^{3D} project - XXV. Two-dimensional kinematic analysis of simulated galaxies and the cosmological origin of fast and slow rotators”. In: MNRAS 444.4 (Nov. 2014), pp. 3357–3387. arXiv: 1311.0284 [astro-ph.CO].

[184] S. Noll et al. “An atmospheric radiation model for Cerro Paranal. I. The optical spectral range”. In: A&A 543, A92 (July 2012), A92. arXiv: 1205.2003 [astro-ph.IM].

[185] K. O’Neil and G. Bothun. “The Space Density of Galaxies through $\mu_B(0)$=25.0 Magnitudes per Inverse Arcsecond Squared”. In: ApJ 529 (Feb. 2000), pp. 811–815.

[186] C. Opitom et al. “MUSE observations of comet 67P/Churyumov-Gerasimenko. A reference for future comet observations with MUSE”. In: A&A 644, A143 (Dec. 2020), A143. arXiv: 2010.05064 [astro-ph.EP].

[187] C. Opitom et al. “TRAPPIST monitoring of comet C/2012 F6 (Lemmon)”. In: A&A 574, A38 (Feb. 2015), A38.

[188] P. Papaderos et al. “Extremely metal-poor star-forming galaxies. New detections and general morphological and photometric properties”. In: A&A 491.1 (Nov. 2008), pp. 113–129. arXiv: 0809.1217 [astro-ph].

[189] V. Patrício et al. “A young star-forming galaxy at z = 3.5 with an extended Lyman α halo seen with MUSE”. In: MNRAS 456 (Mar. 2016), pp. 4191–4208. arXiv: 1512.01212.

[190] Renuka Pechetti et al. “ω Centauri: a MUSE discovery of a counter-rotating core”. In: MNRAS 528.3 (Mar. 2024), pp. 4941–4957. arXiv: 2401.15149 [astro-ph.GA].

[191] A. Peimbert et al. “Physical conditions derived from O II recombination lines in planetary nebulae and their implications”. In: RMxAA 50 (Oct. 2014), pp. 329–340. arXiv: 1408.4835.

[192] Ying-jie Peng et al. “Mass and Environment as Drivers of Galaxy Evolution in SDSS and zCOSMOS and the Origin of the Schechter Function”. In: ApJ 721.1 (Sept. 2010), pp. 193–221. arXiv: 1003.4747 [astro-ph.CO].

[193] C. Péroux et al. “Multiphase circumgalactic medium probed with MUSE and ALMA”. In: MNRAS 485 (May 2019), pp. 1595–1613. arXiv: 1901.05217.

[194] C. Péroux et al. “Spatially resolved metal gas clouds”. In: MNRAS 479 (Sept. 2018), pp. L50–L54. arXiv: 1805.07192.

[195] Ismael Pessa et al. “A galactic outflow traced by its extended Mg II emission out to a ∼30 kpc radius in the Hubble Ultra Deep Field with MUSE”. In: A&A 691, A5 (Nov. 2024), A5. arXiv: 2408.16067 [astro-ph.GA].

[196] T. E. Pickering et al. “Neutral Hydrogen Distributions and Kinematics of Giant Low Surface=20 Brightness Disk Galaxies”. In: AJ 114 (Nov. 1997), p. 1858.

[197] Adriano Poci et al. “Combining stellar populations with orbit-superposition dynamical modelling: the formation history of the lenticular galaxy NGC 3115”. In: MNRAS 487.3 (Aug. 2019), pp. 3776–3796. arXiv: 1904.11605 [astro-ph.GA].

[198] H. Rahmani et al. “Observational signatures of a warped disk associated with cold-flow accretion”. In: MNRAS 474 (Feb. 2018), pp. 254–270. arXiv: 1710.08398.

[199] J. Richard et al. “MUSE observations of the lensing cluster SMACSJ2031.8-4036: new constraints on the mass distribution in the cluster core”. In: MNRAS 446 (Jan. 2015), pp. L16–L20. arXiv: 1409.2488.

[200] Johan Richard et al. “BlueMUSE: Project Overview and Science Cases”. In: *arXiv e-prints*, arXiv:1906.01657 (June 2019), arXiv:1906.01657. arXiv: 1906.01657 [astro-ph.IM].

[201] Adam G. Riess et al. “A Comprehensive Measurement of the Local Value of the Hubble Constant with 1 km s^{-1} Mpc^{-1} Uncertainty from the Hubble Space Telescope and the SH0ES Team”. In: ApJ 934.1, L7 (July 2022), p. L7. arXiv: 2112.04510 [astro-ph.CO].

[202] T. Emil Rivera-Thorsen et al. “Gravitational lensing reveals ionizing ultraviolet photons escaping from a distant galaxy”. In: *Science* 366.6466 (Nov. 2019), pp. 738–741. arXiv: 1904.08186 [astro-ph.GA].

[203] J. G. Rivero González et al. “Nitrogen line spectroscopy in O-stars. III. The earliest O-stars”. In: A&A 543, A95 (July 2012), A95. arXiv: 1205.4444 [astro-ph.SR].

[204] M. M. Roth et al. “MUSE crowded field 3D spectroscopy in NGC 300. I. First results from central fields”. In: A&A 618, A3 (Oct. 2018), A3. arXiv: 1806.04280.

[205] Martin M. Roth. “Scientific Impact of Novel Instrumentation: The Case of MUSE”. In: *Research Notes of the American Astronomical Society* 8.3, 54 (Mar. 2024), p. 54.

[206] Martin M. Roth et al. “Integral Field Spectroscopy: a disruptive innovation for observations of Planetary Nebulae and the PNLF”. In: *arXiv e-prints*, arXiv:2311.14230 (Nov. 2023), arXiv:2311.14230. arXiv: 2311.14230 [astro-ph.GA].

[207] Martin M. Roth et al. “Toward Precision Cosmology with Improved PNLF Distances Using VLT-MUSEI. Methodology and Tests”. In: ApJ 916.1, 21 (July 2021), p. 21. arXiv: 2105.01982 [astro-ph.GA].

[208] J.-R. Roy and D. Kunth. “Dispersal and mixing of oxygen in the interstellar medium of gas-rich galaxies”. In: A&A 294 (Feb. 1995), pp. 432–442. eprint: astro-ph/9410023.

[209] Kate H. R. Rubin et al. “Galaxies Probing Galaxies in PRIMUS. II. The Coherence Scale of the Cool Circumgalactic Medium”. In: ApJ 868.2, 142 (Dec. 2018), p. 142. arXiv: 1806.08801 [astro-ph.GA].

[210] S. F. Sánchez et al. “A characteristic oxygen abundance gradient in galaxy disks unveiled with CALIFA”. In: A&A 563, A49 (Mar. 2014), A49. arXiv: 1311.7052 [astro-ph.CO].

[211] S. F. Sánchez et al. “CALIFA, the Calar Alto Legacy Integral Field Area survey. I. Survey presentation”. In: A&A 538, A8 (Feb. 2012), A8. arXiv: 1111.0962 [astro-ph.CO].

[212] Laura Sánchez-Menguiano et al. “Arm-interarm gas abundance variations explored with MUSE: the role of spiral structure in the chemical enrichment of galaxies”. In: MNRAS 492.3 (Mar. 2020), pp. 4149–4163. arXiv: 2001.03450 [astro-ph.GA].

[213] Giulia Santucci et al. “The SAMI Galaxy Survey: The Internal Orbital Structure and Mass Distribution of Passive Galaxies from Triaxial Orbit-superposition Schwarzschild Models”. In: ApJ 930.2, 153 (May 2022), p. 153. arXiv: 2203.03648 [astro-ph.GA].

[214] Fabian Scheuermann et al. “Planetary nebula luminosity function distances for 19 galaxies observed by PHANGS-MUSE”. In: MNRAS 511.4 (Apr. 2022), pp. 6087–6109. arXiv: 2201.04641 [astro-ph.GA].

[215] E. Schinnerer and A. K. Leroy. “Molecular Gas and the Star-Formation Process on Cloud Scales in Nearby Galaxies”. In: ARA&A 62.1 (Sept. 2024), pp. 369–436. arXiv: 2403.19843 [astro-ph.GA].

[216] E. Schmälzlin et al. “Raman Imaging with a Fiber-Coupled Multichannel Spectrograph”. In: *Sensors* 14 (Nov. 2014), p. 21968.

[217] Elmar Schmälzlin et al. “Nonscanning large-area Raman imaging for ex vivo/in vivo skin cancer discrimination”. In: *Journal of Biomedical Optics* 23, 105001 (Oct. 2018), p. 105001. arXiv: 1810.03363 [astro-ph.IM].

[218] Nicholas Scott et al. “The SAMI-Fornax Dwarfs Survey I: sample, observations, and the specific stellar angular momentum of dwarf elliptical galaxies”. In: MNRAS 497.2 (Sept. 2020), pp. 1571–1582. arXiv: 2007.04492 [astro-ph.GA].

[219] A. E. Shapley et al. “Q1549-C25: A Clean Source of Lyman-Continuum Emission at z = 3.15”. In: ApJ 826, L24 (Aug. 2016), p. L24. arXiv: 1606.00443.

[220] B. Sharpee, J. A. Baldwin, and R. Williams. “Identification and Characterization of Faint Emission Lines in the Spectrum of the Planetary Nebula IC 418”. In: ApJ 615 (Nov. 2004), pp. 323–343. eprint: astro-ph/0407186.

[221] Joshua D. Simon. "The Faintest Dwarf Galaxies". In: ARA&A 57 (Aug. 2019), pp. 375–415. arXiv: 1901.05465 [astro-ph.GA].

[222] Russell J. Smith. "Discovering novae in early-type galaxies with MUSE: A chance find in NGC 1404, and twelve more candidates from an archival search". In: *arXiv e-prints*, arXiv:2001.08221 (Jan. 2020), arXiv:2001.08221. arXiv: 2001.08221 [astro-ph.GA].

[223] Azlizan A. Soemitro et al. "MUSE crowded field 3D spectroscopy in NGC 300. IV. Planetary nebula luminosity function". In: A&A 671, A142 (Mar. 2023), A142. arXiv: 2301.03437 [astro-ph.GA].

[224] C. C. Steidel et al. "The Keck Lyman Continuum Spectroscopic Survey (KLCS): The Emergent Ionizing Spectrum of Galaxies at $z \sim 3$". In: ApJ 869, 123 (Dec. 2018), p. 123. arXiv: 1805.06071.

[225] Peter B. Stetson. "DAOPHOT: A Computer Program for Crowded-Field Stellar Photometry". In: PASP 99 (Mar. 1987), p. 191.

[226] V. Strazzullo et al. "Galaxy Evolution in Overdense Environments at High Redshift: Passive Early-type Galaxies in a Cluster at z ~ 2". In: ApJ 772, 118 (Aug. 2013), p. 118. arXiv: 1305.3577.

[227] D. A. Thilker et al. "A Search for Extended Ultraviolet Disk (XUV-Disk) Galaxies in the Local Universe". In: ApJS 173 (Dec. 2007), pp. 538–571. arXiv: 0712.3555.

[228] E. Toloba et al. "Formation and evolution of dwarf early-type galaxies in the Virgo cluster. I. Internal kinematics". In: A&A 526, A114 (Feb. 2011), A114. arXiv: 1011.2198.

[229] A. Travascio et al. "X-ray view of a massive node of the Cosmic Web at z~3 I. An exceptional overdensity of rapidly accreting SMBHs". In: *arXiv e-prints*, arXiv:2410.03933 (Oct. 2024), arXiv:2410.03933. arXiv: 2410.03933 [astro-ph.GA].

[230] M. Trebitsch et al. "Fluctuating feedback-regulated escape fraction of ionizing radiation in low-mass, high-redshift galaxies". In: MNRAS 470 (Sept. 2017), pp. 224–239. arXiv: 1705.00941.

[231] Ignacio Trujillo et al. "A distance of 13 Mpc resolves the claimed anomalies of the galaxy lacking dark matter". In: MNRAS 486.1 (June 2019), pp. 1192–1219. arXiv: 1806.10141 [astro-ph.GA].

[232] Y. G. Tsamis et al. "Heavy elements in Galactic and Magellanic Cloud HII regions: recombination-line versus forbidden-line abundances". In: MNRAS 338 (Jan. 2003), pp. 687–710. eprint: astro-ph/0209534.

[233] Y. G. Tsamis et al. "Integral field spectroscopy of planetary nebulae: mapping the line diagnostics and hydrogen-poor zones with VLT FLAMES". In: MNRAS 386 (May 2008), pp. 22–46. arXiv: 0802.0774.

[234] Jason Tumlinson, Molly S. Peeples, and Jessica K. Werk. "The Circumgalactic Medium". In: ARA&A 55.1 (Aug. 2017), pp. 389–432. arXiv: 1709.09180 [astro-ph.GA].

[235] H. Übler et al. "The Evolution and Origin of Ionized Gas Velocity Dispersion from z $\sim$ 2.6 to z $\sim$ 0.6 with KMOS^{3D}". In: ApJ 880.1, 48 (July 2019), p. 48. arXiv: 1906.02737 [astro-ph.GA].

[236] H. Umehata et al. "Gas filaments of the cosmic web located around active galaxies in a protocluster". In: *Science* 366.6461 (Oct. 2019), pp. 97–100. arXiv: 1910.01324 [astro-ph.GA].

[237] T. Urrutia et al. "The MUSE-Wide Survey: survey description and first data release". In: A&A 624, A141 (Apr. 2019), A141. arXiv: 1811.06549.

[238] F. Valentino et al. "A Giant Lyα Nebula in the Core of an X-Ray Cluster at Z = 1.99: Implications for Early Energy Injection". In: ApJ 829, 53 (Sept. 2016), p. 53. arXiv: 1605.03194.

[239] Lucas M. Valenzuela et al. "The PICS Project. I. The impact of metallicity and helium abundance on the bright end of the planetary nebula luminosity function". In: *arXiv e-prints*, arXiv:2501.17926 (Jan. 2025), arXiv:2501.17926. arXiv: 2501.17926 [astro-ph.GA].

[240] J. van de Sande et al. "GECKOS: Turning galaxy evolution on its side with deep observations of edge-on galaxies". In: *Early Disk-Galaxy Formation from JWST to the Milky Way*. Ed. by Fatemeh Tabatabaei, Beatriz Barbuy, and Yuan-Sen Ting. Vol. 377. IAU Symposium. Jan. 2024, pp. 27–33. arXiv: 2306.00059 [astro-ph.GA].

[241] J. van de Sande et al. “The SAMI Galaxy Survey: Revisiting Galaxy Classification through High-order Stellar Kinematics”. In: ApJ 835, 104 (Jan. 2017), p. 104. arXiv: 1611.07039.

[242] Jesse van de Sande et al. “The SAMI Galaxy Survey: a statistical approach to an optimal classification of stellar kinematics in galaxy surveys”. In: MNRAS 505.2 (Aug. 2021), pp. 3078–3106. arXiv: 2011.08199 [astro-ph.GA].

[243] Jesse van de Sande et al. “The SAMI galaxy survey: Mass and environment as independent drivers of galaxy dynamics”. In: MNRAS 508.2 (Dec. 2021), pp. 2307–2328. arXiv: 2109.06189 [astro-ph.GA].

[244] R. P. van der Marel and M. Franx. “A new method for the identification of non-Gaussian line profiles in elliptical galaxies”. In: ApJ 407 (Apr. 1993), pp. 525–539.

[245] P. van Dokkum et al. “A galaxy lacking dark matter”. In: Nature 555 (Mar. 2018), pp. 629–632. arXiv: 1803.10237.

[246] Pieter G. van Dokkum et al. “Spectroscopic Confirmation of the Existence of Large, Diffuse Galaxies in the Coma Cluster”. In: ApJ 804.1, L26 (May 2015), p. L26. arXiv: 1504.03320 [astro-ph.GA].

[247] E. Vanzella et al. “Direct Lyman continuum and Ly α escape observed at redshift 4”. In: MNRAS 476 (May 2018), pp. L15–L19. arXiv: 1712.07661.

[248] E. Vanzella et al. “Hubble Imaging of the Ionizing Radiation from a Star-forming Galaxy at Z=3.2 with fesc>50%”. In: ApJ 825, 41 (July 2016), p. 41. arXiv: 1602.00688.

[249] E. Vanzella et al. “Magnifying the Early Episodes of Star Formation: Super Star Clusters at Cosmological Distances”. In: ApJ 842.1, 47 (June 2017), p. 47. arXiv: 1703.02044 [astro-ph.GA].

[250] C. M. Vaughan, D. M. Pierce, and A. L. Cochran. “Jet Morphology and Coma Analysis of Comet 103P/Hartley 2”. In: AJ 154, 219 (Dec. 2017), p. 219.

[251] Daniel Vaz et al. “The MUSE-Faint survey. IV. Dissecting Leo T, a gas-rich relic with recent star formation”. In: A&A 678, A59 (Oct. 2023), A59. arXiv: 2308.16263 [astro-ph.GA].

[252] A. Verhamme et al. “Using Lyman-α to detect galaxies that leak Lyman continuum”. In: A&A 578, A7 (June 2015), A7. arXiv: 1404.2958.

[253] M. Villar-Martín et al. “Kinematically quiet haloes around z˜ 2.5 radio galaxies. Keck spectroscopy”. In: MNRAS 346 (Nov. 2003), pp. 273–294. eprint: astro-ph/0309012.

[254] J. S. Vink. “Very massive stars: a metallicity-dependent upper-mass limit, slow winds, and the self-enrichment of globular clusters”. In: A&A 615, A119 (July 2018), A119. arXiv: 1803.08042 [astro-ph.SR].

[255] Jorick S. Vink et al. “Very Massive Stars in the local Universe”. In: *Highlights of Astronomy* 16 (Mar. 2015), pp. 51–79. arXiv: 1302.2021 [astro-ph.SR].

[256] N. R. Walborn and E. L. Fitzpatrick. “Contemporary optical spectral classification of the OB stars - A digital atlas”. In: PASP 102 (Apr. 1990), pp. 379–411.

[257] J. R. Walsh et al. “An imaging spectroscopic survey of the planetary nebula NGC 7009 with MUSE”. In: A&A 620, A169 (Dec. 2018), A169. arXiv: 1810.03984.

[258] Chen Wang et al. “Stellar mergers as the origin of the blue main-sequence band in young star clusters”. In: *Nature Astronomy* 6 (Feb. 2022), pp. 480–487. arXiv: 2202.05552 [astro-ph.SR].

[259] T. Wang et al. “Discovery of a Galaxy Cluster with a Violently Starbursting Core at z = 2.506”. In: ApJ 828, 56 (Sept. 2016), p. 56. arXiv: 1604.07404.

[260] Peter M. Weilbacher et al. “A MUSE map of the central Orion Nebula (M 42)”. In: A&A 582, A114 (Oct. 2015), A114. arXiv: 1507.00006 [astro-ph.GA].

[261] Peter M. Weilbacher et al. “Lyman-continuum leakage as dominant source of diffuse ionized gas in the Antennae galaxy”. In: A&A 611, A95 (Apr. 2018), A95. arXiv: 1712.04450 [astro-ph.GA].

[262] Martin Wendt et al. “The blue multiunit spectroscopic explorer (BlueMUSE) on the VLT: end-to-end simulator BlueSi”. In: *Software and Cyberinfrastructure for Astronomy VIII*. Ed. by Jorge Ibsen and Gianluca Chiozzi. Vol. 13101. Society of Photo-Optical Instrumentation Engineers (SPIE) Conference Series. July 2024, p. 1310123.

[263] J. H. Wise et al. “The birth of a galaxy - III. Propelling reionization with the faintest galaxies”. In: MNRAS 442 (Aug. 2014), pp. 2560–2579. arXiv: 1403.6123.

[264] L. Wisotzki et al. “Extended Lyman α haloes around individual high-redshift galaxies revealed by MUSE”. In: A&A 587, A98 (Mar. 2016), A98. arXiv: 1509.05143.

[265] L. Wisotzki et al. “Nearly all the sky is covered by Lyman-α emission around high-redshift galaxies”. In: Nature 562 (Oct. 2018), pp. 229–232. arXiv: 1810.00843.

[266] Maosheng Xiang and Hans-Walter Rix. “A time-resolved picture of our Milky Way’s early formation history”. In: Nature 603.7902 (Mar. 2022), pp. 599–603. arXiv: 2203.12110 [astro-ph.GA].

[267] R. Xue et al. “The Diversity of Diffuse Lyα Nebulae around Star-forming Galaxies at High Redshift”. In: ApJ 837, 172 (Mar. 2017), p. 172. arXiv: 1611.03510.

[268] J. Zabl et al. “MusE GAs FLOw and Wind (MEGAFLOW) II. A study of gas accretion around z $\sim$ 1 star-forming galaxies with background quasars”. In: MNRAS 485 (May 2019), pp. 1961–1980. arXiv: 1901.11416.

[269] Johannes Zabl et al. “MusE GAs FLOw and Wind (MEGAFLOW) IV. A two sightline tomography of a galactic wind”. In: MNRAS (Dec. 2019), p. 3236.

[270] Johannes Zabl et al. “MusE GAs FLOw and Wind (MEGAFLOW) VIII. Discovery of a MgII emission halo probed by a quasar sightline”. In: MNRAS 507.3 (Nov. 2021), pp. 4294–4315. arXiv: 2105.14090 [astro-ph.GA].

[271] Sebastiaan L. Zoutendijk et al. “The MUSE-Faint survey. I. Spectroscopic evidence for a star cluster in Eridanus 2 and constraints on MACHOs as a constituent of dark matter”. In: A&A 635, A107 (Mar. 2020), A107. arXiv: 2001.08790 [astro-ph.GA].

[272] Sebastiaan L. Zoutendijk et al. “The MUSE-Faint survey. II. The dark-matter density profile of the ultra-faint dwarf galaxy Eridanus 2”. In: A&A 651, A80 (July 2021), A80. arXiv: 2101.00253 [astro-ph.GA].